YUNIBESITI YA BOKONE-BOPHIRIMA
NORTH WEST UNIVERSITY
NOORDWES UNIVERSITEIT

Novel Method of Improving Squirrel Cage Induction Motor Performance by using Mixed Conductivity Fabricated Rotors (MCFR)

Constantin Danut PITIS

Presented in the fulfillment
of the requirements for the degree

PHILOSOPHIAE DOCTOR

in the
Faculty of Engineering
North West University

Promoter: Prof. Marius Kleingeld

Pretoria, March 2006

Abstract

Title: Novel method of improving squirrel cage induction motor performance by using MIXED CONDUCTIVITY FABRICATED ROTORS (MCFR)

Author: Constantin Danut PITIS

Promoter: Prof. Marius Kleingeld

Keywords: Induction motors, squirrel cage rotors, application engineering, mining industry

The ideal squirrel cage motor should have a varying rotor resistance; large at standstill, and decreasing as the speed rises. Overseas-designed high impedance rotors try to fulfil these conditions – mostly used are double cage rotors and die cast aluminium rotors. However, in the South African coal-mining industry these rotors recorded high rate failures with heavy financial losses. As a result, the need for an alternative rotor type that was able to comply with basic conditions ignored before appeared on the market:

- Higher reliability with extended life expectancy
- Lower total ownership costs
- Easy re-manufacturing with components available on the market
- Specific performance stability at competitive price

Over the years, only two principles were tacitly accepted in designing squirrel cage rotors:

1. For a single cage rotor, in a circumferential direction around the rotor the squirrel cage bars are placed in the same cylindrical shell, with the same shape and same conductivity.
2. For a double cage rotor, the same rule as above applies; however, in the radial direction, the bars have different shapes and typically different conductivities.

The invention is based on a new principle, i.e. "in a circumferential direction around the squirrel cage rotor, squirrel cage bars may have different conductivities and same shapes, or different conductivities and different shapes".

Mixed Conductivity Fabricated Rotors (MCFR) are designed and manufactured based on this new principle, and are able to withstand the harsh South African mining conditions.

Since patented, the invention has been materialised in a set of special rotors powering continuous miners of a reputable coal-mining house, which was spending about R5 million annually on replacing specific imported die cast aluminium rotors only.

Fully complying with the above-mentioned basic conditions, the patent offers a large variety of technical and economical advantages, increasing mining processes efficiency beyond expectations.

The thesis describes the MCFR's design adaptability by altering the rotor design to meet the demands of a specific engineering application as a base line of drives design.

The patent is part of the new South African trend of increasing processes efficiency. It offers large possibilities of designing dedicated motors with a positive impact on the South African economy. Some socio-economical advantages are worthy of considerable study:

- Being locally manufactured, the MCFR may reduce the country's economical dependence.
- Requiring no special expertise, the MCFR can be produced in any quantity and size without excessive investment.
- The MCFR offers an alternative option (product interchangeability) on the market as well as sound competition (with export potential).
- The patent ensures business sustainability conditions which diffuse financial constraints on motor manufacturers and end-users during the re-capitalisation process (very loaded in South African economic and industrial environment).

Acknowledgements

The author wishes to acknowledge with gratitude all mining houses and engineers who have encouraged him in this venture.

Special thanks goes to Voest Alpine Mining and Tunneling, South Africa who gave author the opportunity of designing and developing this patent.

Thanks to Mr Theuns du Toit and Mr Dave Birch, directors of Custom Electric Motors (Cullinan Electric) – one of the oldest South African motor manufacturers – for changing my future and my life in many ways.

Many individuals expressed their opinions when this patent was presented on various occasions. I acknowledge with gratitude these contributions, especially from South African Rotating Machines Working Group specialists and academics, as well as the generous comments of many who have written and spoken to me. The number is so large that it would be inappropriate to name them all and the risk of omission would be great.

I would like to thank Mr Lino do Lago for his patience in changing drawings and specifications during a painful designing process, and Mr Kessary Mtunzi for his direct contribution in manufacturing prototypes.

Thanks to Mr Bruno Penzhorn, FEMCO Mining Director, who made the administrative arrangements, and facilitated orders and customer relationships.

I thank my wife Rodica and my daughter Alina who were a constant and active source of support throughout the endeavour.

Last but not least, I express my profound gratitude to Prof. Marius Kleingeld, Messrs Johann van Rensburg and Dieter Krueger, and Prof. Eddy Matthews from the Centre for Research and Continued Engineering Development, Pretoria, Faculty of Engineering, North-West University, who again spent many hours reading and correcting the text. Their friendship, valuable council and continued encouragement are greatly appreciated.

Pretoria, South Africa **C.D. PITIS**

2005/2006

Contents

Abstract ii
Acknowledgements iv
List of Abbreviations viii
List of Symbols ix
List of Figures xii
List of Photos xiii
List of Tables xv
CHAPTER 1: Introduction 1
1.1 The global concept of efficiency 1
1.2 South African industry evolution at the beginning of this millennium 1
1.3 Global approach towards efficiency 2
1.4 Example of efficiency in action 3
1.5 New specific trends in the electric motor industry 3
1.6 Designing and manufacturing "dedicated motors" for specific applications 5
1.7 Repairing (re-manufacturing) old motors to meet new specific requirements 5
1.8 Contribution of this research 6
1.9 Thesis overview 7
1.10 References 10
CHAPTER 2: Essentials of Application Engineering 12
2.1 Conversion process in electric motors 12
2.2 Squirrel cage electric motors in application engineering 13
2.3 Shortcomings of squirrel cage motors 15
2.4 Five essentials of application engineering 15
2.5 Matching the driven machine conditions (load) 16
2.6 Matching the power supply conditions 17
2.7 Matching environmental conditions and reliability indicators 17
2.8 Specific working conditions in South African coal mine industry 17
2.9 How rotor design changes motor characteristics 18
2.10 References 21
CHAPTER 3: General Overview of Squirrel Cage Rotors in Induction Motors 23
3.1 Particulars of this specific bibliographic research (overview) 23
3.2 General description of the squirrel cage rotor 25
3.3 Short description of the magnetic circuit of the rotor 26
3.4 Short description of electric circuit of the rotor 28
3.5 Slot profiles of squirrel cage rotors 29
3.6 Theoretical considerations regarding squirrel cage rotors 34
3.7 Single cage fabricated rotors (homogenous) 37
3.8 Double cage fabricated rotors 40

3.9 Skin-effect rotors 43
3.10 Idle-bar rotors 44
3.11 Die cast aluminium rotors 45
3.12 References 46
CHAPTER 4: Shortcomings of High Impedance Rotors on the Market 50
4.1 Basic conditions enforced on a high impedance rotor 50
4.2 Shortcomings of double cage rotors 51
4.3 Economical implications of double cage rotor failures 58
4.4 Shortcomings of aluminium die cast rotors 58
4.5 Manufacturing costs or outsourcing (imported rotor) cost of a dedicated die cast aluminium rotor 67
4.6 Estimations of economical implications of die cast aluminium rotor failures 69
4.7 General conclusions regarding economical losses 70
4.8 Common characteristics of "P" family of motors 70
CHAPTER 5: A Novel Solution: Mixed Conductivity Fabricated Rotor 73
5.1 Previous trials in replacing GAM and CM on VAMT machinery 73
5.2 Defining requirements for a new model of a specific type of rotor 77
5.3 Existing principles in building rotors 78
5.4 Summary of the invention aspects 79
5.5 Description of preferred versions of the patent 80
5.6 Mathematical expressions of flux density and current density variation in "deep bars" 81
5.7 The MCFR's operating principle 90
5.8 Mathematical equations of the MCFR1 model 91
5.9 References 93
CHAPTER 6: Design and Manufacturing Process of the MCFR 95
6.1 Basic conditions and inputs for new the design 95
6.2 Initial data required for the MCFR 97
6.3 Main steps in designing the MCFR 98
6.4 Main steps in re-designing an aluminium rotor 100
6.5 MCFR1 design for a new 36 kW spinner motor 102
6.6 Investigations on the MCFR after 1.8 years' continuous running underground 108
6.7 Advantages of the MCFR 111
6.8 References 112
CHAPTER 7: Experimental Results, Validation and Verification 114
7.1 Test conditions 115
7.2 Typical tests performed for SABS approval 116
7.3 Declared nameplate rated values 123
7.4 Comparison of performance to products on the market 123
7.5 Special tests performed in DOL starting conditions 124
7.6 Thermal assessment of the MCFR 128

7.7 Technical and economical assessments during validation and verification activity.. 132
7.8 References 133
CHAPTER 8: Conclusions and Recommendations 135
8.1 Conclusions 135
8.2 Recommendations 137
Annexure 1.1: MCFR Patent Forms 138
Annexure 4.1: Typical Continuous Miner 141
Annexure 4.2: Design Limits of Double Cage Rotors 142
Annexure 4.3: Quotation of a New Die Cast Aluminium Rotor 145
Annexure 5.1: MCFR Presentation to the South African Rotating Machines Working Group 146
Annexure 6.1: MCFR Enquiries 148
Annexure 6.2: Design Iterations 150
Annexure 7.1: MCFR1 Design for the 36 kW Spinner Motor 152

List of Abbreviations

A Tq	Acceleration Torque
DME	Direction of Minerals and Energy
DOL	Direct-on-line (starting motor by direct connection to power supply)
EEM	Energy efficiency motors
e.m.f.	Electromotive force
FLCrt	Full-load current
FLTq	Full-load torque
HV	High voltage
IACS	International Annealed Copper Standard
IEC	International Electro-technical Commission
LTC	Load Torque Curve (counter-torque) Tl = φ (N)
m.m.f.	Magnetomotive force
MCFR	Mixed Conductivity Fabricated Rotor
MV	Medium voltage
NEMA	National Electrical Manufacturers Association, USA
No	Speed of stator magnetic field (synchronous speed) [r/m]
Nr	Rotor speed [r/m]
Npu	Rotor speed corresponding to Pull up torque (PUT)
Nb	Rotor speed corresponding to Pull out torque (POT)
Nnom	Motor (rotor) full load (rated) speed [r/m]
Ns	Synchronous speed
OD	Outside diameter
POT	Pull-out torque or breakdown torque
PUT	Pull-up torque (saddle torque)
SABS	South African Bureau of Standards
SANS	South African National Standard
spp	Slots per pole per phase
Sq.CEM	Squirrel cage electric motor
Sq.CR	Squirrel cage rotor
STC	Speed-torque curve of a motor Tm = f(N)
St.Tq.	Starting torque or Breakaway torque
TOC	Total ownership costs
Tl	Load torque (counter-torque)
Tm	Motor torque
Tq	Torque
VAMT	Voest Alpine Mining and Tunnelling, GmbH, Austria

List of Symbols

Capitals

A	cross-section	[m2]
B	flux density	[Tesla]
C	degrees Celsius	[°C]
D	stator bore diameter	[m]
E	e.m.f.	[Volt]
F	magnetomotive force	[Newton]
G	output coefficient	[kW / (m3 x r/m)]
G	weight	[kg]
H	inertia constant	
I	current	[A]
J	current density	[A/mm2]
K	constant or factor	
L	core length	[m]
L	inductance	[Henry]
L	length or distance dimension	[m]
M	mutual inductance	[Henry]
M	torque	[Newton-meter]
N	rotational speed	[r/m]
No	synchronous speed	[r/m]
N	number of phases or rings	
P	active power	[kW]
Q	reactive power	[kilo Volts-Ampere]
R	radius	[m]
R	resistance	[Ohm]]
R	reluctance	[A.turns / Wb]
S	number of slots	
S	rating apparent power	[kVA]
S	slip = [No – N_r]/No	
T	absolute temperature	[°K]
T	number of turns	
V	voltage	[V]
W	width	[m]
X	reactance	[Ohm]
Z	impedance	[Ohm]
Z	number of conductors	

Small letters

a	cross-section
c	conductivity
d	slot (bar) depth
d	diameter
d	diameter of copper wire
e	e.m.f.
f	factor, function
f	frequency
h	height or depth
i	current
j	complex operator $\sqrt{(-1)}$, or + 90° rotation operator
k	constant
l	length
m	mass
n	harmonic number
n	integer
n	speed [rotation per second]
no	synchronous speed
p	number of pole-pairs
2p	number of poles
p	operator d/dt
r	radius
r	ratio
r	resistance
r'	equivalent resistance
s	slip
t	time
u	velocity or peripheral speed
v	voltage
w	width or dimension
x	fraction, multiplier
x	reactance
x'	equivalent reactance
x	unknown
y	unknown

Greek letters

α	Angle
	= r2/x2
β	angle
	phase coefficient
δ	current-density
ε	base of natural logarithms
	eccentricity
	permeability
η	efficiency
λ	permeance coefficient
	wavelength
μr	relative permitivity
Φ	magnetic flux
φ	component flux
Ψ	total flux
ψ	angle between coil e.m.f.s (electric)
Λ	permeance [Wb / A. turns]
μ	absolute permitivity
μo	magnetic space constant = 4Π / (10exp.7)
ll	productivity
ρ	resistivity
ρi	thermal resistivity of insulation
θ	angle
	arctang (x/r)
	arcos (r/z)
	temperature rise
τ	time constant
ω	angular frequency = 2Π f
ωr	angular velocity

List of Figures

Figure 1.1 TOC structure of an induction motor driving a particular mining process....2
Figure 1.2 Evolution of specific costs indicators function of the process speed "v"....3
Figure 2.1 Typical example of a speed-torque curve (STC) of an induction motor....13
Figure 2.2 Five essentials of application engineering when choosing an electric motor....16
Figure 2.3 Typical STC for a motor with a letter "A" NEMA Class design....19
Figure 2.4 Typical STC for a motor with a letter "B" NEMA Class design....20
Figure 2.5 Typical STC for a motor with a letter "C" NEMA Class design....20
Figure 2.6 Typical STC for a motor with a letter "D" NEMA Class design....20
Figure 3.1 A typical assembly drawing of a double cage rotor....25
Figure 3.2 Typical manufacturing drawing of a double cage rotor lamination....27
Figure 3.3 Typical short-circuit test characteristic graph (Ik = f(Uk) in p.u.) lot tips....30
Figure 3.4 Rotor slot profiles used for electromagnetic design purposes....31
Figure 3.5 Typical rotor slots used for fabricated rotors (prefabricated rotor bars)....32
Figure 3.6 Typical rotor slots used for die cast aluminium rotors....32
Figure 3.7 Theoretical torque-slip relation....36
Figure 3.8 Partial cross-section of single cage fabricated rotor....37
Figure 3.9 Partial cross-section of a double cage fabricated rotor....40
Figure 3.10 Schematic diagram of a torque-slip (STC) curve for a double cage motor....42
Figure 3.11 Cross-section of a Wall's composite rotor conductor....43
Figure 3.12 Cross-section of an idle-bar rotor slot....44
Figure 4.1 Simulating rotor load thermal conditions in order to detect a local thermal vector....63
Figure 4.2 Sketch of heat flux transferred unevenly from the rotor to the shaft and to the winding...64
Figure 5.1 Speed-Torque curves of 36 kW, fitted with an aluminium and a copper rotor....75
Figure 5.2 Illustration to classic principle no. 1 of the rotor construction....78
Figure 5.3 Illustration to classic principle no. 2 of the rotor construction....78
Figure 5.4 Schematic diagram of one of the simplest versions of the MCFR1....81
Figure 5.5 Cross-section of a deep bar linked by a leakage flux....82
Figure 5.6 Phasor diagram of the mutual flux and induced voltage....83
Figure 5.7 MCFR1 reactance and resistance ratio evolution during motor starting....89
Figure 6.1 Initial cast aluminium and fabricated bar rotor slot profiles....101
Figure 6.2 Stator lamination design for 36 kW spinner motor....103
Figure 6.3 Design of the rotor lamination for a 36 kW spinner motor fitted with the MCFR1....103
Figure 6.4 Manufacturing instructions for the electric circuit of the MCFR1....105
Figure 6.5 Assembly drawing of the MCFR1....107
Figure 7.1 Functional block diagram of the testing bay....115
Figure 7.2 3D picture of a spinner motor used for confirmation of MCFR1 performances....116
Figure 7.3 Oscillogram of DOL starting current for a 36 kW fitted with MCFR....125
Figure 7.4 Speed-torque curve of the 36 kW prototype....128

List of Photos

Photo 3.1 Rotor bars separation from the short-circuit ring....26
Photo 3.2 Magnetic steel laminations stacked in a rotor core....27
Photo 3.3 Manufactured copper rotors....28
Photo 3.4 Cast aluminium squirrel cage profiles....28
Photo 3.5 A "broken bars" situation on a "T" bar profile....39
Photo 3.6 Cutting the top corners of the end of the bars to prevent dangerous vibrations....39
Photo 3.7 Typical double cage rotor....41
Photo 3.8 Example of a "skin effect" rotor....43
Photo 3.9 Cross-section of a die cast aluminium rotor....46
Photo 4.1 Prolonged and heavy operational thermal stresses on a double cage rotor....52
Photo 4.2 End-stopper separation on a double cage rotor....53
Photo 4.3 Thermal stress is present on the starting cage bars as the first phase of deterioration....53
Photo 4.4.Electrolytic activities around the brazed joints....54
Photo 4.5 Erosion of starting cage bars is present in the region of brazed joints....54
Photo 4.6 Starting cage distortions occurred as a result of motor rapid re-closures....55
Photo 4.7 Starting cage regarded as a "weak point" in a double cage rotor....56
Photo 4.8 Double cage rotors are not suitable for specific South African conditions....56
Photo 4.9 "Hot spots" with temperatures reaching melting point of the brass bars....57
Photo 4.10 Brass bars of a starting cage in a "broken bar" situation....57
Photo 4.11 Casting voids on a short-circuit ring of an MV die cast rotor....59
Photo 4.12 Interbars "short-circuits" on an aluminium cast rotor....60
Photo 4.13 "Partial rotor broken bars" on a short-circuit ring of a die cast aluminium rotor....61
Photo 4.14 Short-circuit ring expelled from the rotor body causing a rotor broken bar situation....62
Photo 4.15 A "rotor broken bar" situation as a result of rotor rubbing against the stator bore....62
Photo 4.16 Incipient rotor failure as the aluminium tends to leak from the slots....63
Photo 4.17 "Bow" rotor on a die cast aluminium....63
Photo 4.18 Collateral damage of an aluminium rotor rubbing against the stator bore....65
Photo 4.19 Degradation of the electric circuit of the die cast aluminium rotor....66
Photo 4.20 Corrosion of rotor electric circuit cast material....66
Photo 5.1 Brass rotor specially manufactured for the VAMT 36 kW spinner motor....76
Photo 6.1 Rotor manufactured by Loher (Flender), Germany....96
Photo 6.2 Rotor manufactured by DAMEL, Poland....96
Photo 6.3 Rotor manufactured by Luck & King, RSA....97
Photo 6.4 Rotor iron core pack build-up on the shaft for the MCFR1, 36 kW spinner motor....104
Photo 6.5 Sequence of different bar conductivities fitted in an MCFR1....106
Photo 6.6 The MCFR1 fitted with a unique short-circuit ring....107
Photo 6.7 MCFR1 manufactured with two pairs of short-circuit rings....108
Photo 6.8 A spinner motor fitted with an MCFR returned after 1,8 years running underground....108

Photo 6.9 The MCFR1 after 1.8 years of running underground 109
Photo 6.10 Water ingress into the motor during storage 110
Photo 6.11 The stator was rusted due to water in the motor enclosure 111
Photo 7.1 The MCFR iron core in excellent condition after running on load for 1.8 years 131

List of Tables

Table 2.1 Comparison performances of motors according to NEMA Design A, B, C and D 21
Table 3.1 Rotor slots properties, application and use in conjunction with bars 33
Table 3.2 Double cage reactance and resistance variation during starting and running of the motor 41
Table 4.1 Financial losses estimation for a specific motor fitted with double cage rotor 58
Table 4.2 Price structure for a 36 kW imported die cast aluminium rotor 68
Table 4.3 Financial losses estimation for a specific motor fitted with die cast aluminium rotor 69
Table 4.4 Identification of VAMT motors "weak points" 71
Table 5.1 Conditions imposed on a new rotor replacing die cast imported aluminium rotors 77
Table 6.1 Initial estimations of $C_{av.b}$ used in new design situations 98
Table 7.1 Comparison of performances of various spinner motors 124
Table 7.2 Comparison of windings temperature rise 129
Table 7.3 Comparison of the temperature rise of bearings 129
Table 7.4 Rotor temperature rise and DOL starts 130
Table 7.5 Estimations of rotor and motor life span 131
Table 7.6 Comparison of specific technical and economical performances 132
Table 7.7 Predicted events on 36 kW spinner motors for a projected 15-year period 132
Table 7.8 Comparison of economical indicators and savings obtained per 36 kW spinner motor 133
Table 8.1 Comparison of economical indicators and savings obtained per 36 kW spinner motor (15-year projection) 136

CHAPTER 1: INTRODUCTION

This thesis forms part of the South African movement towards the global concept of efficiency. Some features of the global approach towards efficiency are highlighted. A particular example of application engineering in mining industry reveals hidden economical implications.

Contributions of this research and invention have formed part of new trends in electric motor manufacturing and the repairing industry.

1.1 The global concept of efficiency

This millennium is marked by a new trend: **EFFICIENCY**.

The new monetary policy promoted by the South African Reserve Bank together with the energy and materials crisis in the world has had a huge impact on the South African industry by introducing the new concept of efficiency at all horizontal and vertical levels (technical, economical, financial, etc.).

The efficiency concept is present at all levels of industrial activity. This concept is actually driven by "**energy efficiency**" concept as mentioned in the Intergovernmental Panel on Climate Change [1], and specifically re-defined by the Federal Energy Management Plan [2].

The Johannesburg World Summit on Sustainable Development concluded that changing unsustainable patterns of energy use is a key area for global action to ensure the survival of our planet.

Numerous international scientific conferences [3], [4], [5], [6], [7] stressed that energy efficiency improvements in various industrial processes, residential appliances, heating equipment, and lighting can play a key role in assuring a sustainable energy future and socio-economic development, and at the same time mitigate climate change.

1.2 South African industry evolution at the beginning of this millennium

South Africa's real growth rate in value-added manufacturing in the mining industry was 1.4% for the period between 1997 and 2002. This figure compares poorly to the average rate of 3.9% for developing countries and the average of 5.8% for "transitional economies" [8]. In 2005 the Department of Trade and Industry (DTI) revealed that employment in the industry was falling at an average of 8.4% a year.

"The declining share of manufacturing is perhaps the best evidence that the business-economics environment for manufacturing is poor versus the competitors", says Roger Baxter, Chief economist of Chamber of Mines in an interview with Mining Weekly [9].

A potential spanner in the beneficiation wheel is the declining contribution of manufacturing to the GDP in South Africa.

One of the explanations can be the misunderstanding of the global efficiency concept. To date, there are not any specific references on this subject. However, focusing on South Africa, a short discussion is necessary.

1.3 Global approach towards efficiency

The global approach towards the efficiency concept rejects the excessive profit taken from a specific business. In the author's opinion this concept must also incorporate the following:

- Process efficiency control
- Planning and prediction based on the "critical path" method
- An energy efficiency policy (currently in use)
- Logistics efficiency
- Planning regarding total ownership costs (TOC)
- Co-operation of Unions and employees with management
- Encouraging indigenous participation in the process (R&D, products, software)

Figure 1.1 illustrates a particular TOC structure as a component of the concept of global efficiency.

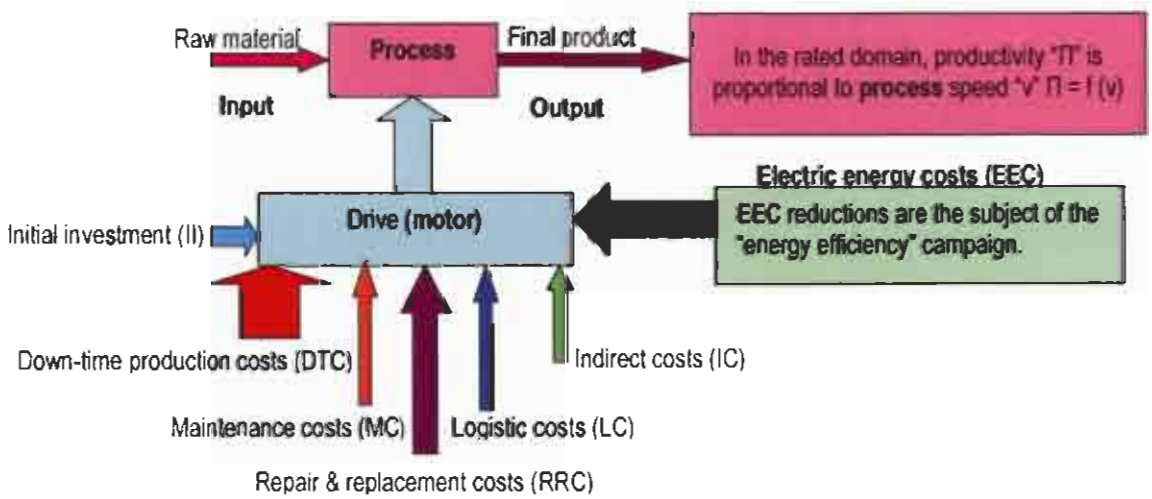

Figure 1.1 TOC structure of an induction motor driving a particular mining process

This thesis does not intend to develop this complex subject, but some interesting directions may be investigated.

1.4 Example of efficiency in action

In the actual economical environment, business sustainability requires high-efficiency technological processes. In the case of a specific mining house, overseas mining equipment was considered suitable for technological processes in South African mines. In order to maximize productivity, performances of continuous miners were increased by 200% to 300% (rated monthly). This "improved efficiency" obtained by increasing the speed of the process contradicted the concept of global efficiency.

After a while, it became obvious that overseas-designed electric motors that were used to power imported mining machinery were not satisfying the harsh South African requirements. In this situation the essentials of application engineering were not taken into account when the technical solution was assessed. The results became obvious: high financial losses.

Figure 1.2 shows specific costs indicators variation function of the process speed "v".

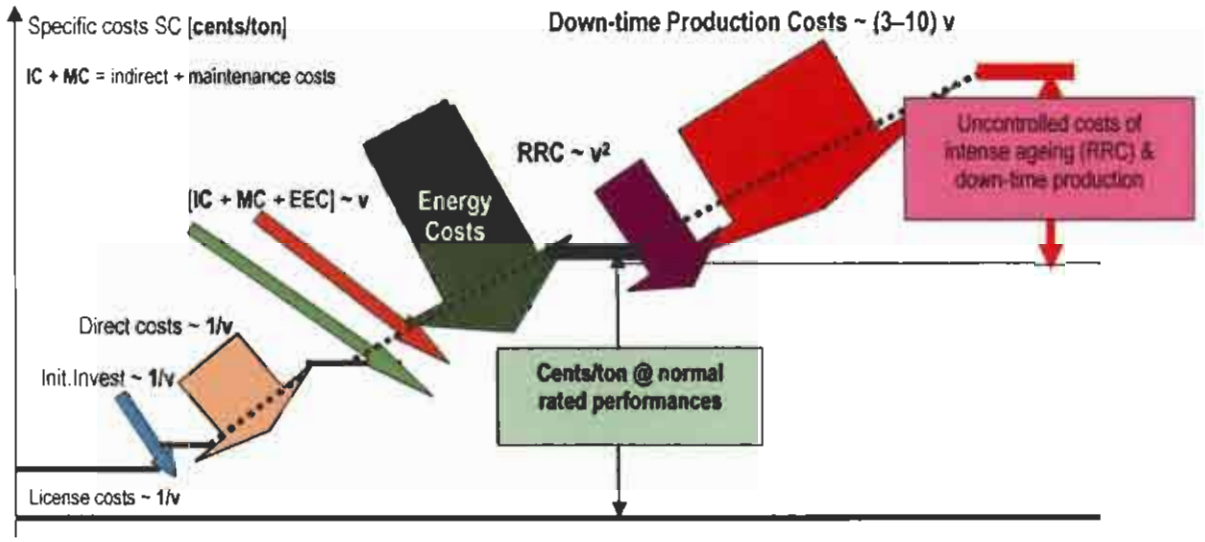

Figure 1.2 Evolution of specific costs indicators function of the process speed "**v**"

According to the efficiency rule, design, concepts and technical requirements, including drives and equipment, are becoming more specific. As a result, the performance requirements of electric motors are becoming more detailed too.

Increasing efficiency of technological processes thus requires so-called "dedicated motors" for specific drives!

1.5 New specific trends in the electric motor industry

During the last decade some new trends have appeared on the market for motor manufacturers, repairers and end users:

- According to new regulations in USA [10], [11] and Europe [12], energy efficiency motors (EEM) are currently replacing standard motors (available at reduced prices in South Africa).
- Low cost standard motors produced in "mass production" have restricted access to high efficiency drives as a result of restrictive regulations and customer requirements.
- For specific applications even EEM cannot always compete with so-called "dedicated motors".
- Besides high efficiency, the generation of new-dedicated electric motors requires basic conditions ignored before (see also paragraph 1.6).
- Increased efficiency of processes is reflected in the escalation of customers' more specific requirements in the motor range from low to medium and high voltage (high power) [13].
- The market is offering technical solutions of "dedicated motors", but at higher prices [14].
- The demand for "dedicated motors" does not always justify a "mass production" level.
- Business sustainability conditions impose financial constraints on motor manufacturers, repairers and end-users during the re-capitalisation process. This process is a characteristic of the actual South African economic and industrial environment [15].

The targets prescribed by the South African Department of Minerals and Energy (DME) in the last decade [16], [17], [18] indicate that new efficiency concepts are now breaking the old rules that dictate, "As long the initial investment cost is cheap, it is good enough."

The South African electric motors market industry is still divided into two distinct tiers [19]:

- Discerning motor market
- Non-discerning motor market

Both segments have a place in the electric motor market.

The "non-discerning market" is price driven and the initial cost is usually the chief driver of the purchasing decision. This market segment is not specification driven and its focus is not on total cost of ownership (TOC).

The "discerning market" has made great strides in raising the bar in terms of motor specifications. Terms like "high efficiency", "class H insulation", "vacuum impregnation", "reliability", "TOC", "class B temperature rise" and "increased degree of protection" are frequently mentioned and often specified.

The impact of the energy efficiency concept on the South African industry is already present in the detailed specifications of electric motor performance requirements [20].

This market segment has been responsible for driving continuous product development.

As a result, new trends are present in the South African electric motor industry [21], [22].

- Designing and manufacturing new "dedicated motors" according to specific processes
- Repairing (re-manufacturing) old motors to meet new specific requirements of the drives

1.6 Designing and manufacturing "dedicated motors" for specific applications

The new trend in designing and manufacturing "dedicated motors" for specific applications has to accept basic challenges that were ignored before:

- Higher reliability of motor and components
- Extended warranty period and life expectancy
- Easy maintenance and repair
- Easy re-manufacturing of components
- Lower total ownership costs (TOC) of the motor
- Motor and components available on the market at competitive prices

The proposed MCFR is part of a new trend of designing and manufacturing dedicated motors and may contribute to some general impacts on the South African economy [23]:

- Improving technical and economical performances in mining activities by reducing ageing process and down-time production losses
- Increasing life expectancy of specific dedicated motors and reducing TOC
- Increasing competitiveness of South African products to international standards
- Creating new job opportunities as promoting new technology
- Promoting Reserve Bank policy by reducing the import costs
- Developing possibilities of exporting know-how technologies
- Defusing the incipient energy crisis in the country

New trends in designing and manufacturing dedicated motors for specific applications are related to application engineering, the interdependence being presented in Chapter 2.

1.7 Repairing (re-manufacturing) old motors to meet new specific requirements

A specific characteristic of our country is that a very large variety of electric motors are running in the country's industry, providing little satisfaction when referring to TOC.

As a result, in the South African industrial environment about 20 to 25% of the repaired squirrel cage motors need rotor replacement.

For old motors with cast aluminium rotors this becomes a "writing-off" problem, especially when manufacturers ceased the production of rotors (aluminium cast rotors cannot be repaired) [24].

By discarding motors, investment expenses related to the **re-capitalisation process** may reach unacceptable values. Typical situations experienced frequently are presented below.

- Damaged aluminium cast rotors cannot be repaired.
- Aluminium cast rotors replacement is economically prohibitive when production of these specific rotors was ceased.
- A motor's application becomes redundant and it cannot be used for other applications because of its very specific performances.
- Dedicating motors to specific applications always requires restrictive performances when rotors have to be replaced.

1.8 Contribution of this research

The thesis presents a new type of rotor known as a "Mixed Conductivity Fabricated Rotor" (MCFR). This invention holds patent since 2004.

It is regarded as an original contribution towards the design and manufacturing of "dedicated motors" with reference to low voltage motors, used especially in mining activities.

Although less spectacular than giant high-voltage motors, low-voltage motors' total power ranges from 60 to 68% of the total motor's power. For example, in 1994, it was estimated that the summated ratings of the 20 million motors in the UK approached 100 GW, made up largely (65 %) of induction motors rated below 150 kW and of an average rating less than 5 kW [25].

The thesis offers alternative methods to the market demand according to new specific trends existing in the low-voltage electric motor industry.

The proposed MCFR can be designed and manufactured at a competitive price, regardless of the production volume and can be used to repair old motors according to specific requirements, especially when squirrel cage rotors have to be replaced.

By using the MCFR, the motor speed-torque curve (STC) can be adjusted to drive requirements, being a useful tool for application engineering in choosing the right performances of squirrel cage motors.

At least two major advantages in promoting this patent as an alternative method in adjusting the motor performances must be highlighted:

1. For the new motors, the patent offers an alternative method of designing and manufacturing new "dedicated motors" by using the MCFR with adjustable performances according to drive requirements.
2. For old motors, the patent offers an alternative method of replacing damaged or obsolete rotors by using the MCFR to give old motors a new life extension.

This proposed technical solution has proven to have some relevant advantages related to the manufacturing process, costs and reliability.

- Design and manufacturing of new custom-made motors and squirrel cage rotors at competitive prices to suit specific application requirements.
- The MCFR offers a useful tool in application engineering.
- The MCFR with high-reliability indicators can be manufactured at competitive prices, regardless of the production volume (for new or repaired electric motors).
- Increased rotor reliability indicator extends the entire electric motor life span.
- The MCFR prevents an early re-capitalisation process.
- It reduces the total ownership costs of squirrel cage motors.

For these reasons, the patent has been considered a real contribution towards the global efficiency concept.

The proposed method of manufacturing MCFRs has been registered as a National South African patent [26], [27] (see also Annexure 1.1).

Since priority claimed in 2004, the patent has been manufactured, tested, verified and validated by various tests and site measurements.

1.9 Thesis overview

The essentials of applications engineering are necessary as an input, emphasising how rotor design can change motor characteristics. The most significant design variable of the motors is the effective resistance of the rotor cage circuits.

Chapter 3 presents a comprehensive description of the squirrel cage rotor and its circuits and components. This is essential in understanding this complex part of an induction motor. Various slot profiles with all related properties are discussed. Presentation of various types of high-impedance rotors, focusing on double cage and die cast aluminium rotors, completes the bibliographic research.

Chapter 4 presents shortcomings of high-impedance rotors on the market. Photos support the original descriptions of failure mechanisms, including the rubbing process.

General conclusions regarding economical losses on high-impedance rotors with reference to South African operational conditions represent the author's contribution to establish a unitary approach in various activities related to mining activities. The need for another type of rotor becomes obvious.

Specific South African conditions in designing dedicated electric motors and identification of the "weak points" for a unitary motor model were the base lines in designing the "P" family of motors.

***Note 1.1**: "Weak points" of complex equipment were the components with highest failure intensity indicator (λ) and major weight in increasing value of motor failure intensity λ **motor**.*

In this "P" family, the MCFR represents one of the major solutions to improving the efficiency of the mining processes with all other consequences already presented above.

Chapter 5 starts with a short story of a specific motor conversion revealing the need for a Mixed Conductivity Fabricated Rotor. Specific die cast aluminium rotors, currently used by a reputable mining house, generate annually replacement costs in the range of R5 million. Losses related to downtime production and repair activities are not included.

The invention principle is totally different than that currently on the market and no references and similar manufactured types could be found. Specialists and academics attending various presentations of the invention, acknowledged the novelty of the invention principle.

A summary of the invention aspects and a description of the preferred embodiments of the patent are provided for two main types: MCFR1 and MCFR2. This is followed by a description of the basic manufacturing process, operating principles and relevant advantages of the patent.

Chapter 6 provides a theoretical background justifying why the "deep-bar effect" of various bar profiles and sizes was chosen for the MCFR design. The author presents main steps in designing the MCFR1 for new motors and re-designing an aluminium rotor to become an MCFR. A complete design of the MCFR1 is described with drawings and photos of different stages of the manufacturing process.

Investigations into the MCFR1's condition after 1.8 years' continuous running underground are presented as part of the validation and verification activities. It was confirmed that, as a novel rotor solution, the MCFR has a sound design representing a reliable long-term solution.

Savings obtained by using a specific MCFR1 on a 36 kW spinner motor were estimated at R150 000 per year, per motor. There are 4 motors of 36 kW on a continuous miner machine, while the number of VAMT continuous miners operating in the world total to about 5 550 units. The reader can make his own calculations in order to obtain a global economical picture.

Chapter 7 details typical tests performed according to SABS regulations to obtain product approval.

The dynamic response of the rotor during starting conditions was obtained as a result of special transient tests. Main parameters of the MCFR1 have been assessed confirming the design and new principle of invention:

- Assessment of inrush current and modulation of starting current waveform.
- Assessment on possible dips on transient speed-torque curve.
- Assessment on breakdown (pullout) and pull up torque
- Surge factor estimation
- Presence of harmonic induction torques and harmonic synchronous torques

It was confirmed that the MCFR offers reliable torques with no major parasitic torques during the start-up sequence. No parasitic harmonics are present during the steady state or transient state.

Thermal assessment of the MCFR was another direction of investigating:

- Heat radiation in a radial direction towards stator winding
- Heat transmission in axial directions towards bearings
- Rotor temperature rise on load and per start (in DOL starts from COLD and HOT conditions)
- Investigation of the presence of local thermal vectors on the rotor iron core

These tests enabled favourable comparison of the product's performance to that of similar products on the market.

The MCFR life span was estimated to be net superior to that of existing rotors on the market. On-site validation and verification confirmed the life span estimation and project soundness.

The patent offers a large variety of technical and economical advantages, which increase the mining processes' efficiency beyond expectations.

The thesis emphasises the MCFR's design adaptability, i.e. the rotor design can be altered to meet the demands of a specific engineering application.

As a fabricated rotor, the MCFR patent has higher reliability indicators compared to existent high impedance rotors.

The performance stability, including the fact that the rotor can keep the starting torque value very constant even after the motor has reached its thermal stabilised condition known as "hot conditions", represents one of the salient performances of this invention.

Being materialised in a set of special rotors powering continuous miners of a reputable coal-mining house, the MCFR patent represents a breakthrough regarding large manufacturers' monopoly in deciding market prices. It will enable medium-sized organisations to become rotor and motor manufacturers. Establishing sound competition will offer an alternative option to the market.

The patent is part of the new South African trend of increasing the efficiency of processes. It offers the possibility of designing dedicated motors with a positive impact on the South African economy. Some socio-economical advantages are worthy of considerable study:

- Being locally manufactured, the MCFR may reduce the country's economical dependence.
- Requiring no special manufacturing expertise, the MCFR can be produced in any quantity and size without excessive investment.
- The MCFR offers an alternative option (product interchangeability) on the market and sound competition (with export prospective).

- The patent ensures business sustainability conditions diffusing financial constraints on motor manufacturers and end-users during the re-capitalisation process (very significant in South African economic and industrial environment).

The patent and calculations presented in this thesis set up some base lines for some further research regarding squirrel cage electric motors.

1.10 References

1. IPCC (Intergovernmental Panel on Climate Change); "Revised 1996 guidelines for national greenhouse gas inventories", Organization for Economic Co-operation and Development, Paris, 1996.
2. Department of Energy Federal Register; "Federal Energy Management Plan – FEMP", USA, New York, March 2004.
3. EEDAL; "International Conference on Energy Efficiency in Domestic Appliances and Lighting", Florence, 1997.
4. EEDAL, Ibidem, Naples, 2000.
5. EEDAL, Ibidem, Turin, 2003.
6. ICUE/DUE; "1st ICUE International Conference of Industrial & Commercial Use of Energy", Cape Town, May 2004.
7. ICUE/DUE; "2nd ICUE International Conference of Industrial & Commercial Use of Energy", Cape Town, May 2005.
8. Department of Trade and Industry; "Gold in South Africa" Annual Report of Industrial Development Corporation, New York, 2002.
9. Creamer, M.; "Golden Sunset in South Africa", Mining Weekly, Feb. 17–23, 2006, pp10–11.
10. Department of Energy Federal Register; "Energy Policy and Conservation Act EPACT", Public Law 102 – 486/1992, USA, 1992.
11. NEMA – MG1, Motors and Generators; "Table 12–10: Electric Motors Efficiencies", USA, 1998.
12. European Committee of Manufacturers of Electric Machines and Power Electronics; "Energy Efficiency Electric Machines", CEMEP, EU, Paris, 2000.
13. Anglo Gold Ashanti; "Medium and High Voltage (3300, 6600 &11000 Volts) Squirrel Cage and Wound Rotors Induction Motors", 438/11 Specification, Johannesburg, 1998.
14. Pitis, C.D.; "Power Efficiency becoming Important in Electric Motors", Materials Handling & Logistics TODAY, Johannesburg, Sept. 2003, pp 35–36.
15. Pitis, C.D.; "New trends in electric motor industry", Engineering News, Johannesburg, May 31–June 6, 2002, p 42.
16. Department of Minerals and Energy; "White paper in Energy Policy", Pretoria, 1998.

17. Department of Minerals and Energy; "Energy efficiency in South Africa", AMEU, Pretoria, 2005.
18. Legodi, M. and Tshikalanke, P.; "Using Energy Efficiency to Maximize Energy Savings in South Africa", AMEU, 59th Convention, Polokwane, 2005.
19. Teixeira, A.; "High Efficiency Low Voltage Motors", Electricity + Control, Johannesburg, July 2005, pp 44–45.
20. Chrissoulis, C.; "Current trends in rotating machines ownership in South Africa", (ZEST Electric Motors), Electricity + Control, August 2004, pp 45–48.
21. SASOL Technology Pty.; "Induction and Synchronous Motors", Specification SP-46-11, Revision 3, SASTECH Engineering Division, March 1999.
22. Anglo Americans Technical Service; "Electrical Induction Motors: Medium Voltage (3300 V to 11000 V) Three phase Motors", AATS. Spec. 538/011, Issue 3, Johannesburg, Oct. 2002.
23. Pitis, C.D., Livingstone, A.; "Energy efficient fans in underground auxiliary ventilation systems", Proceedings, 1st ICUE International Conference of Industrial & Commercial Use of Energy, Cape Town, May 2004, pp 103–106.
24. Pitis, C.D.; "Electric Motors Life Extension by Renewal of Squirrel Cage Rotors", Proceedings, 2nd ICUE International Conference of Industrial & Commercial Use of Energy, Cape Town, May 2005, pp 87–93.
25. Say, M.G; "Alternating Current Machines", Chapter 12, 5th Edition, Longman Scientific & Technical Singapore Publishers Ltd, 1995.
26. Pitis C.D.; Provisional patent registered as "Mixed Conductivity Fabricated Rotors – MCFR" patent registration no. 6886, Spoor and Fisher, Johannesburg, August 2004.
27. Pitis, C.D.; "Mixed Conductivity Fabricated Rotor", South African Patent No. 2005/07280, Johannesburg, September 2005.

CHAPTER 2: ESSENTIALS OF APPLICATION ENGINEERING

It is obvious that overseas-designed electric motors powering mining machinery are not satisfying harsh South African requirements.

The problem can be addressed by understanding the essentials of application engineering with reference to the special conditions imposed by the South African mining industry.

The invention is actually a solution to specific application engineering problems in South Africa. In application engineering consideration must be given to the motor design, the electrical supply, the attached mechanical load, and the environment within which the motor operates. The most significant design variable in squirrel cage motors is the effective resistance of the rotor cage circuits. This is the area on which the invention actually focuses.

2.1 Conversion process in electric motors

Drives always require mechanical power. There are very diverse industrial needs.

Squirrel cage induction motors (Sq CEM), as induction machines, convert electric power into mechanical power with the ideal being simplicity and reliability.

The induction machine is the most rugged and the most widely used machine in the industry. One simply couples the motor to the load shaft, connects the three motor leads to the terminals of a 3-phase power supply and closes the switch.

- At this moment the applied voltage "**U**" drives an input current "**+I**" against "**Er**" (counter e.m.f.) to give an electric input power **Pe = U . (+I).**
- The part "**I Er**" is converted from the electric input **Pe.**
- The conversion process means the development of an electromagnetic torque **Me** which drives the motor against the mechanical input torque **Mm** at the speed **Ωm** to produce the negative mechanical input **Pm = (- Mm) Ωm,** corresponding in effect to a positive mechanical output **Pm.**

But the motor doesn't always come to speed or run efficiently. The reason for this is that too often an application design is left unfinished. The application design as such receives careful attention while the electric motor to power the application is largely left to chance.

Typically, the designer's only guidance when selecting a motor, "Be sure to get one large enough!" To be on the safe side, the motor is thus oversized, with all the consequences related

to the initial investment capital and cost of the electricity bill, unless the non-discerning market is price driven and the initial cost is usually the chief driver of the purchasing decision.

On the other hand, the most dangerous situation occurs when the motor does not match specific load requirements. A motor never operates in isolation!

To eliminate the guesswork involved in motor selection, the following is necessary:

- Understanding of the motor Speed-Torque Curve (STC) and
- How electric motors react to changes in load demand, power supply, environment, etc.

To meet the various starting and running requirements of a variety of industrial applications, several standards designs of squirrel cage motors are available on the market.

The proper application of electrical motors requires some fundamental application engineering knowledge, a suspicious mind, and a lot of common sense.

2.2 Squirrel cage electric motors in application engineering

The principal characteristic of an electric motor is the Speed-Torque Curve (STC) [1]. Used in application engineering, the STC is basically a motor's fingerprint.

The speed-torque characteristics of the most common designs are standardised in accordance with various criteria.

A typical example of STC is shown in figure 2.1.

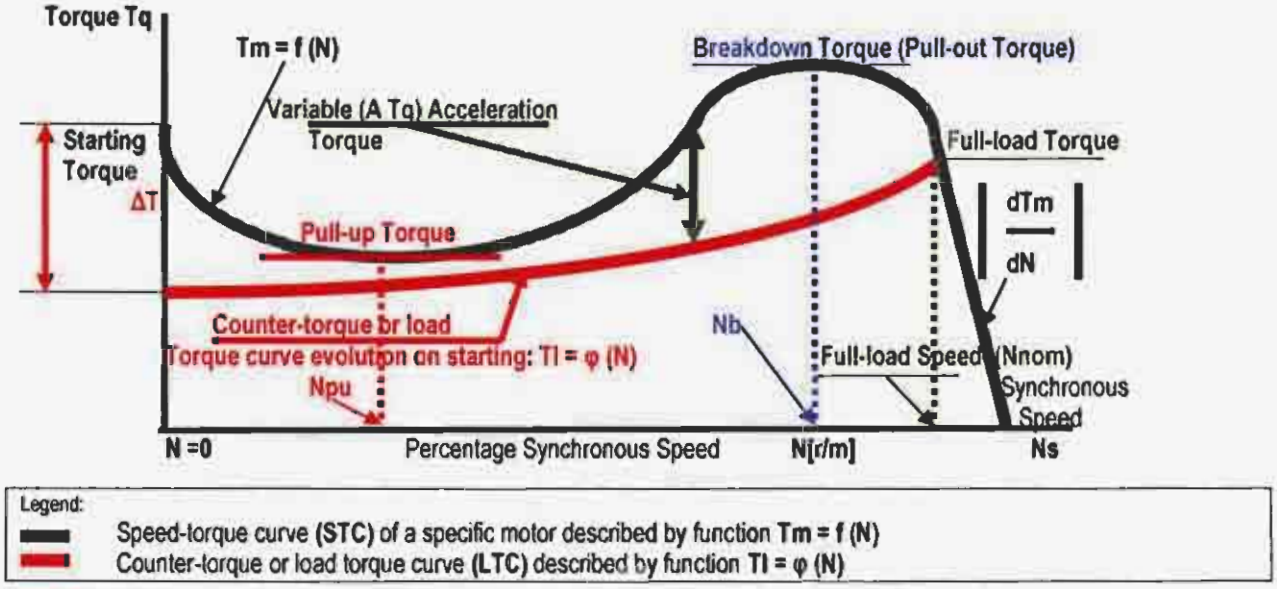

Figure 2.1 Typical example of a speed-torque curve (STC) of an induction motor

STC has four characteristics that describe motor operation:

1. **Starting torque (St.Tq)** is the amount of torque it takes to start the machine rotating from its position of rest – the torque needed to break it away which is also called the ***breakaway torque***. The difference **ΔT>0** between motor starting torque and load breakaway torque ensures starting of the application.
2. **Pull-up torque (PUT)** is the lowest torque developed by the motor between ZERO speed and the speed, which corresponds to the breakdown torque or pull-out torque (**Nb**).
3. **Breakdown torque** or **pull-out torque (POT)** is the maximum torque developed by the motor during that period of acceleration between the speed corresponding to pull-up torque (**Npu**) and the full load speed (**Nnom**).
4. **Full-load torque (FLTq)** is the operating torque, the torque developed at full-load speed (**Nnom**) to produce the nameplate output power of the motor.

Counter-torque or load torque curve **(LTC)** characterises the load torque evolution of the application.

In application engineering, the STC must always correlate with the LTC.

The difference between the STC and LTC gives the so-called "**Acceleration Torque**" (A Tq). Acceleration torque value is variable at all speed functions of applications and motor characteristics.

$$\textbf{A Tq} = \text{Motor Torque} - \text{Load Torque} = \textbf{Tm - Tl} \qquad (2.1)$$

The motor must be able to exert enough torque **Tm** to overcome the load's accelerating torque demand at all speeds, otherwise the drive will not reach full speed but hang up at some intermediate r/m until the motor is tripped off the line.

Acceleration torque, together with first derivative of the Tm = f (N) function in the (Nb, Ns) interval influences the energy efficiency process of the application.

The first derivative of the function **Tm = f (N)** is expressed as follows:

$$\left|\frac{d\,Tm}{dN}\right| = \{f'(N)\}\Big|_{(Nb,\,Ns)} \qquad (2.2)$$

One of the common design philosophies to achieve a "higher efficiency" is to increase flux density "**B**" values in order to reduce the rotor conductor losses **RI²**. The drawback of this approach is an increase in some values related to the motor starting process as well as:

- **Starting current (locked rotor current)**
- **Inrush current and modulation of starting current wave form**
- **Locked rotor torque**

The starting performances of cage induction motors are regulated according to standard designs designated by adopted standards [2], [3].

If the electric design is not well controlled, the motor can become inadequate for a specific application.

When choosing these values, caution must be taken not to enhance the motor shortcomings.

2.3 Shortcomings of squirrel cage motors

When motors are started direct on line (DOL), high starting currents (characterised by x = surge factor of the motor) could cause problems with switchgear. This can lead to a higher rating of switchgear having to be selected for new installations or the replacement of switchgears on existing installations.

In addition, unusual higher starting torques could place increased stress on driven equipment. This could lead to premature mechanical load failure.

Both scenarios have cost implications that need to be included in motor purchasing decisions.

In choosing the best motor for a job or when sizing a motor for a specific application, we must take into consideration that squirrel cage motors have some major shortcomings.

- Relatively high starting current is required to achieve some essential performances
  - Adequate efficiency when running on load
  - Conditions related to pull-out or breakdown torque
  - Acceptable values of starting torque and Pull up torque
- Inability to run efficiently at higher slip (since rotor power losses = slip [pu] x Output power is dissipated in rotor heating)

2.4 Five essentials of application engineering

When selecting a squirrel cage electric motor design, five essentials must be considered [4], as shown in figure 2.2.

- Matching the driven machine conditions
- Matching the power supply conditions
- Matching the environmental conditions
- Matching the reliability conditions
- Matching the business sustainability conditions

Only selective considerations related to technological process improvement will be discussed.

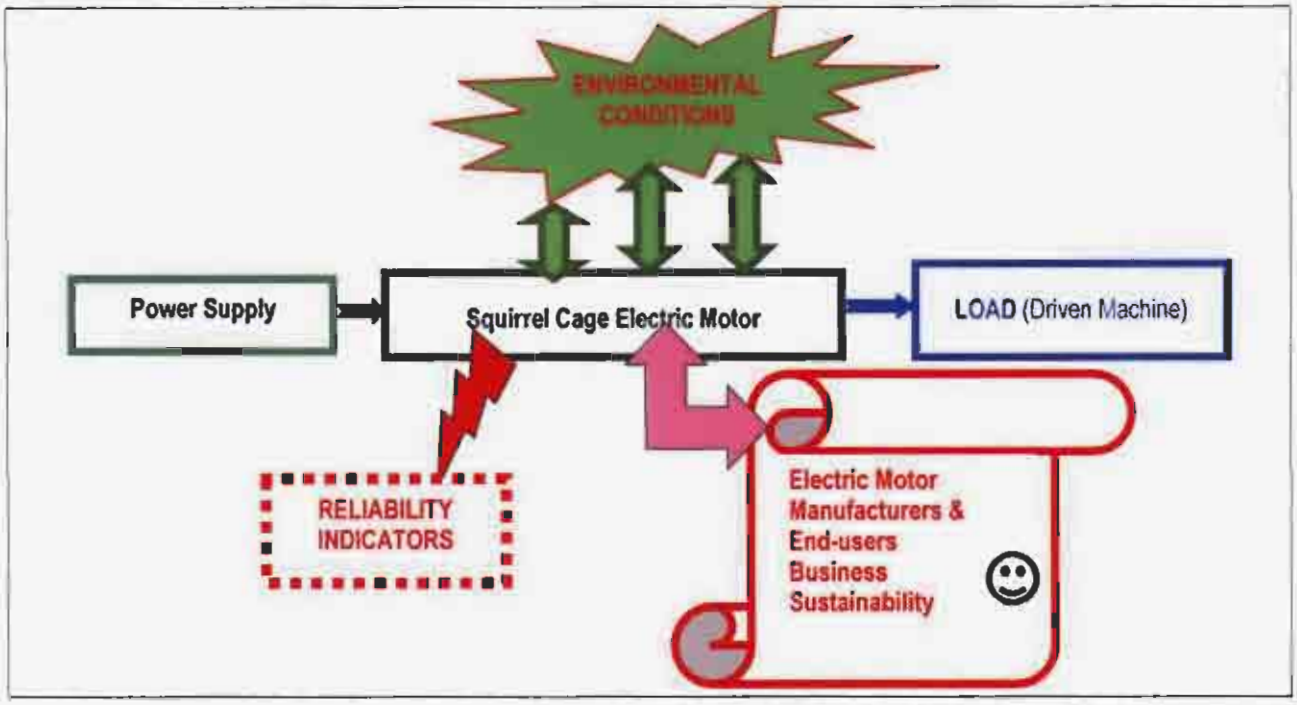

Figure 2.2 Five essentials of application engineering when choosing an electric motor

2.5 Matching the driven machine conditions (load)

LOAD represents all the numerical values of the electrical and mechanical quantities that signify the demand to be made at a given instant on a motor by a mechanism (application).

In matching the motor to a specific load, the motor's STC must be considered with torque values as the most required performances.

- Required values of starting torque
- Imposed value of POT or breakdown torque
- Acceptable value of PUT
- Adequate value of FL Tq

Improved efficiency of an application is reflected in LTC shape. Requiring **specific values of starting torque** this shape being influenced by:

- Increased mass inertia (improved technological process) is to be driven
- Material strength conditions on mechanical driven components
- Avoiding intermediate starting procedures, such as clutches, starting procedure, etc.
- Acceptable number of DOL startings

Note 2.1: *The standards and specifications provide only guidelines for the number of starts and successive starts per hour [5]. However, the information is not applicable to repetitive START-RUN-STOP-REST cycles resulting from energy management programs. It should be recognised that each start is one factor in the life expectancy and reliability of the motor.*

Function of motor and rotor designs especially, some reduction in life expectancy and reliability must be accepted when a motor is used at the upper range of the starting duty.

Imposed values of pull-out torque are more restricted than before and are related to improved application performances.

- Technological process as such
- Material strength of mechanical transmission chain

Note 2.2: *Some standards [5] regulate specific values of starting torque, PUT, and the POT function of motor and rotor designs especially.*

2.6 Matching the power supply conditions

In matching the power supply conditions, low starting current is required the most. This condition is related to the motor's influence on the incoming power and electrical distribution [5].

- Switchgears, transmission lines and transformers costs
- Quality of power supply affected by the motor starting procedure
- Quality and conditions of the power supply

2.7 Matching environmental conditions and reliability indicators

In matching environmental conditions, the electric design must comply with the required motor enclosure (protection) that actually has a great influence on heat transfer conditions.

Obviously, heat transfer has a big influence on reliability indicators.

These essentials, together with the two essentials presented previously, are always related to the motor manufacturer's and end-user's business sustainability.

All these conditions are standardised. However, in the South African coal mine industry the real conditions do not always match these standards.

2.8 Specific working conditions in South African coal mine industry

According to overseas original documentation and machine presentations, specific performances of this machinery are rated. For example, a continuous miner powered by a 270 kW, 1 000 V, 4-poles cutter motor has been designed for a monthly cutting load of 40 000 tons of coal.

In South Africa, the same continuous miner is currently cutting a monthly coal load of between 80 000 and 120 000 tons.

The high volume of coal load reduces the cents/ton price, but electric motors become subjected to accelerated degradation, with high failure rates.

It has been found beyond any doubt that in South African coal mines, electric motors have to withstand specific working conditions, which induce severe multiple stresses, for example:

- Frequent stop/starting
- Unbalanced or reduced voltage (under acceptable conditions)
- Prolonged stall conditions
- Motors operating at large slip values (5 to 10 times bigger than normal), in overload conditions, with torque values close to breakdown (pull-out) torque
- Quality of the power supply (unbalanced voltage, dips, sags, transients, voltage and frequency variation beyond standard limits, etc.)

2.9 How rotor design changes motor characteristics

By altering the stator or rotor design, the STC shape can be tailored to meet the demands of a specific application (load).

Further on in the thesis, we will consider changes of Tm = f (N) by only altering the rotor design.

It must be mentioned that the most significant design variable in these motors is the effective resistance of the rotor cage circuits.

Many types of the rotor bars provide a variable rotor resistance function of the motor speed. When a motor is connected DOL, at zero speed, the rotor current frequency is 50 Hz.

After breakaway and running at low speeds, the current frequency values continuously drop towards low values before reaching operating speed (at 0.5 to 2 Hz).

Because of this frequency variation, at starting, the rotor leakage reactance $\mathbf{x_2 = 2\ \Pi\ f\ L_2}$ records high values at the bottom of the bars where the linking leakage flux is greater (related to 50 Hz frequency).

As a result, most of the rotor current flows very near the surface of the rotor (top of the bar). If this portion of the bar is very narrow, it appears as high resistance during start up (very high current density in the top region of the bar).

This provides a high starting torque and the minimum starting current.

Calculations made on a 500 kW, 6 600 V motor revealed that at the "zero" moment of motor starting, the current density in the top filament of the rotor bar have values in the region of 150 A/mm^2 [6].

Once the motor approaches operating speed, the frequency of the rotor current drops to low values (1 to 2 Hz) and the leakage reactance value becomes insignificant.

Therefore, the rotor current will flow evenly through the rotor bars.

Rotor bars resistance will determine further the motor efficiency.

***Note 2.3**: Motor starting process has special characteristics [7]. The entire starting process of an induction motor can be divided into specific stages (which are not discussed in this thesis).*

- *Voltage surge stage*
- *Inrush current stage*
- *Locked rotor current stage*
- *"Synchronisation" stage*

Classic solutions use expensive and sophisticated methods of design and manufacturing.

For exemplification, the NEMA design class letters A, B, C, and D will be discussed only [8].

According to NEMA standards, these four typical design classes have some salient characteristics, which distinguish one from the other.

Figures 2.3, 2.4, 2.5 and 2.6 show examples of various rotor designs that change according to motor mechanical characteristics (STC).

In these figures some useful design characteristics will be presented that have to be taken into consideration in application engineering:

- Rotor slot cross-sections with bars in the slot
- Useful and leakage flux paths
- Typical motor STC for these specific rotor designs

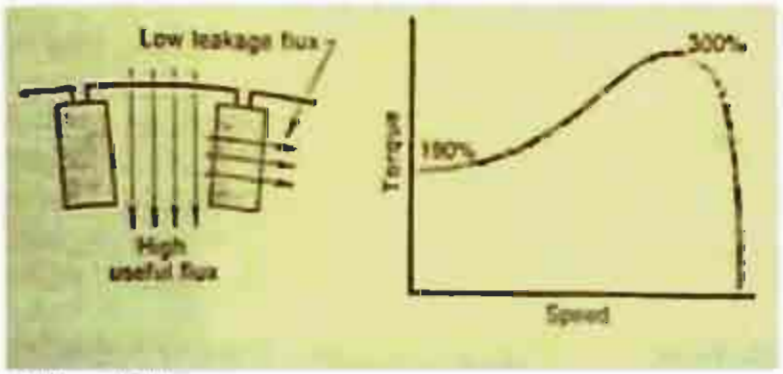

Useful flux = HIGH
Leakage flux = LOW

Figure 2.3 Typical STC for a motor with a letter "A" NEMA Class design

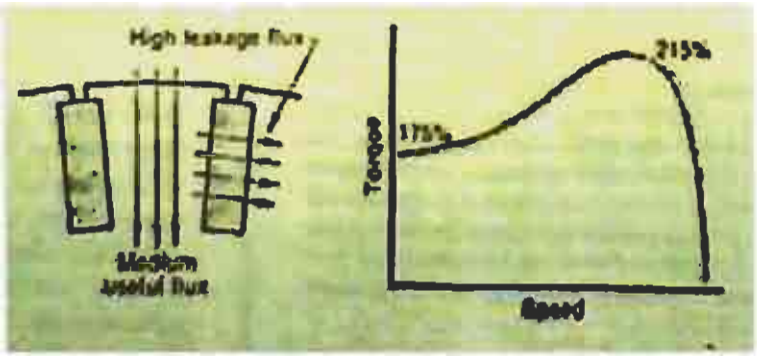

Useful flux = MEDIUM
Leakage flux = HIGH

Figure 2.4 Typical STC for a motor with a letter "B" NEMA Class design

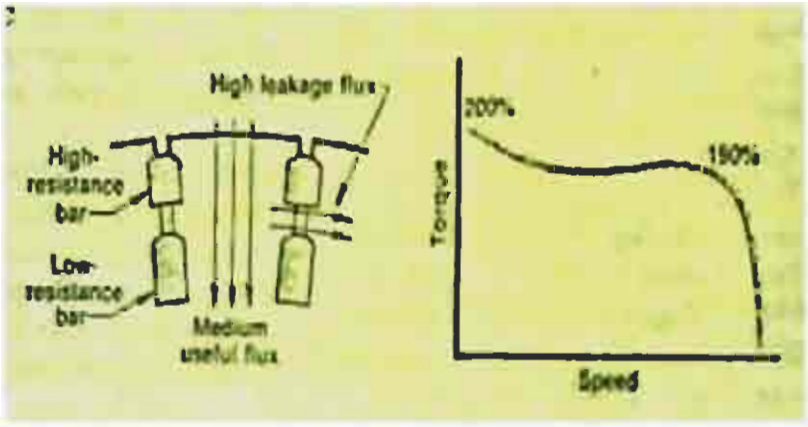

Useful flux = MEDIUM
Leakage flux = HIGH

Figure 2.5 Typical STC for a motor with a letter "C" NEMA Class design

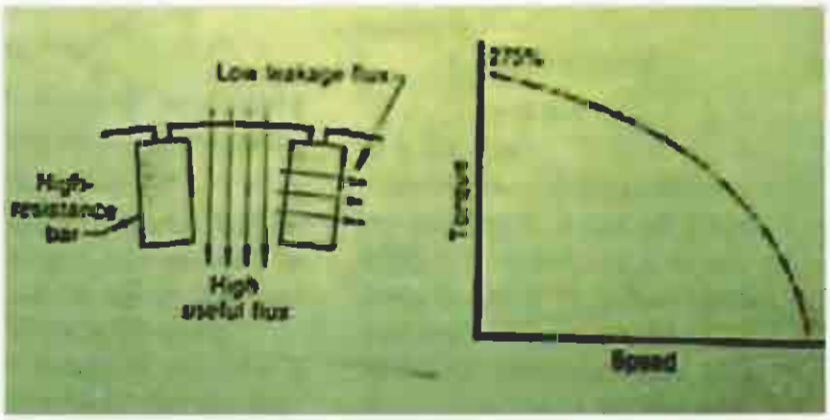

Useful flux = HIGH
Leakage flux = LOW

Figure 2.6 Typical STC for a motor with a letter "D" NEMA Class design

Motor characteristics related to various NEMA Class designs are presented in table 2.1.

Table 2.1 Comparison performances of motors according to NEMA Design A, B, C and D

ITEM/NEMA Class	Design Class "A"	Design Class "B"	Design Class "C"	Design Class "D"	Design Class "E"	Design Class "F"
Starting torque	Normal	Normal	High	Very High	Normal	Low
Starting current	High	Low	Low	Low	High	Low
Full-load current	Normal	Normal	High	High	Normal	Normal
Breakdown torque	High	Normal	Low or no POT	No POT or very high	High	Normal
Efficiency	High	Normal	Low	Low	Low	Normal
Full-load slip	Low	Low	High	High	Low	Normal
Power factor	Normal	Normal	Low	Low	Normal	Low
Rotor circuit	Low resistance	High leakage reactance (deep bars, D.cage)	Double cage	High resistance, high losses		
Load Torque Characteristic	Low load torque at start	POT lower than A. No demand for St.Tq	High load torque at start	V.high load Tq at start. POT @ slip 0.5 or higher		
Applications	Fans, Pumps	General purposes	Compressors, Conveyors, Crushers, Cutters	Intermittent, high impact loads + fly wheel		

Design class E and F have been supplementary introduced [9].

"Dedicated motors" as defined above are not included in this table.

A Mixed Conductivity Fabricated Rotor (MCFR) can be designed and easily manufactured to match performances of any of the above-mentioned rotors. As a result, the motor's characteristics and performances may be changed according to any of the NEMA Class designs.

As a typical feature, MCFR allows re-design of a motor for a given application (frame and stator winding specification) by using a cheap and reliable manufactured rotor solution.

2.10 References

1. SANS 1804; "Induction Motors", Part 2, South African Bureau of Standards (SABS), Pretoria, 1998.
2. SABS IEC 60034-12 © IEC: 2000; "Starting performance of single speed three phase cage induction motors", SABS, Pretoria, 1998.
3. NEMA, MG1-12; "Tests and Performance – AC and DC Motors", USA, 1998.
4. Nailen, P.E.; "Managing Motors", Chapter 3–5, 2nd Edition, Barks Publication Inc. Chicago, 1966.

5. NEMA – MG 10; "Energy Guide for Selection and Use of Polyphase Motors", USA, 1998.
6. Pitis, C.D.; "A consideration of how to adjust the performance of MV squirrel cage motors during rebuilding", Electricity + Control, Johannesburg, January 2006, pp 22–24.
7. Melaia, R.; "A Closer Look at the Problems of Direct-On-Line Motor Starting", ABB, Energize, Sept/Oct 1998, pp 57–68.
8. Koningsveld, v. Ch.; "Getting power to the pump", Louis Allis Co. Milwaukee, Wis. USA, Machine design, Tegniese Inligtingsdiens, Pretoria, Feb. 1981.
9. Anderson, E.P.; "Electric Motors", Chapter 3, 3rd Edition, Theodore Aurel & Co. division of Howard W. Sams & Co., Inc. Indianapolis, USA, 1985.

CHAPTER 3: GENERAL OVERVIEW OF SQUIRREL CAGE ROTORS IN INDUCTION MOTORS

A comprehensive description of the squirrel cage rotor and its components was deemed necessary in order to understand this complex part of an induction motor.

Short theoretical considerations are essential in understanding general overview of the rotors.

Various types of high impedance rotors have been presented, focusing on double cage and die cast aluminium rotors.

3.1 Particulars of this specific bibliographic research (overview)

Before continuing with the discussion, it is important to mention the difficulty of completing the present study and literature overview.

One of the paramount requirements to obtain suitable performances for an induction motor is the ability to design specific slot shapes. The slot shape design also influences the technological manufacturing process with all the technical improvements (novelties) and related economical consequences. That is why the slot profiles and all related information are one of the best-kept secrets of the motor manufacturers.

By protecting their designs, motor manufacturers control the selling of some specific motors by contractual conditions (including a confidential agreement between the manufacturer and end-user) regarding stripping and repairing. The minimum time duration of these contracts ranges from five years and up. As a result, only authorised repair shops are chosen to perform the work on the motors, i.e. commissioning, warranties, monitoring, refurbishment, repair, etc. Some relevant examples in this regard are:

- In South Africa only Reid & Mitchell Pty is the sole representative of General Electric regarding motors repairs and restoration.
- Voest Alpine Mining and Tunneling GmbH Austria bought the exclusivity for specific motors (used on continuous mining machinery) from Breuer Motoren GmbH Germany; in South Africa Femco Mining Motors Pty exclusively repairs the motors.
- Reliance and Harnishphegger Inc. USA allow motor repairs in South Africa to be done only by JOY Machinery Pty.

- SAMINCO, Inc. USA, obtained exclusivity from Transvaal Electric Pty to use specific AC traction motors driving coal-mining machinery.

Another example of protecting intellectual property is the so-called "contract on exclusivity" between manufacturer and suppliers regarding deliveries of specific "critical" motor components. These contracts ensure manufacturers that the supplier will not sell similar parts of the motor to competitors or other motor repairers. As a matter of interest, the following can be mentioned in this regard:

- UNILAM Pressing Pty has contract exclusivity and a confidentiality agreement for specific laminations with various motors manufacturers, including Transvaal Electric, Alstom, Femco Mining, Power Mote, etc.
- DOVAC Engineering Pty signed a confidentiality agreement with Femco Mining Motors for specific parts of new types of scrapper winch motors – mostly used in the gold, platinum and diamond mining industry.
- Transvaal Electric Pty has contract for exclusivity with Mc. Kechnie Brothers Pty. South Africa on delivering specific sizes and conductivities of bronze bars for conveyor motors mostly used in the coal-mining industry.
- Morgan Carbon Pty has contract exclusivity with Joy Manufacturing Pty in South Africa for various electric motor parts.
- For special JOY Reliance rotors, the bars with specific conductivity are not manufactured in South Africa but imported from the USA.

These examples explain the lack of information on this specific subject. The documentary activity, which included gathering information, data collection and understanding related market trends, was based on the following:

- Studying classic literature, scientific papers and articles published sporadically
- South African and international standards, catalogues of reputable motor manufacturers and official documents issued by DME, SABS and other official bodies
- Training sessions and courses attended at the Witwatersrand University, Electrical Engineering Department and Stellenbosch University, Center of Electric Engineering
- Specific projects conducted for various customers over the past 13 years
- Site investigations (including failure investigations reports) and monitoring activity of various squirrel cage motors in specific applications in mining and heavy engineering industries
- Consultancy activity for various mining houses and heavy industry groups
- Design and repair activities as designer, technical and project manager in two reputable motor manufacturer houses

3.2 General description of the squirrel cage rotor

A rotor is a moving part of a motor. It converts electrical power into mechanical power. Among their advantages, squirrel cage induction motors have a simple and sturdy, highly reliable rotor structure [1], [2], [3], [4]. A large variety of rotor types are available on the market.

The thermal and mechanical strength of the rotor are often limiting factors due to stresses imposed by starting the motor, because start-up cannot be achieved with a controlled starting current [5]. A normal running situation can be also detrimental if the design does not match customer requirements. Solving this problem would considerably expand the already wide field of applications that their inherent advantages have secured for Sq.CEM. However, there are some restrictions on the slot profiles imposed by the design and manufacturing capabilities [6].

In practice, the rotor consists of a set of uniformly spaced bars (electrical conductive active materials) accommodated in the rotor slots (magnetic steel active material) and connected at each end to conducting rings. The rotor is a complex component of the motor. It is the result of a combination of various disciplines linked in an inter-disciplinary design activity:

- Electromagnetic design
- Mechanical design
- Strength of material and rotor stiffness to electrodynamic forces and unbalanced magnetic forces
- Thermo-dynamics and thermal assessment

Figure 3.1 shows the results when a rotor's electric circuit is designed and manufactured for a typical double cage 200 kW cutter motor.

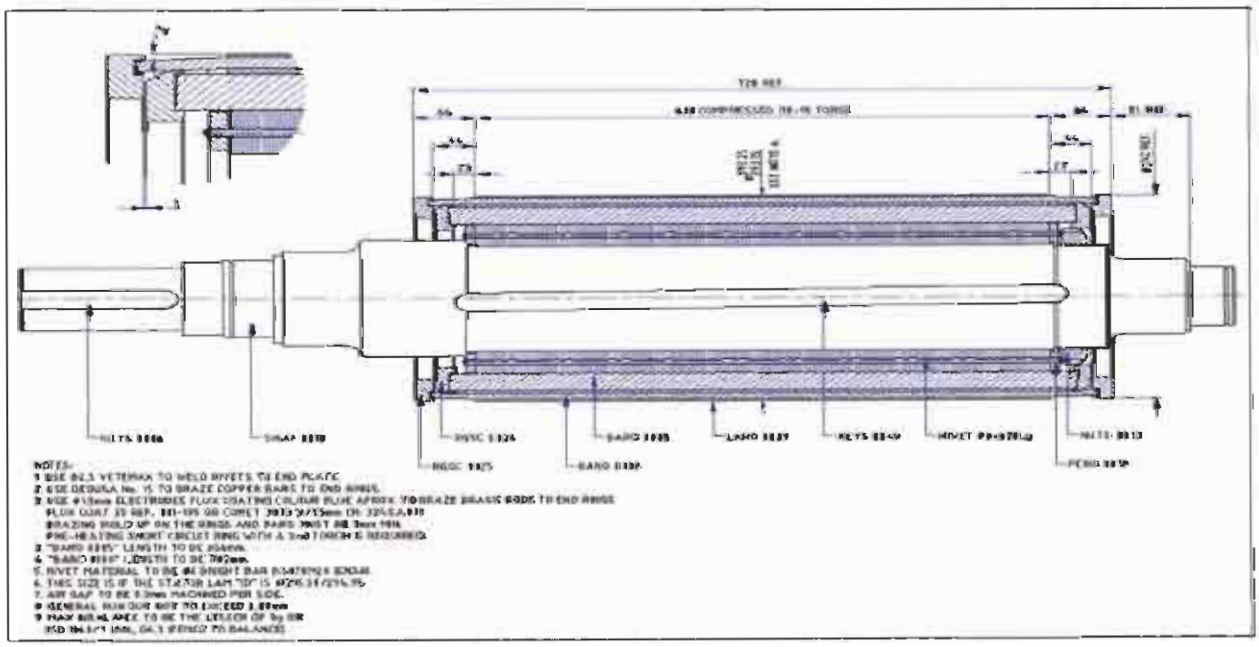

Figure 3.1 A typical assembly drawing of a double cage rotor

Note the shaft diameter in the region of the rotor core. The designer preferred to reduce the rotor core back iron in order to increase the rotor stiffness. The air gap between the rotor and the stator must be very small in order to obtain the best power factor. The shaft must, therefore, by very rigid and be furnished with the highest grade of bearings. Special keys, splines, or special joints facilitate torque transmission between the rotor core and the shaft.

Working under thermal and mechanical stresses, the rotor's technological process requires a special mechanic design regarding tolerances and interference fit of the components.

Mechanical vibration, together with thermal expansion and contraction due to slip-frequency currents, are very damaging to a slack bar.

The connection of the rotor slot bars to their short-circuit rings must be carefully designed, being the most likely source of weakness in a cage rotor. Photo 3.1 shows a rotor's electric circuit designed and manufactured without proper consideration of such typical thermal and mechanical stresses.

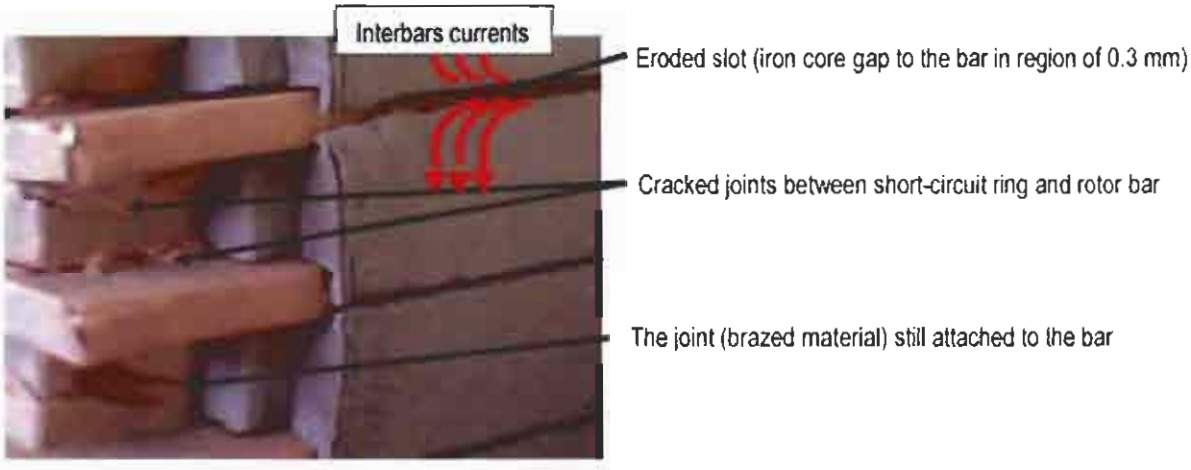

Photo 3.1 Rotor bars separation from the short-circuit ring

Reliable electrical and mechanical design methods assisted by suitable manufacturing processes and adequate machinery have to be used in order to avoid deterioration of electrical and mechanical rotor performances, thus preventing early failures

3.3 Short description of the magnetic circuit of the rotor

A magnetic circuit comprises numerous magnetic steel lamination discs stacked together in the form of a cylindrical magnetic path [7].

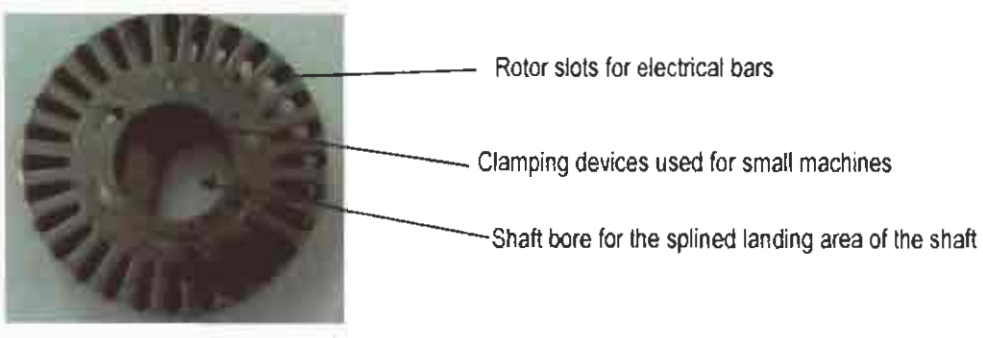

Photo 3.2 Magnetic steel laminations stacked in a rotor core

Each disc has equispaced perforations in a circle near its edge determined by a slot profile specified by the rotor design and manufacturing technology.

When laminations are stacked, the perforations are aligned in order to create channels or slots situated close to the surface of the rotor assembly as shown in photo 3.2.

A typical manufacturing drawing of a rotor lamination is shown in figure 3.2.

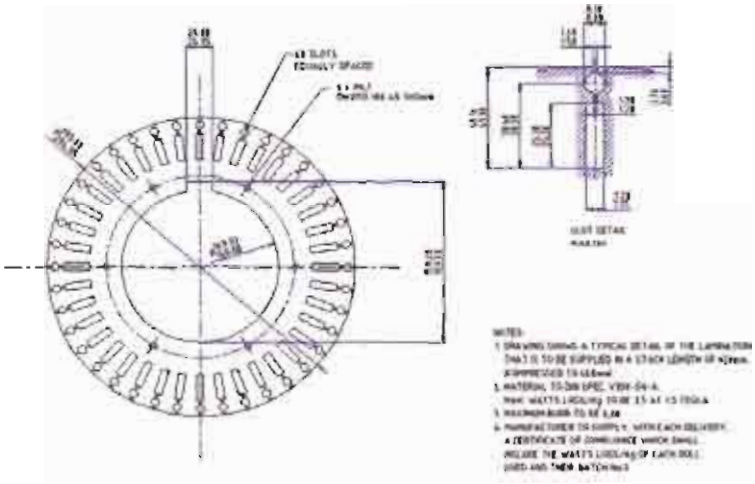

Figure 3.2 Typical manufacturing drawing of a double cage rotor lamination

There are five basic elements influencing design and manufacturing rotor cores and packs [8]:

- Component design
- Material
- Pressing and ancillary equipment
- Tooling
- Quality of the product

Ferromagnetic materials that are used have a high relative permeability because for relative small values of magnetic field strength "**H**", big values of flux density "**B**" can be obtained [9].

3.4 Short description of electric circuit of the rotor

Bars manufactured of conductor materials are fitted in the rotor slots. Together with short-circuit rings, they form the electrical circuit of the rotor. Even though the rotor bars are in direct contact with steel laminations, practically all the rotor current flows through the bars and not in the laminations, because of conductivity difference.

The bars are connected by short-circuit rings at each end of the rotor, simulating a squirrel cage. Photo 3.3 shows two manufactured "spider" copper rotors.

In the case of die cast rotors, the bars are aluminium cast. Aluminium cast short-circuit rings connect the bars at both ends thus creating a rotor electric circuit. An aluminium squirrel cage is shown in photo 3.4 (after steel laminations forming the rotor core have been removed).

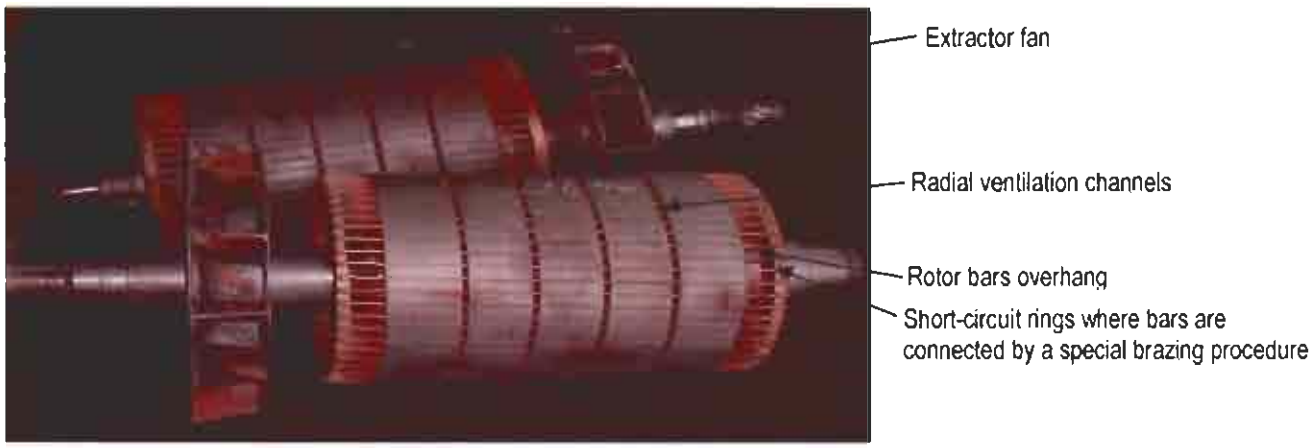

Photo 3.3 Manufactured copper rotors

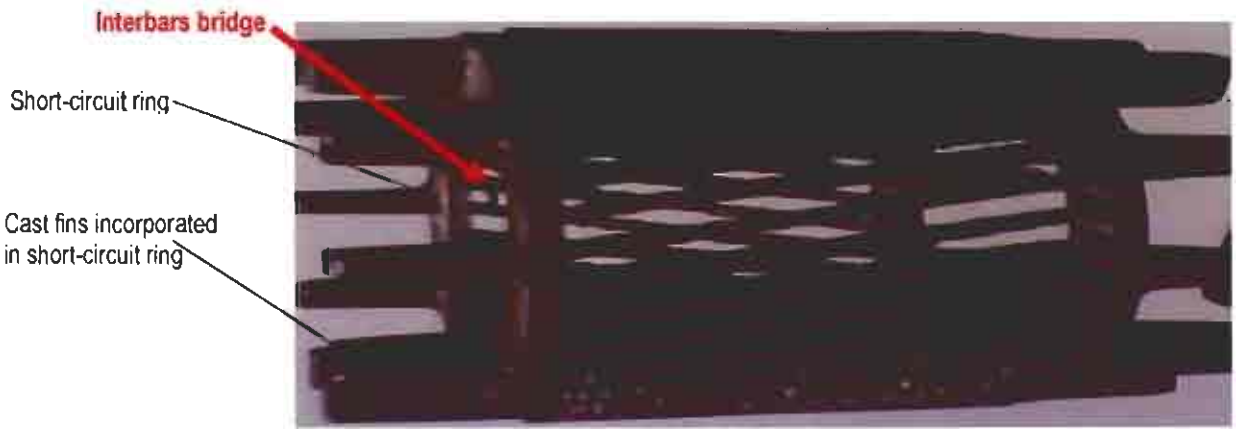

Photo 3.4 Cast aluminium squirrel cage profiles

This cage has a failure because an interbars bridge is positioned on the left-hand side. Cast fins at both ends of the rotors are incorporated on the short-circuit rings in order to cool the rotors by fanning effect.

Electrical circuits (bars and short-circuit rings) for the squirrel cage rotor can be made of different conductive materials, such as:

- Copper bars connected with copper short-circuit rings
- Copper alloys, such as stannum copper alloy, zinc copper alloy, nickel copper alloy, silicon copper alloy, and arsenical copper.
- Brass alloys bars connected with copper or brass alloy short-circuit rings
- Bronze alloys bars connected with copper, brass or bronze alloys short-circuit rings
- Aluminium alloys bars cast together with short-circuit rings
- Special conductive materials connected with short-circuit rings with material according to design requirements

According to IACS, electrical materials used for electrical circuit for rotors are characterised by conductivity measured in % compared to pure electrolytic copper [10].

Conductivities of currently used materials available in RSA for manufacturing rotors' electrical circuit [11] are:

- EC = Electrolytic copper has 99.9–97% IACS conductivity, for bars and short-circuit rings
- CC = Cast copper has 90–82% IACS conductivity, for bars and short-circuit rings
- AC = Aluminium cast, has 55–65% IACS conductivity for bars and short-circuit rings
- SC = Siluminium cast has 20–35% IACS conductivity for bars and short-circuit rings
- BA = Brass alloy has 26 or 42% IACS conductivity for bars and short-circuit rings
- BZ = Bronze alloy, has 12, 15 or 16% IACS conductivity for bars and short-circuit rings

Classification of squirrel cage rotors can be done function of the technological process in manufacturing electric circuit. This actually refers to the rotor type and can be obtained by using one of the following main procedures:

- Pressing the profiled bars into the slot and then attaching the short-circuit rings (by brazing or other thermal procedure) [12], referred to as fabricated rotor
- Casting a specific material into the slots, and at the same time casting the short-circuit rings, referred to as a die cast rotor

3.5 Slot profiles of squirrel cage rotors

3.5.1 Influence of the rotor slot profiles on motor performances

Leakage reactance of a motor is function of the slot profile design. The leakage reactance of a motor determines the locked-rotor current at full-rated voltage. This reactance is generally smaller than the reactance that determines the full load power factor or the breakdown torque.

Motor designers are permanently trying to bring these extreme values of the reactance together: either to reduce the starting current, or to increase the power factor and breakdown torque, whichever is preferred [13].

In view of the fact that over 95% of squirrel cage induction motors are started directly on line, prediction of the accurate starting parameter is of paramount importance, as is the application engineer's understanding of the related phenomena.

A main cause of reduced reactance at locked rotor, i.e. under DOL starting conditions, is magnetic saturation of the stator and rotor tooth tips. This is due to the combined effects of zigzag and slot-leakage fluxes.

Researchers and designers studied the nature and prediction of the DOL starting current of Sq.CEM, with particular reference to leakage path saturation, inrush current and other related phenomena [14], [15], [16].

A paper recommended by the AIEE Rotating Machinery Committee and approved by AIEE Technical Operation Department presented at the AIEE Full General Meeting, Chicago Oct. 1960 [17], **demonstrated that the reactance saturation factor is sharply reduced if the angle between the air gap periphery and the slope of the teeth overhang is small.**

3.5.2 Influence of teeth magnetic saturation on motor performances

The influence is manifested in the common case of "semi-closed" slots (small opening of the rotor slots), "closed" slots or a relatively small air gap value. The bridges covering the slots partially or totally are rapidly saturated when applied voltage Uk reaches values in a range of 30% to 50% of rated value Un. At these values the saturated zone extends rapidly starting from the teeth lips and extending towards the bottom of teeth. For these type of motors, a "short-circuit characteristic" Ik = f (Uk) has a non-linear shape, as shown in figure 3.3 [18].

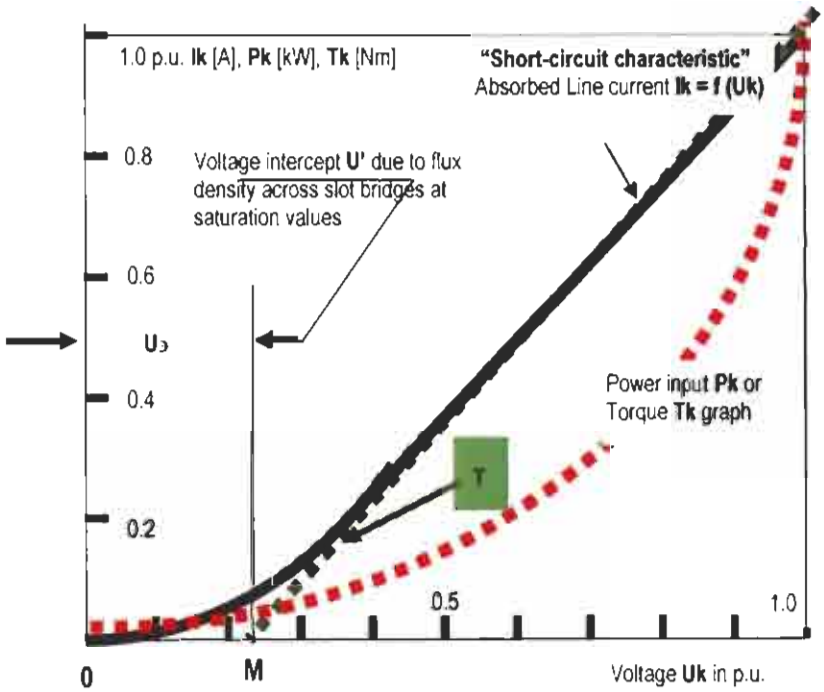

I_k = short-circuit current and U_k = applied voltage on short-circuit test

Figure 3.3 Typical short-circuit test characteristic graph (Ik = f(Uk) in p.u.) lot tips

The tangent line on the graph Ik = f (Uk) is represented by a **straight (green) line T**, with a slope fixed by the non-saturating portion of the leakage reactance, that cut zero-current axis at a **voltage U'** (point "M" on the graph).

U' is the voltage induced by the flux in the saturating portion of the reactance when these paths are saturated. This has been experimentally demonstrated by drawing the graph current Ik versus applied voltage Uk for an induction motor on locked rotor conditions [20].

3.5.3 Typical rotor slot profiles used as design base line

Typical slot profiles are presented in figure 3.4. Other types of slot profiles used for stamping laminations for fabricated rotors are shown in figure 3.5. For die cast rotors, other slot types are presented in figure 3.6.

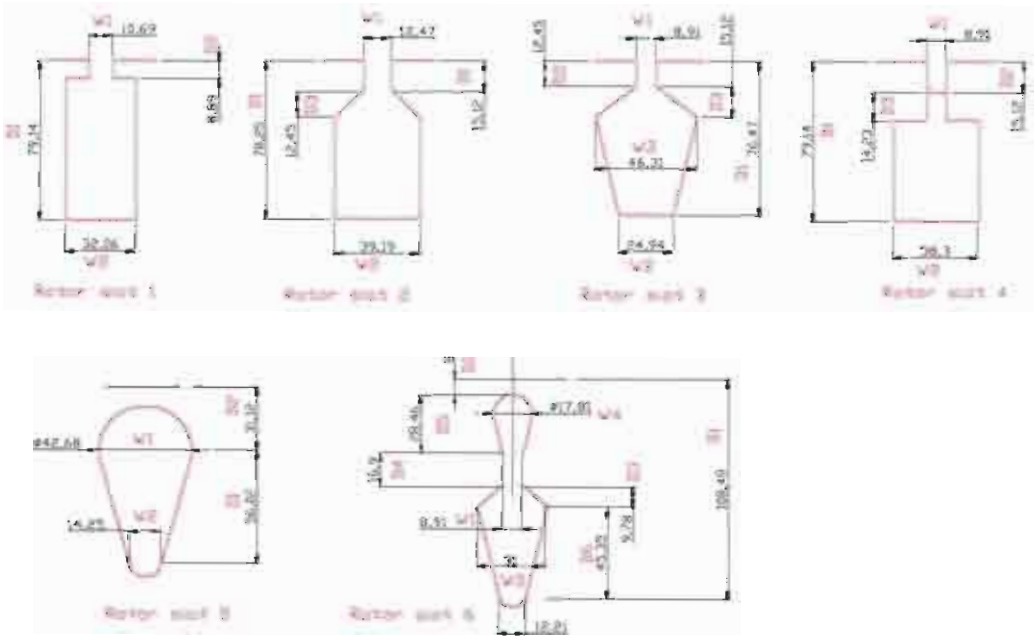

Figure 3.4 Rotor slot profiles used for electromagnetic design purposes
(Classification according to [21])

3.5.4 Special rotor slot profiles used for fabricated rotors

Besides the typical rotor slots presented in figure 3.4, there are more types, shown in figure 3.5, which determine the salient features of the motors as described in table 3.1. These types are used in specific conditions and need to be mentioned as variations of high impedance rotors.

Toshiba Works currently uses rotor slot no. 7 for high power motors.

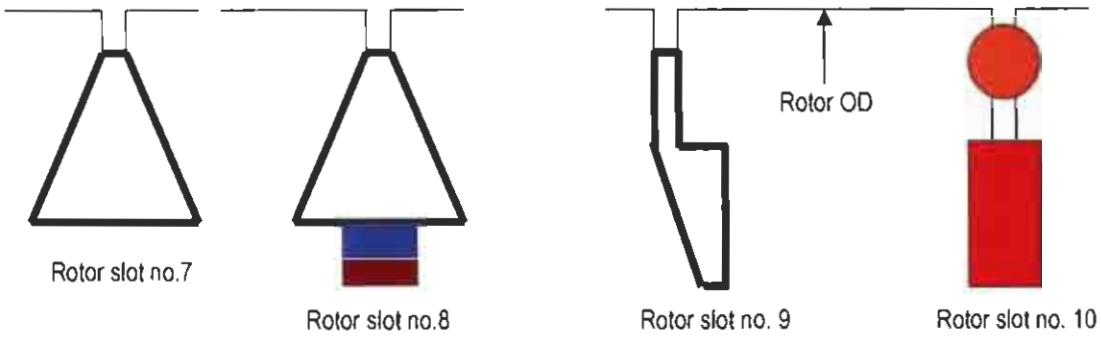

Figure 3.5 Typical rotor slots used for fabricated rotors (prefabricated rotor bars)

Rotor slot no. 8 is a "Toshiba" slot type used for high-voltage, high-power and high-speed machines. To position the bar in the slot, two tapered wedges are driven into the slot below the bar, one from each end of the rotor tightly near the rotor surface. This pushes the bar to the rotor surface and tightly clamps it in position. The outer edge is then "swaged" (tight fit and bend) to ensure that no movement occurs.

Rotor slot no. 10 is a "double cage" rotor mostly used by Breuer Motoren GmbH, Germany in mining applications.

3.5.5 Special rotor slot profiles used for die cast rotors

Initially, die cast rotors were used in manufacturing low-voltage machines with the power ranging from fractional up to 160 kW [22].

Improved designs and processes enabled motor manufacturers to increase the rated power of the motors equipped with die cast aluminum motors [23].

Figure 3.6 shows slot profiles for die cast rotors, used by various well-known motor manufacturers in a case of high power motors [24].

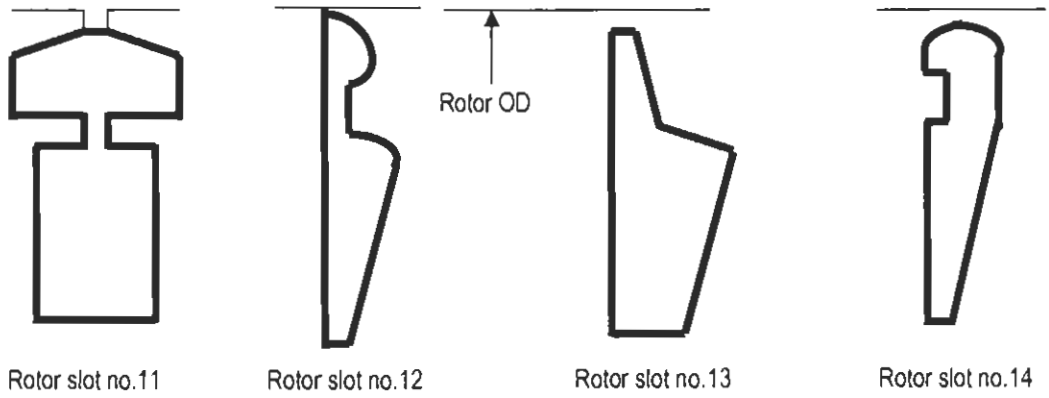

Figure 3.6 Typical rotor slots used for die cast aluminium rotors

In 2005, Alstom launched the LS4 series high efficiency motors (Eff. 1) fitted with die cast aluminium rotors. This performance was achieved with a relatively low starting current as well as with high starting torque values [25].

With die cast rotor designs and the manufacturing process being permanently improved, some motor manufacturers emerged on the market with medium voltage motors with rated power breaking the limit of 1 000 kW [26]. Typical rotor slot profiles used for these machines are shown in figure 3.6.

When the market validated these designs, the manufacturers restricted or ceased production of some specific (non-economical) die cast (and fabricated) low-voltage rotors [27], [28].

3.5.6 Properties, applications and features of rotor slots

Table 3.1 presents the features of rotor slots shown in figure 3.4, figure 3.5, and figure 3.6 in conjunction with possible rotor bar materials fitted into the slots.

Table 3.1 Rotor slots properties, application and use in conjunction with bars

Type	Application	Motor features	Material
No.1 – rectangular	Widespread load range	Function of design	Copper, Co. alloys
No.1a – **deep bars**	Freq. heavy starts	Relative high torques	Copper, Co. alloys
No.2 – rectangular	Heavy inertia load	Standard, 150–500 kW	Copper
No.3 – "knife" bars Type SA 0	Freq. starts, small load	Low starting currents	Copper
No.4 – "Sash" bar	Heavy loads	500–4 000 kW	Copper, Co. alloys
No.5 – "Egg" bar	Normal loads	Small motor up to 37 kW	Copper
No.6 – Cast classic	Heavy frequent starts Widespread	Good starting conditions 22–500 kW	Aluminium cast
No.7 – Triangular "Toshiba"	1–2 MW power	Good starting conditions	Copper, Co. alloys
No.8 – Triangular and tapered wedges – Toshiba – Japan	1–4 MW power High speed	Good starting conditions Preventing bar damage	Copper, Co. alloys
No.9 –"Special Alstom"	Widespread loads	Good starting conditions	Copper
No.10 – Double cage "Breuer" Germany	Heavy frequent starts (10–15 starts per hour)	Good starting conditions 110–400 kW	Copper, Co. alloys, Brass
No.11– "Trislot GE"	Normal loads	Good starting conditions 110–600 kW	Aluminium cast
No.12 – "Alstom"	Heavy loads	110–800 kW	Aluminium cast
No.13 – "Siemens"	Heavy loads	110–1 000 kW	Aluminium cast
No.14 – "WEG"	Heavy loads	110–1 300 kW	Aluminium cast

3.6 Theoretical considerations regarding squirrel cage rotors

3.6.1 Power flow distribution in the rotor

Squirrel cage rotors can be differentiated from one another by the functioning of the developed torque when performing STC. For a given motor design, the classification is made according to the spatial position of the cage and the conductivities into the cylindrical shell, the slot profile of the rotor and the material used for the bars and short-circuit rings. Special reference will be made to high impedance rotors in this classification [29].

For a given main flux and a stator voltage [30]:

- Rotor e.m.f. E'_2 and current I'_2 are settled by the slip, while
- Phase angle φ_2 is a function of r_2 and s x_2 and
- The rotor power P_2 is then a function of slip, as mechanical power, too.

From the power P_2 delivered to the rotor (via air gap), the fraction "s" is lost in RI^2 and the reminder fraction "(1 – s)" appears as mechanical power (including friction and windage losses) [31], [32] so that:

$$P_2 : P_m : I_2^2 r_2 = 1 : (1 - s) : s \qquad (3.1)$$

Mechanical power being: $P_m = (1 - s) P_2$.

3.6.2 General expression of torque

Motor torque is consequently:

$$M = P_m / 2 \Pi n = (1 - s) P_2 / 2 \Pi n_s (1 - s) \qquad (3.2)$$

$$M = P_2 / 2 \Pi n_s \text{ Newton} - m = P_2 \text{ synchronous Watts}$$

Note 3.1: *Definition of 'synchronous watt' is that torque which, at the synchronous speed of the machine, develops a power of 1 Watt.*

The torque is thus directly proportional to the rotor input power, regardless of the speed, and therefore to the stator input power (small stator losses were not taken into consideration).

The motor input is therefore proportional to the torque: a given torque at a low speed requires the same input as the same torque at higher speed.

Although the torque is produced by a series of conductors, each of which carries a pulsating current and lies in a pulsating magnetic field, the total torque of a polyphase machine has a constant value. This is because the sum of the phase powers in a balanced polyphase system is invariant with time [33]. This property was used by the MCFR invention.

From equation 3.2 results:

$$M = P_2 = E_2\ I'_2 \cos \varphi_2 \text{ synchronous watts per phase}$$

With: $I'_2 = E'_2 / Z'_{s2} = s\ E_1 / \sqrt{r'^2_2 + s^2 x'^2_2}$ and $\cos \varphi_2 = r'_2 / Z'_{2s}$

The result: $M = [s\ E_1^2\ r'_2\ ] / [\ r'^2_2 + s^2 x'^2_2\ ]$ synchronous Watts per phase (3.3)

Where r'_2 is rotor equivalent standstill resistance

x'_2 is rotor equivalent standstill reactance

Let the ratio be $\alpha = r'_2 / x'_2$ – the quotient of the rotor phase resistance and standstill reactance.

For a 3-phase machine, the torque is:

$$\mathbf{M = [3\ E_1^2\ s\ \alpha\ ] / [\ x'_2\ (s^2 + \alpha^2)] = K_t\ s\ \alpha\ / [(s^2 + \alpha^2)]\ synchronous\ Watts} \quad (3.4)$$

Where $K_t = 3\ E_1^2 / x'_2$ (3.5)

For constant flux and a given arrangement of rotor winding, K_t is a constant.

The torque/slip curve depends on slip "s" and ratio $\alpha = r_2 / x_2$.

3.6.3 Torque expression at various speeds (slips)

At full load (normal), speed ($s^2 \approx 0$) and torque equation becomes:

$$M = s\ [\ 3\ E_1^2 / x'_2\ ] / \alpha \quad (3.6)$$

For a given machine, $[3\ E_1^2 / x'_2] / \alpha$ is a constant, so that the torque is directly proportional to motor slip "s". An increase in load torque is developed by a nearly proportional increase in slip, giving the machine a speed/torque curve nearly rectilinear in the region of synchronous speed and breakdown speed.

At low speeds and at starting, the motor slip "s" approaches unity. Further, "α" is usually small in normal motors, a typical value being $\alpha = r_2 / x_2 = 0.2$. The term α^2 is then small compared to s^2, and can be ignored.

Thus, at low speeds, the torque equation becomes:

$$M = [\ 3\ s\ E_1^2 / x'_2\ ]\ \alpha / s^2 = [\ 3\ E_1^2 / x'_2\ ]\ \alpha / s \quad (3.7)$$

For a given machine, $[3\ E_1^2 / x'_2]\ \alpha$ is a constant and the torque is inversely proportional to the motor slip "s": i.e. the torque/slip curve is a rectangular hyperbola.

3.6.4 Theoretical shape of torque/slip graph with POT

Torque calculations [34] for the slip ranges s = 0 to s =1 gives the approximate straight-line and hyperbolic shapes of the torque (shown in figure 3.7). These were compared to equation 3.4 results for a case in which $\alpha = r_2 / x_2 = 0.2$. The torque is scaled in terms of constant Kt.

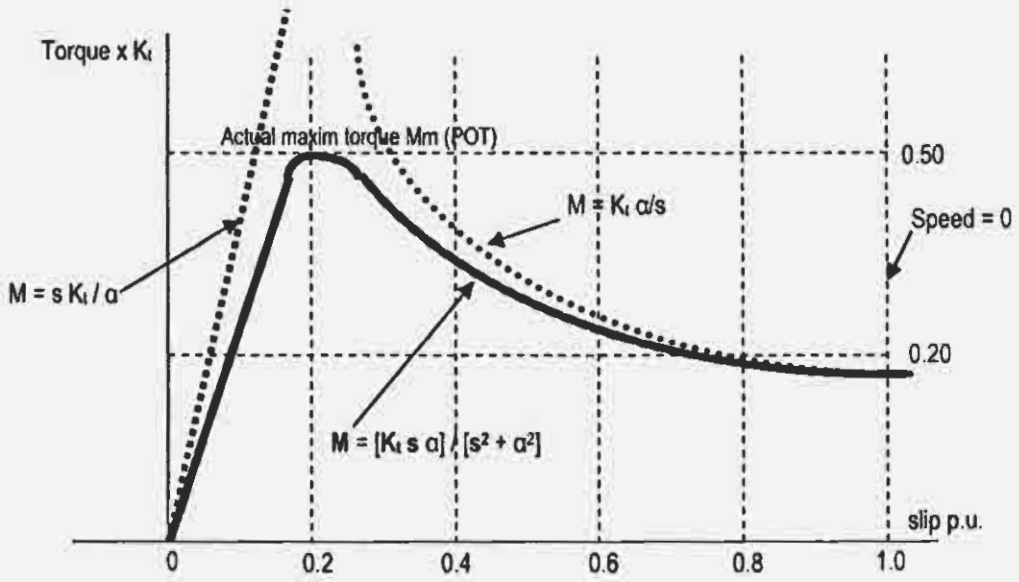

Figure 3.7 Theoretical torque-slip relation

Condition for maximum torque is: [d M / d s] = 0

Equation 3.4 becomes:

$$[(s^2 + \alpha^2)]\,[\,d(s\,\alpha) / d\,s] - s\,\alpha\,[d\,[(s^2 + \alpha^2)] / d\,s] = 0$$

Which gives:

$$\alpha\,[(s^2 + \alpha^2)] = 2\,s^2\,\alpha, \text{ so that } \alpha = 0 \text{ or } \mathbf{s^2 = \alpha^2 \rightarrow s = \alpha}$$

Maximum torque expression is then:

$$\mathbf{M_m = + K_t\,\alpha^2 / 2\,\alpha^2 = \tfrac{1}{2}\,K_t = 3 / 2\,E_1^2 / x'_2} \qquad (3.8)$$

If $\mathbf{s = \alpha = r_2 / x_2}$, or $\mathbf{r_2 = s\,x_2}$, then the torque attains its greatest value at a slip such that the resistance r_2 and the actual reactance ($s\,x_2$) are equal.

Maximum torque depends on the rotor reactance, but given this, it will be independent of r'_2.

The speed for maximum torque will, however, depend on the ratio $\mathbf{\alpha = r'_2 / x'_2}$.

Varying r'_2 will merely change the motor slip (speed) at which maximum torque occurs, not its magnitude.

Comparing equations 3.6 and 3.7, the two curves will cross when

$$s\,[\,3\,E_1^2 / x'_2\,] / \alpha = [\,3\,E_1^2 / x'_2\,]\,\alpha / s$$

i.e. **when s = α** with a maximum torque value according to 3.8.

***Note 3.2**: It must be mentioned here that torque is also related to rotor sizes as per the well-known output coefficient*

$$G = kW / D^2\,L\,n \qquad (3.9)$$

Where: *D = rotor outside diameter in m*

L = rotor iron core length in m

N = motor speed in r/m

3.7 Single cage fabricated rotors (homogenous)

3.7.1 General description of single cage fabricated rotors

These rotors are manufactured by using a specific profiled bar as shown in figures 3.4 and 3.5. The bars are inserted in rotor slots situated in the same cylindrical shell and connected at both ends by two short-circuit rings.

The bars and short-circuit rings of these rotors are made of the same conductive material.

Typical position of the bars in the rotor slots is shown in figure 3.8.

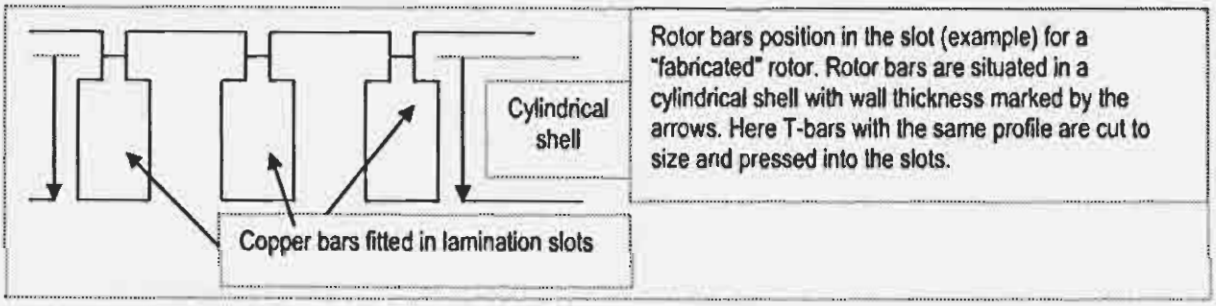

Figure 3.8 Partial cross-section of single cage fabricated rotor

The bars (Sash bars or "T" bars) are placed in the rotor slot. The bar shape is the same as rotor slot no. 4 shown in figure 3.4.

The "T" bar shape has a mechanical advantage over the parallel-sided deep bar in that the bar shoulders keep the bar tighter in the slots against the centrifugal forces.

3.7.2 Thermal stress applied to single cages fabricated rotors

For this specific "T" bar, during starting procedure, the current is confined chiefly to the upper part of the rotor bar. This part of the conductor has a smaller width (cross-section) than the rest of the bar.

That means that, on the top of the bar, the current density reaches high values (10 to 20 times higher than normal) at start or stall conditions [35].

As a result, the top of the bar will become hot with a great temperature gradient compared to the rest of the bar.

Due to thermal conductivity, the heat is dissipated to the lower portion, especially where a greater section of copper is used.

However, during frequent startings this great thermal gradient imposes a considerable thermal stress on the bar overhang, especially where the bar protrudes from the rotor iron core.

3.7.3 Thermo-mechanical stress applied to single cage fabricated rotors

Thermo-mechanical stress occurs as a result of short-circuit ring thermal expansion. The maximum acceptable temperature rise in rotor components is specified by various standards. A maximum value of 350°C has been generally agreed [36].

During frequent startings or prolonged stall conditions, the short-circuit ring temperature will increase as a result of the high currents circulation.

Thermal expansion of the short-circuit rings will occur.

If the short-circuit rings are brazed at the bottom of the bars, they will create thermo-mechanical stress on the brazed joints and the bar overhangs.

The axial movement of the rotor bar as a result of longitudinal thermal expansion was not taken into consideration.

Let's calculate the short-circuit ring expansion for a temperature rise of only 150°C [37].

A short-circuit ring has the following characteristics:

- Material copper with coefficient of linear expansion $\alpha = 0.0000168$ /°C
- Geometric sizes @ 20°C are: OD = 400 mm, ID = 350 mm, width w = 40 mm

To calculate the final sizes of the outside diameter D_{150} for a temperature rise $\Delta T = 150°C$, the medium line @ 20°C has a diameter of $D_{20} = 375$ mm and circumference is $\Pi D_{20} = 1178.6$ mm

Short-circuit ring linear expansion for a temperature rise of 150°C is

$$\Pi D_{150} = \Pi D_{20} (1 + \alpha \Delta T) = 1181.54 \text{ mm}$$

The result is an expansion of the short-circuit ring = 2.97 mm or 1.48 mm per side, i.e. the bar overhang has to be bent for approximately 1.5 mm when hot, and the retracting and the cycle could be repeated until the fatigued material cracks.

An example of this complex "broken bar" situation is shown in photo 3.5.

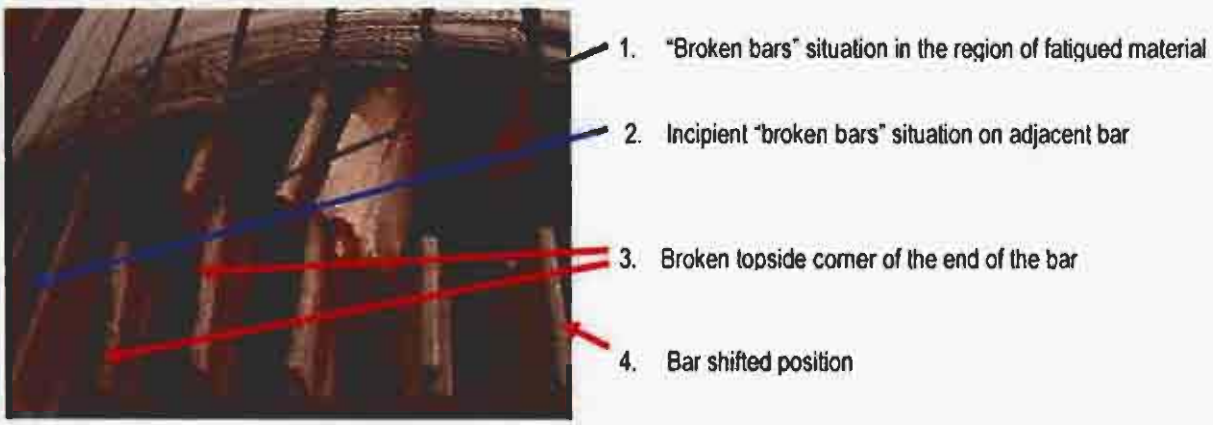

Photo 3.5 A "broken bars" situation on a "T" bar profile

3.7.4 Mechanical stress caused by vibrations on single cage fabricated rotors

Mechanical stresses caused by vibrations: During start up, a transitionary vibrating torque occurs at supply frequency. The effect of inrush current on the rotor (as a multiple of the starting current value) is predominantly mechanical. The torque is proportional to the current. That means the inrush current produces very high transient torques in the rotor and particularly high electro-dynamic forces on the rotor bars overhangs.

The rotor bars overhangs are not placed in the iron rotor core. Electro-dynamic forces exerted on the bars in the iron core and overhangs will be different.

Photo 3.6 Cutting the top corners of the end of the bars to prevent dangerous vibrations

In the rotor iron core of length "L" and a relative permeability μ_r for bar currents I_b which are supposed to be equal on adjacent bars placed at "x" distance, the electrodynamic force on the bar is:

$$F_b = \mu o \, \mu_r \, I_b^2 \, L / 2 \, \Pi \, x \qquad (3.10)$$

On the rotor bar overhang of the length "l", the electrodynamic force is: $F_{oh} = \mu o \, I_b^2 \, l / 2 \, \Pi \, x$

Because the ratio $F_b / F_{oh} >> 1$, the electrodynamic forces generating the vibrations on the bars and bar overhangs have different values.

This will produce a phase shift of the oscillating wave, very noticeable on the top corner of the bar overhang free of any supporting points (the short-circuit ring reinforcement is situated far from this oscillating point with a lagging phase shift). As a result, these corners will always break, as shown in photo 3.5, comment no. 3. To prevent this situation, the top corners of the end of the bars are cut off, as shown in photo 3.6.

3.7.5 Single cage fabricated rotors (non-homogenous)

These rotors are the same as the previous but the bar's material has a different conductivity than the material used for short-circuit rings.

Joining bars to short-circuit rings is done by using a special brazing procedure.

The difference in the conductivity of short-circuit ring material helps in adjusting the starting torque of the motor rated speed. For example, a lower conductivity of the short-circuit ring will not only increase the starting torque, but the motor slip as well, with negative effects on motor efficiency.

The bars are also situated in the same cylindrical shell, as indicated in figure 3.8.

3.8 Double cage fabricated rotors

3.8.1 General description of double cage rotor

Double cage rotors invented by Boucherot [38], [39] have different kinds of slotting (dumb-bell, staggered, trislot).

The cages are manufactured by using specific profiled bars already prefabricated by another supplier (preferably rectangular and round bars), as shown in figure 3.5, slot no. 10.

Typically, the bars in the starting cage have a different profile and are made of a different material than the bars used in the running cage. A typical example is shown in figure 3.9.

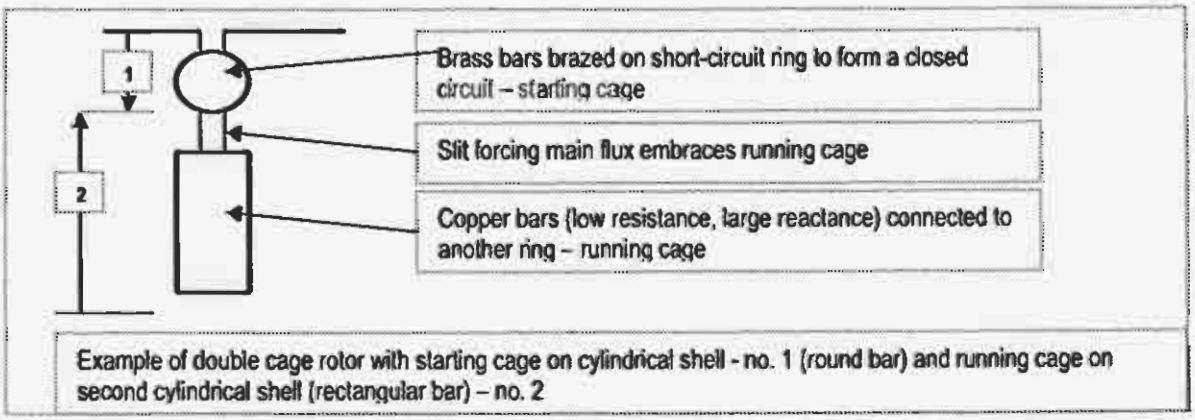

Figure 3.9 Partial cross-section of a double cage fabricated rotor

These rotors have two different cages: starting cage – no. 1, and running cage – no. 2. These cages are installed at different diameters in two different cylindrical shells. The cages are connected separately at both ends by different short-circuit rings as shown in photo 3.7.

Photo 3.7 Typical double cage rotor

3.8.2 Operating principles of double cage rotor

The round bars of the starting cage are placed on cylindrical shell no. 1. These bars are made of material with a lower percentage IACS conductivity (higher resistance) and brazed on a short-circuit ring to form the close circuit of starting cage.

The rectangular bars of the running cage are placed on cylindrical shell no. 2, and are connected to another set of short-circuit rings.

A slit cut into the "leakage slot", forces the main flux to embrace the running cage manufactured of high percent conductivity (IACS) copper bars (lower resistance).

Close to the periphery of the rotor, starting cage 1 has a high resistance and a low reactance. The inner cage 2 has a low resistance, but is set deeply in slots with a considerable leakage flux because of the "leakage slot" with a long narrow slit. Leakage slots with a large reactance are necessary in the deep slotting to prevent the main flux from missing the running cage bars.

Double cage comportment during starting and running of the motor is described in table 3.2.

Table 3.2 Double cage reactance and resistance variation during starting and running of the motor

Motor state	Starting cage 1 (high resistance)		Running cage 2 (low resistance)	
	Reactance	Resistance	Leakage Reactance	Resistance
Starting	Normal	High I^2R losses – high Starting Torque	LARGE	Low – no current flows
Full speed	Negligible	High	NEGLIGIBLE	Low – high current

The starting cage (close to the rotor periphery) has a low reactance and high resistance, which produces a considerable RI^2 loss and consequently a good starting torque.

The running cage (inner cage), set deeply in slots with a considerable leakage flux because of the "leakage slot" with a long narrow slit, has a low resistance and large reactance (especially at start) causing the rotor current to flow with high resistance mainly in the outer cage.

At normal speed the reactance of both cages are almost negligible.

Cages are electromagnetically parallel connected and carry rotor currents in inverse proportions to their resistance. So, most of the rotor full load current will flow through running cage no.2.

The shape of the speed/torque curve of a motor with a double cage rotor can be regarded as the sum of two STC motors, as shown in figure 3.10:

- One with a squirrel cage similar to the starting cage, and
- Another with a squirrel cage similar to the running cage.

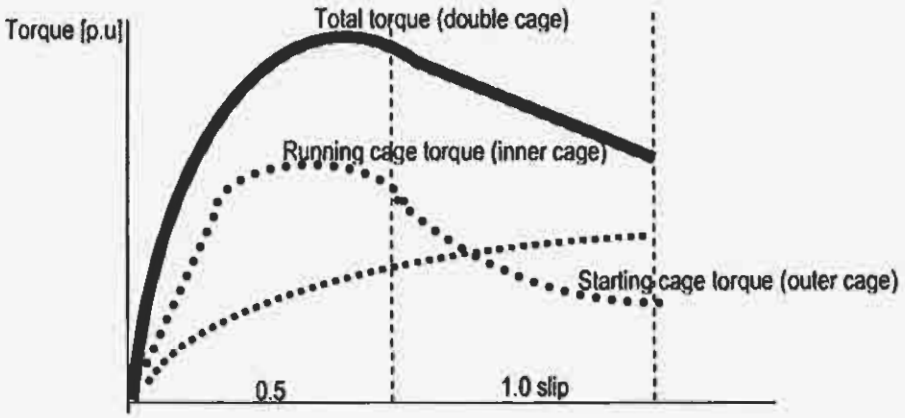

Figure 3.10 Schematic diagram of a torque-slip (STC) curve for a double cage motor

As a result, the STC of a double cage motor can be modified in order to obtain the desired starting torque, within limits, by choosing the suitable parameters involved in the rotor design.

- Resistances of the two cages
- Number of slots combination
- Breadth of the slot opening's diameter
- Depth of the inner cage (running cage) slots
- Width of the leakage slot

3.8.3 Specific problems of a double cage rotor

Sometimes the performances of a double cage fabricated rotor may be compared to that of a die cast aluminium rotor. Both of them have some problems.

- Thermo-mechanical stresses developed in the starting cage (when heavy starting occurs) produce frequent cage damage in the joints, especially.

- The additional leakage that takes place in the inner cage (that is far from stator winding) results in a drop in the power factor at full load.
- The high resistance of the outer cage increases the motor temperature and the losses at full load.
- During frequent startings, motor reclosure and prolonged stall conditions, the starting cage works as a fuse.

3.9 Skin-effect rotors

The variation of rotor frequency provides a means of changing the effective rotor resistance, since inductive impedance loses almost all of its reactance at the low frequencies (when operating at normal slip) [40].

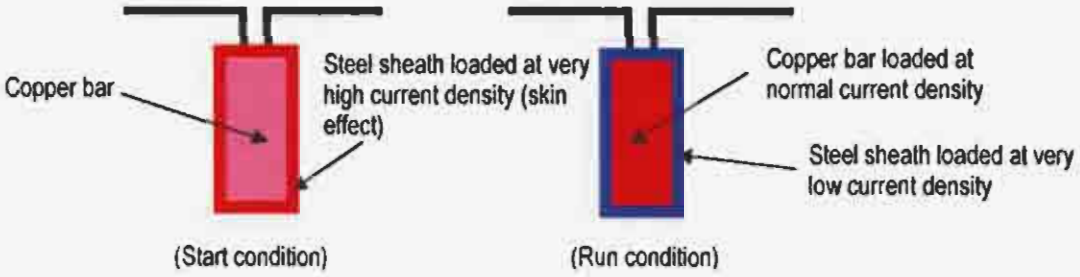

Figure 3.11 Cross-section of a Wall's composite rotor conductor

A number of composite conductors have been developed using this variable reactance to produce a skin effect in the rotor conductors (bars or short-circuit rings). The result is greater effective rotor resistance at low speeds – during starting especially.

Wall's composite conductor consists of a central copper rod covered in the slot portion by a seamless steel sheath. A typical example is shown in photo 3.8.

Photo 3.8 Example of a "skin effect" rotor

The sheath is copper-plated on the outside, care having been taken to ensure that the plating overlaps the ends and makes good contact with the central rod, as shown in figure 3.11. Tests show that the resistance to alternating current may reach values 2 to 3.5 times that of direct

current: $Z_{bar} \approx 2$ to 3.5 $R_{bar\ DC}$. This will enable a starting torque value that is at least equal to full load torque.

At resting and at low speeds, the skin effect, assisted by a steel sleeve, tends to confine the current to the sleeve so that the uniform distribution is upset and the effective resistance rises.

At normal running speed the rotor frequency is so low that the low resistance rod carries the current substantially.

A similar effect is obtained by using iron end-rings, preferably sectionalized in order to dissipate the heat developed during starting process more readily.

Manufacturing this type of rotor requires a very precise process design and execution. Breaking of the steel sheet may occur at any stage when inserting so-called composite bars into the rotor slot. If only one slot failed, the entire manufacturing process would have to be restarted.

During rotor life, it was found that performance deterioration might likely occur if frequent starting took place. The explanation lay in the fact that, during starting of the motor, electric discharges occurred between the sheath and the laminations. These discharges are facilitated by small air gaps (related to fitting tolerances of the conductors in the slots). These discharges eroded the sheath cover of the copper bars increasing further the air gaps.

As a result, rotor bars vibrations during starting degenerate in rotor broken bar situation. Winding overheating because of rotor non-performance at starting is another side effect.

3.10 Idle-bar rotors

Placing open-circuited conductors, or "idle-bars", in the slot above a depressed squirrel cage produces a low starting current at a moderate torque performance [41], as shown in figure 3.12.

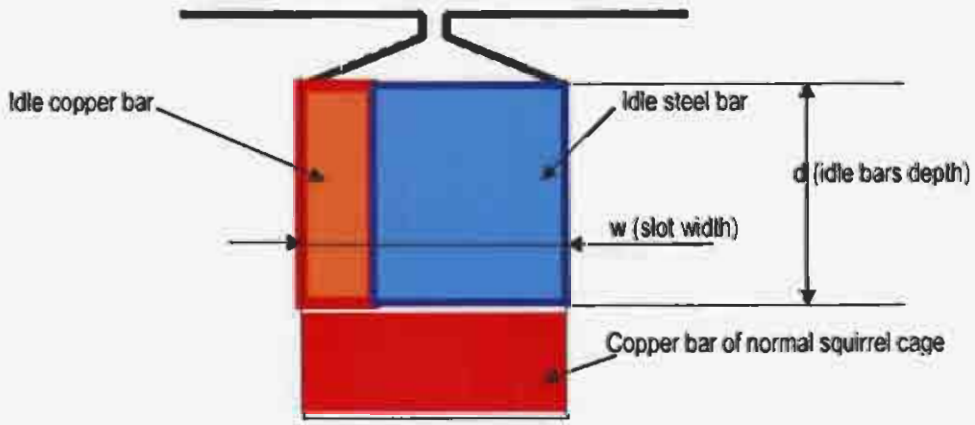

Figure 3.12 Cross-section of an idle-bar rotor slot

The copper bar (leakage slot) must be wide enough to give a reactance value at full speed Xo, corresponding to the desired value of breakdown torque. The remainder of the normal slot width may be filled with a steel bar.

At standstill, the full-frequency leakage flux (due to the current in the squirrel cage bar) passes across both the idle bars inducing opposing eddy currents. These eddy currents will create I^2R losses, and also a counter mmf opposing the passage of the flux. Thus, the effective resistance of the squirrel cage is increased and its reactance is reduced during the starting period

The performance of this design may be assessed by considering the idle bars to form a short-circuited tertiary "3" winding, which is linked by the slot-leakage flux of the squirrel cage.

Assuming that the leakage flux paths through the idle bars are directly across the slot, the separate copper and steel bars may be replaced by a fictitious single idle bar with the same depth, d, and the same width, w, as the air gap (slot width).

The fictitious bar conductance must be equal to that of the two actual bars in parallel.

This specific design's shortcoming is the looseness of the bars as a result of the unequal dilatation of the various materials, thus creating an accelerated tendency towards rotor broken bars. The design and manufacturing processes require high skills and technology.

3.11 Die cast aluminium rotors

Just as double cage rotors, die cast rotors are regarded as high impedance rotors.

When the double-cage construction is used with die cast aluminium or siluminium rotors, the starting cage and the running cage have the same material conductivity.

A wide range of the aluminium alloy's chemical compositions and mechanical and electrical properties are regulated by standards [42]. However, as far as the conductivity is concerned, the alloys mostly used in the die cast rotor manufacturing industry have restricted conductivity values (as specified in paragraph 3.4) [43].

When using a specific Boucherot slot shape during the casting process, the upper and the lower parts of the "dumbbell" slot (shown in figure 3.4) are connected by an aluminium fillet. This fillet, situated in the "leakage slot", provides electrical contact between the cages along their length. That is why the rotors are sometimes called and classified as "triple cage rotors" [44].

However, analysis and experiments both show that the assumption of using separate cages may be a reasonable practical approximation [45], [46].

A typical example of rotor bars with slot shape no. 6 (figure 3.4) is shown in photo 3.9.

The bars in a specific squirrel cage are situated in the same cylindrical shell, with the same profile and the same conductivity.

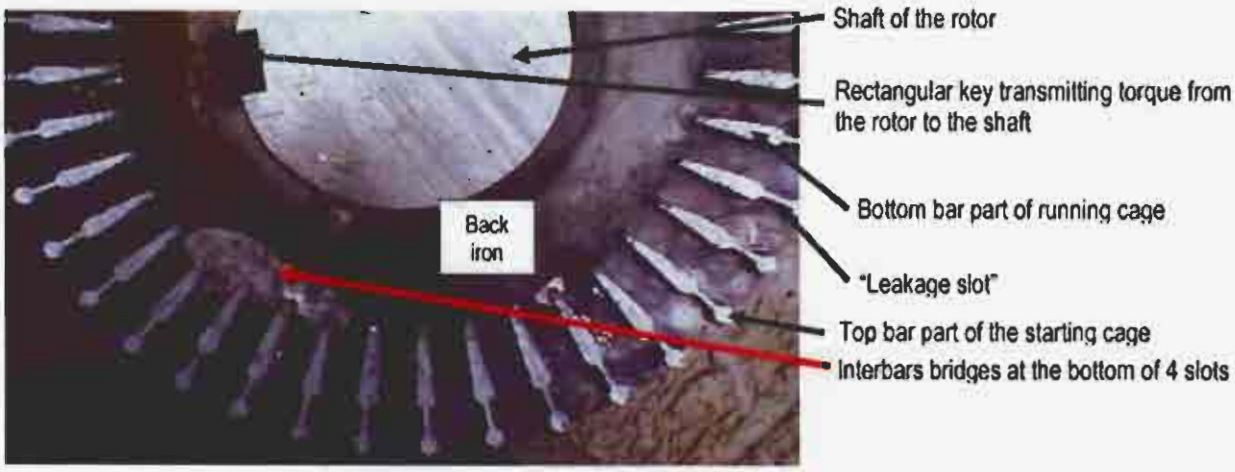

Photo 3.9 Cross-section of a die cast aluminium rotor

The following specific shortcomings cause most of the rotor failures. The indirect failures of the motor components are occurring due to electromagnetic, mechanical and thermal interdependence:

- Casting voids
- Interbars "short-circuits"
- Rotor broken bars (hidden defects)
- Rotor broken bars as a result of rotor rubbing against the stator bore
- "Bow" rotor, locally overheated rotor, and rubbing
- Rotors rubbing, with resulting collateral damage caused by the rotor rubbing
- Design problems

3.12 References

1. Chalmers, B.J., Wooley, I.; "General theory of solid-rotor induction motors", Proceedings IEE, 119, 1301, 1972.
2. Say, M.G.; "Electric Engineering Design Manual", 3rd Edition, Chapman and Hall Ltd, London, 1972, pp 169–177.
3. Mauduit, A.; "Machines electriques – Moteurs d'induction", 3rd Edition, Ed. Dunod, Paris, 1931.
4. Piotrovsky, L.; "Electrical Machines", Romanian translation from Russian, Energetic Publishers, Bucharest 1953.
5. Pitis, C.D.; "Technical report on copper rotor failure investigation" for SA Block, Pty. Oct. 2005.
6. SABS IEC 60034 – 1; "Rotating electrical machines, Part 1: Rating and performances: Table VIII", Council of the SABS, Pretoria, June 2002.

7. Terni, s.p.a.; "Non oriented electrical steel for energy", Steel Lamination catalogue, Rome, Italy, 1981.
8. EURO – Tranciatura; "Production range of laminations for electric machinery", Milan, Italy, 1985.
9. DIN 46400; "Cold rolled non-orientated, finally annealed magnetic sheet and strips" Part 1, DIN-Normen, Berlin, 1984.
10. Copper Development Association; "Coppers and Brasses – Wrought materials: Chemical and physical properties". Data sheets No. A1–No. A6, Edition 1968.
11. Du Preez, H.; "Rotor bars breakage and replacement", GENWEST Industries, Elektron, June 1996, pp 18–19.
12. Kay, G.D.; Welded connections in power supplies", Caldel, SA, Elektron, February 1996, pp 26–28.
13. Chalmers, B., Dodgson, R.; "Saturated leakage reactances of cage induction motors", Proceedings IEE, Vol. I 16, No. 8, 1969, pp 139–144.
14. Grayer, I., Melaia, R.; "Direct-On-Line Starting Current of Cage Induction Motors", ABB, Elektron, June 1996, pp 25–27.
15. Jokiniemi, M.; "Designing Cage Motors to Withstand Direct-On-Line Starting", ABB, Finland, Vector, May, 1981, pp 30–36.
16. Graham, W.I.; "Direct-On-Line Starting of Modern Energy Efficient Low Voltage ac Squirrel Cage Motors", CBI, Electricity + Control, Oct. 1998, pp 7–12.
17. Agarwal, P.D., Alger, P.L.; "Saturation Factors for Leakage Reactance of Induction Motors", AIEE, Paper 60 – 119, Chicago, Feb. 1961.
18. Richter, R.; "Electric Machinery", Vol. IV – "Asynchronous machinery", Technical Publishers, Translation from German Version, Bucharest, 1960.
19. Pitis, C.D.; "Performing locked rotor test on squirrel cage motors", Vector, Feb. 2005, pp 26–28.
20. Voest Alpine TECH HYDRO – WEIZ; "Test Report on asynchronous dPRW280/80-4KL machine" Austria, Dec. 2002.
21. Landy, C.F., Meyer, A.S.; "ELEN 4010: Machine Design – Three phase machines", Univ. of the Witwatersrand, Dept. of Electrical Engineering, Tutorial notes, Johannesburg, 2001.
22. Siemens Aktiengesellschaft; "Three-phase Motors – General Catalog M11.1 TEFC, Squirrel cage Motors Catalog", Germany, 1968.
23. GEC Pty; "GEC Machines in South Africa – Catalog and Presentation", Hortors + CTP Publishers, Cape Town, May 1990.
24. GEC Small Machines Company; "Cage Motors TEFC and Cast Iron, D Frames, D71–D355 – Catalog", Myles & Associates Publishers, Johannesburg, 1985.
25. Teixeira, A.; "High Efficiency low voltage motors" (Alstom), Electricity + Control, July 2005, pp 44–45.

26. WEG LTDA; "1300 kW, 4 pole, 3300 V, 50 Hz, IP23 – Three phase squirrel cage electric motor – Manual" WEG Maquinas Ltda, June 1993.
27. Wood, D.; "Die-cast and copper cage rotors", Alstom, Vector, June 2003, pp 22–23.
28. Sewmungal, G.; "High efficiency motors" (Siemens), Energize, August 2005, pp 58–60.
29. Cioc, I., Nica, C.; "Design of electric machinery", Chapter 4, Didactic and Pedagogic Publishers, Bucharest, Romania, 1994.
30. Van der Merwe, F., Scollay, R.; "Induction Machines: Selection, Maintenance and operation problems", Univ. of Stellenbosch, Faculty of Engineering, Centre of Electric and Electronic Engineering, Tutorial notes, Aug. 2000.
31. Gheorghiu, I.S.; "Electric machinery – Problems and industrial applications" Volume no I, Chapter 2 and 6, Technical Publishers, Bucharest, Romania, 1966.
32. Gheorghiu, I.S.; "Electric machinery – Problems and industrial applications" Volume no II, Chapter 4, Technical Publishers, Bucharest, Romania, 1966.
33. Sen, P.C.; "Principles of Electric Machines and Power Electronics" Chapter 5, 2nd Edition, John Wiley & Sons, New York, 1996.
34. Landy, C.F., Meyer, A. S.; "Squirrel cage electric design program", Univ. of Witwatersrand, Dept. of Electrical Engineering, Johannesburg, 1997.
35. Pitis, C.D.; "A consideration of how to adjust the performance of MV squirrel cage motors during rebuilding", Electricity + Control, pp 22–24, Johannesburg, January 2006.
36. Anglo Gold Ashanti; "Squirrel cage motors for double drum winches", Specification no. 538 – 014, Johannesburg, 2000.
37. Pitis, C.D.; "Thermo-dynamic calculations on over-temperature protection of equipment (sensors)", Vector, April 2005, pp 30–33.
38. Chalmers, B.J., Mulki, A.S.; "Design synthesis of double-cage induction motors", Proceedings IEE, 117, 1970, p. 1 262.
39. Jordan, H.E.; "Synthesis of Double-Cage Induction Motor Design", A.I.E.E. Transactions, Vol.78, Part II, 1959, pp 691–695.
40. Say, M.G.; "The Performance and Design of Alternating Current machines", Chapter 13, 3rd Edition, Isaac Pitman & Sons, Ltd., London, 1990.
41. Alger, L. Ph.; "Induction Machines – Their behavior and uses", Chapter 5, 2nd Edition, Gordon & Breach Science Publishers, New York, 1975.
42. SABS EN 1676; "Aluminium and aluminium alloys – Specifications", Council of the SABS, Pretoria, 1996.
43. SABS EN 1706; "Aluminium and aluminium alloys – Castings – Chemical composition and mechanical properties", Council of the SABS, Pretoria, 1998.
44. Guru, B.S., Hiziroglu, H.R.; "Electric Machinery and Transformers", Chapter 8, Harcourt Brace Jovanovich, Publishers, New York, 1988.

45. Say, M.G.; "Alternating Current Machines", Chapter 8, 5th Edition, Longman Scientific & Technical Singapore Publishers Ltd., 1995.
46. Van der Merwe, H., Jones, C.J.; "Die cast aluminium rotors in HV motors", Alstom Electrical Machines, Elektron, July 1998, pp 19–27.

CHAPTER 4: SHORTCOMINGS OF HIGH IMPEDANCE ROTORS ON THE MARKET

The presentation focuses on the high-impedance rotors mostly used, i.e. double cage and die cast aluminium rotors. Assessment criteria are set up according to some basic conditions.

Design limits of double cage rotors have initiated a comprehensive description of these rotors' shortcomings, which are discussed in this chapter and illustrated by various photos.

The economical implications of double cage rotor failures were analysed for a specific motor fitted with double cage rotor.

Shortcomings of aluminium die cast rotors (with relevant photos), including an original description of the rubbing process are also presented.

Costs of a new locally manufactured cast rotor and costs of an imported cast aluminium rotor give an idea of the high restrictive costs of designing and manufacturing aluminium cast rotors in South Africa. This is proven by financial losses experienced by a South African mining house in using imported cast aluminium rotors.

General conclusions regarding economical losses on high impedance dedicated rotors with reference to South African operational conditions represent the author's contribution to establish a unitary approach in various activities related to mining activities.

Specific South African conditions in designing dedicated electric motors and identification of the "weak points" for a unitary motor model were the base lines in designing the "P" family of motors.

In this "P" family, the MCFR represents one of the major solutions to improving efficiency of the mining processes, with all other consequences already presented in Chapter 1.

4.1 Basic conditions enforced on a high impedance rotor

The rotor is the moving component of the motor, which drives the load. It has to be designed to withstand various permanent or temporary stresses.

- Mechanical (static and dynamic)
- Electrodynamic
- Vibrations
- Thermal

- Thermo-mechanical
- Load influence

As described before, the motor's performances are standardised and often the end-user's drive must be adjusted to the motor's performances. However, for dedicated motors, the design and manufacturing activities must always comply with customer requirements and load characteristics, which result in a large variety of motor types.

High impedance rotors are obtained by increasing the resistance of the rotor's squirrel cage bars in these motors. They are thus able to fulfil some basic and contradictory functions:

- Limit the starting (and inrush) current values
- Increase values of the starting torque per Ampere
- Reduce the RI^2 losses in the stator winding during the starting period
- Withstand prolonged stall conditions
- Allow an unusually high permissible number of starts per hour from "HOT" motor conditions

Rotors mostly used as high impedance rotors are double cage rotors and die cast aluminium rotors.

As specified in Chapter 1, although welcomed in various applications, they are still not able to fulfil all the market demands regarding specific drives (see also paragraph 2.8). Because of this, some technological processes are re-adjusted which lower the efficiency, unless motor failures with all consequences could be recorded (these characteristic failures related to rotors as initial cause will be discussed further).

As mentioned above, the need for an alternative rotor type (able to fulfil absolute specific and contradictory conditions) appeared on the market.

4.2 Shortcomings of double cage rotors

4.2.1 Double cage rotors in the mining industry

The motors powered by double cage rotors have high starting torque values ranging from about 2.2 to 2.7 p.u. (x FLTq). Starting current values are 6.5 to 8.0 p.u (x FLCrt).

They are preferred to die cast aluminium rotors because of a much higher reliability, performance stability and lifetime.

Double cage rotors are mostly used in the mining industry for various motors and applications. The motor powers range from 70 kW to 350 kW and are manufactured by Breuer (Germany), Loher (Germany), Flender (Germany), and Damel (Poland).

The motors are installed on various machines designed and manufactured by Voest Alpine Tunneling GmbH Austria (part of Sandvik Corporation) for coal-cutting operations.

A typical VAMT continuous miner is shown in Annexure 4.1.

These machines operate all over the world: in Africa (about 140 units), the Australasian continent (about 100 units), Europe (about 2 200 units), USA (about 1 200 units), and Russia – Asiatic side (about 1 500 to 2 000 units). China also is using this high productivity machinery.

***Note 4.1**: Another international company, EIKHOFF GROUP, uses long wall continuous miners powered by double cage motors. DBT – Germany and WIRTH – Germany also use double cage rotors. In the thesis we will refer to Voest Alpine Mining and Tunneling.*

However, these manufactured rotors have some limitations caused by motor power, rated voltage and geometrical sizes. The calculations are presented in Annexure 4.2.

Double cage rotor failures presented in the following paragraphs are typical for specific South African conditions (already presented in paragraph 2.8).

4.2.2 General thermal stresses on the double cage rotors

Photo 4.1 shows a German 315 kW 4-poles rotor that is part of a cutter motor installed on a continuous miner.

This specific rotor shows heavy discoloration on different lamination sectors – proof of unusual high values of thermal stress imposed by characteristic South African machine running conditions.

The rotor was manufactured with laminations from different material (coils) with different qualities (specific losses in Watts/kg). This is indicated by the various colours on the rotor segments at the same rotor temperature estimated in excess of 350°C.

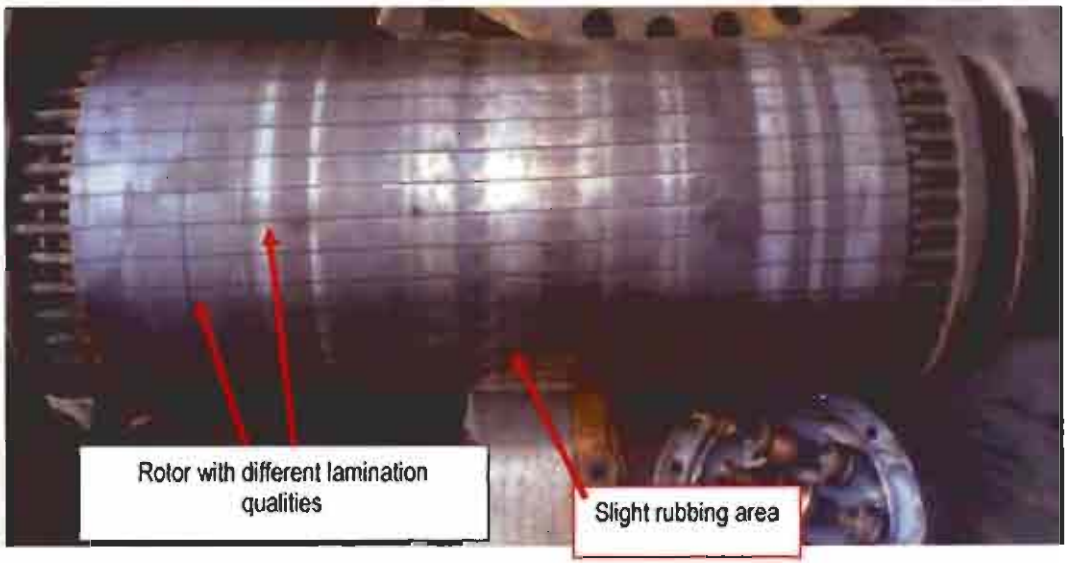

Photo 4.1 Prolonged and heavy operational thermal stresses on a double cage rotor

The slight rubbing seen in the middle of the rotor could be explained by reduction of the air gap possibly due to excess heat developing in the motor internal enclosure, together with unusual flexing of the rotor shaft. The rotor will be discarded.

4.2.3 Mechanical and thermal stress on the starting cage

Because of the load particulars (operation procedure), the rotor is subject to unusual thermal stresses. Photo 4.2 shows the end-ring stopper separated from the laminations pack as a result of frequent longitudinal dilatations and contractions of the rotor.

Photo 4.2 End-stopper separation on a double cage rotor

Vibrations of this loose end-ring during load will cause erosion of the relative tiny brass bars of the starting cage. This can be seen very clearly on the right-end side of the cage. Reduction of the cross-section of these brass bars will cause a local thermal vector – proven by the specific condensation seen on the iron core.

The cross-section of the starting cage bars cannot be increased without altering motor starting performances (function of bars resistance).

4.2.4 Thermal stresses on the starting cage

It was found that the use of special laser cut end-rings as lamination stoppers could prevent end-ring separation on cyclic rotor longitudinal dilatations and contractions.

Photo 4.3 shows a special keeper plate end-ring holding laminations in position. The brass bars of the starting cage are discolored as a result of prolonged high values of currents circulating in the cage. According to tent discoloration, the brass bars were subject to a temperature in excess of 500°C.

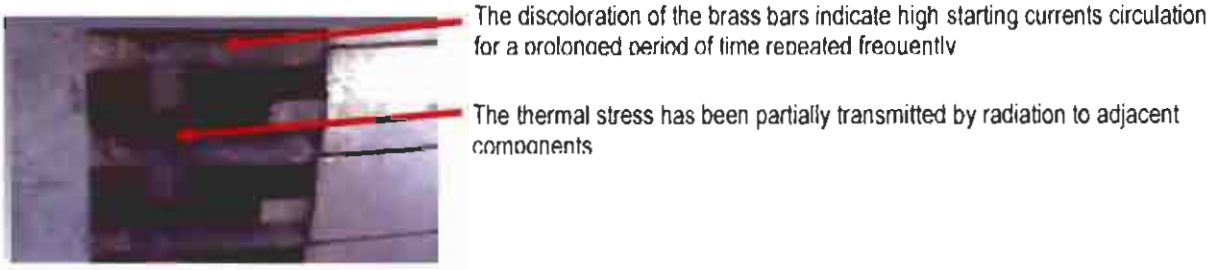

Photo 4.3 Thermal stress is present on the starting cage bars as the first phase of deterioration

This initial thermal stress will be followed by oxidation and electrolytic activities as a result of salt deposits around high temperature spots.

Photo 4.4 shows advanced thermal stress followed by incipient electrolytic activity in the region of the brazed joints.

Photo 4.4.Electrolytic activities around the brazed joints

4.2.5 Erosion of brazed joints

Photo 4.5 shows a classic example of the erosion of brazed joints. The rotor was cleaned before the photo was taken.

The erosion was facilitated by various combined fault conditions present simultaneously in this specific situation:

- High resistance on the joints
- Presence of general thermal stress
- Ingress of salty substances
- Prolonged stall and frequent starts conditions of the motor
- Electric discharges (sparking flashes during stall conditions) throughout air gap

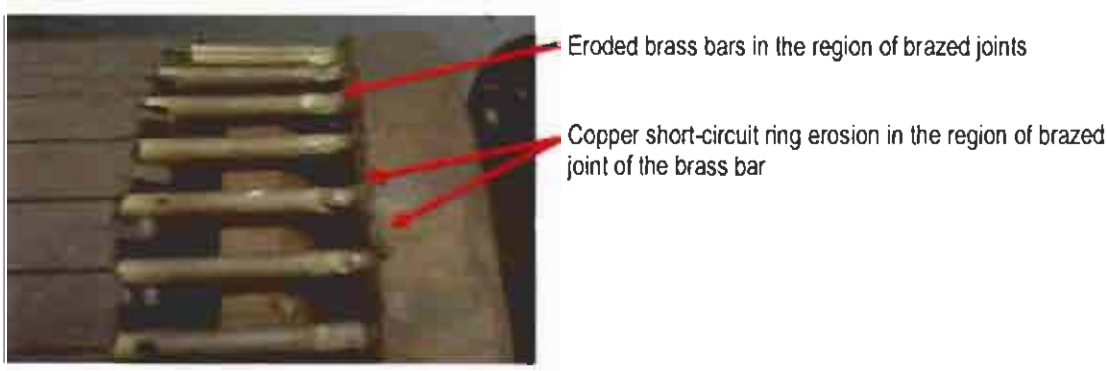

Photo 4.5 Erosion of starting cage bars is present in the region of brazed joints

4.2.6 Mechanical stresses on the starting cage generated by motor re-closure

The specific operational conditions in the South African coal-cutting industry are the chief reasons for starting cage failure.

Photo 4.6 shows severe mechanical distortion of the starting cage as a result of heavy rotor accelerations, which occurred during motor re-closure.

Photo 4.6 Starting cage distortions occurred as a result of motor rapid re-closures

Fast switching of the motor circuit itself can cause spectacular damage: twisted shaft, rotors loosened on the shafts, bending rotor bars with the separation of short-circuit rings, stator coils bending, or machine ripped off its brackets or foundation. These are the results of high transient forces – a sudden, drastic twisting action produced by temporary peak currents, which may be repeated frequently.

Short switching times affect phase relationships between residual and line voltages on motor circuits.

During normal running, a steady-state magnetic field rotates at synchronous r/m within the motor, pulling the rotor after it at a slightly lower speed. If the motor circuit is opened, some residual voltage remains within the winding. Magnetic flux in the laminations cannot disappear instantly when the winding is de-energized. The coasting rotor cage cuts through this field, causing the machine to generate a voltage at its open-circuited terminals that disappears with time. The length of that time depends on how quickly the stored electromagnetic energy dissipates.

As explained earlier, the residual voltage comes into line with rotor r/m, its frequency gradually dropping. The source voltage, however, remains unchanged at its original frequency. When the circuit is re-closed, the two voltages (source and residual) are likely to be out of phase with each another.

In fact, the re-closure yanks the remaining magnetic field back into synchronism and with it the coasting rotor. That abrupt shock also causes a high current pulse, leading to damaging electro-dynamic forces.

Actual re-closure torque can be 8 to 10 times locked-torque value, because the temporary motor behaviour does not match the starting situation. Even during a normal start, a temporary short-time torque of 3 to 5 times the locked-rotor value appears.

Photo 4.7 Starting cage regarded as a "weak point" in a double cage rotor

Typical examples of a starting cage regarded as a "weak point" in South African environments (using frequent re-closures!) are shown in photos 4.7 and 4.8.

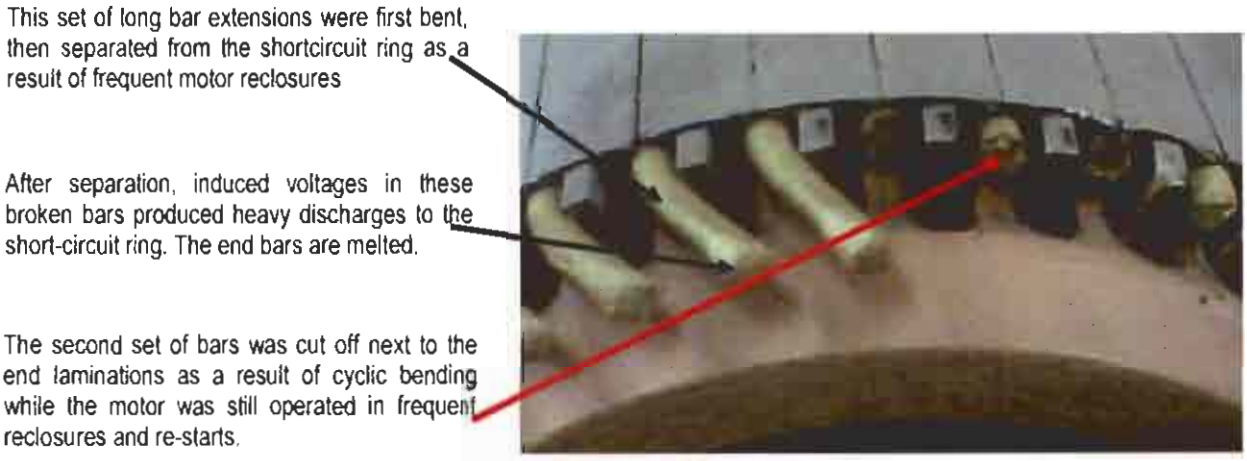

Photo 4.8 Double cage rotors are not suitable for specific South African conditions

4.2.7 Broken rotor bars

Some failures discussed above are similar to "broken rotor bar" situation, manifested on starting cage, especially. There are more specific conditions causing broken bars.

During a locked-rotor condition, the bar current frequency is 50 Hz and the rotor core is subject of same type of iron losses as in the stator core situation. If rotor core laminations are short-circuited, because of the local circulation of the eddy-currents, a "hot spot" will be generated in this specific area. In stall conditions the temperature of this "hot spot" could reach values closer to bar material melting point. Photo 4.9 shows a typical rotor "hot spot" situation.

It must be mentioned that the starting cage distortion indicates that the specific rotor was also subject to frequent motor re-closures. Distorted cages and "hot spots" will produce broken rotor bars.

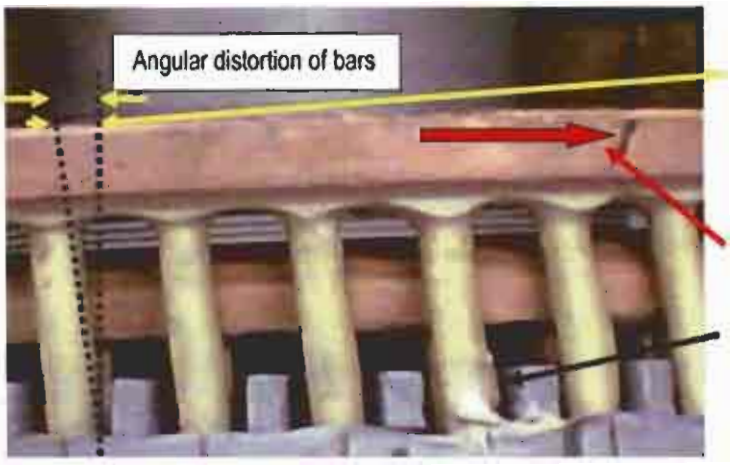

Photo 4.9 "Hot spots" with temperatures reaching melting point of the brass bars

This motor was sent for rewinding. Winding failure occurred at the end of the slot. As a rule the winding failure at the end of the slot is considered a result of poor workmanship. In this case, the winding insulation failed because of heat radiated from the rotor "hot spot". Some brass drops were found next to the point of winding failure proving that during stall condition, besides hot spot radiation, the brass was expelled towards the adjacent point of the stator as a disrupting high-voltage electric discharge.

Note 4.2: *In the chemical industry electric disruptive discharges in the motor air gap can cause ignition of flammable gases existent in the motor enclosure.*

A classic broken rotor bar situation is shown in photo 4.10.

Photo 4.10 Brass bars of a starting cage in a "broken bar" situation

These bars were subject to four combined fault conditions:

- General high temperature generated into the starting cage
- Material expulsion as a result of electric disruptive discharges
- Electro-dynamic and mechanical vibrations
- Possible faulty brass structure in these specific points

Monitoring the motor on site can facilitate the early detection of broken bars.

4.3 Economical implications of double cage rotor failures

As mentioned before, these motors are used in conditions far above the initial design requirements of running the motors in very specific conditions. As a result of financial losses recorded by the customer in repairing and refurbishing these motors, the author has given special attention to these issues during the last 5 to 6 years.

Estimations of financial losses have been done on one of the most used 200 kW cutter motor. The calculations presented in table 4.1 estimate financial losses, which occur when unplanned stoppage takes place.

Table 4.1 Financial losses estimation for a specific motor fitted with double cage rotor

Item	Cost rate	Magnitude	Financial loss (Rand)
Average production	R3 000 / hour		
Down-time production	(10–15) x R3 000 / hour	18–20 hours*	540 000–900 000
New motor	R400 000		
Average repair cost	R180 000 / motor	Max 60% of new	R240 000**
New rotor cost	R70 000 / new rotor***		
Repairer warranty costs		R150 000	R150 000
Repairer production loss		R120 000	R120 000
TOTAL financial loss			**1 020 000–1 510 000**

* From previous experience and according to customer planning, the following activities (with time duration) take place:

Spare motor availability = 6 to 8 hours

Replacing motor and commissioning = 12 hours

** Including rotor replacement

*** Double cage rotor cannot be repaired; shaft replacement average success rate 50%

Conclusion: The financial losses generated by unplanned stoppage as a result of double cage rotor failure of a 200 kW motor are estimated at R1, 2 million.

Other indirect losses regarding logistics, marketing and repairer image are not taken into consideration.

4.4 Shortcomings of aluminium die cast rotors

4.4.1 Characteristic failures of die cast rotors

In spite of various techniques and advanced methods adopted regarding the quality assurance process, a relevant percentage of faulty die cast rotors exist on the market. So-called hidden defects occur because of:

- Quality assurance system failure to perform during rotor manufacturing, before motor assembly
- Occurrence of non-detectable failures (beyond the sensitivity of existing apparatus)

- Failure to perform a load test or to detect the faulty rotor during the load test
- Non-consistent site activity for monitoring and detecting rotor failures

Characteristic failures of aluminium cast rotors can be classified as:

- Voids in the casting
- Interbars "short-circuits"
- Broken bars
- "Bow" rotor, locally overheated rotor, and rubbing
- Cast material
- Design problems

4.4.2 Casting voids

Voids in the casting generate local thermal vectors as a result of a reduction of cast material. The resistance of the casting will increase in proportion. Photo 4.11 shows these characteristic defects.

This specific 350 kW, 6600 V, 4-poles motor has been rewound three times during its warranty period. All these times the rotor passed the quality tests performed with various apparatus and instruments.

Only after the last rewind and with the assembled motor, the vibration spectrum was carefully noted during the load test. Correct interpretation of the vibration spectrum data revealed the rotor failure.

The specific application required 4 to 6 starts/hour. During the start-up period, the "hot spots" of the short-circuit ring radiated heat towards the diamond bar winding. A "fire circle" generated by the short-circuit ring was superimposed on the winding overhangs already thermally stressed during motor start-up. This produced accelerated ageing of the winding insulation, until a weak spot was found to discharge the stress.

The cast voids marked with black circles and grouped together on the side of the short-circuit ring produce an artificial resistance increase of 45%.
This are will act as a "hot spot" radiating heat circularly towards winding overhang and producing a very intensive ageing effect on the winding insulation.
Price of one set coils of diamond windings for this type of motor = R58 000.

Photo 4.11 Casting voids on a short-circuit ring of an MV die cast rotor

After the rotor short-circuit ring was cut off, some data and calculations were available:

- Rotor short-circuit ring rated cross-section = 46 x 35 = 1610 mm^2
- Average cross-section area of voids = 19 x 25 = 475 mm^2
- Normal half ring aluminium volume = 0.86 dm^3
- Actual aluminium volume in half of the ring = 0.47 dm^3
- Volumic resistance increasing due to voids = 45%
- Estimated extra temperature rise in the voids area = 85 to 105°C

4.4.3 Interbars "short-circuits"

The bridges created by the cast aluminium between the rotor slots are known as interbars "short-circuits". Photo 4.12 shows such a hidden defect at the bottom bars.

Photo 4.12 Interbars "short-circuits" on an aluminium cast rotor

In the photo 4.12 there are about 13 to 15 slots (out of a total number of 44 rotor slots) short-circuited by the interbars bridges. These bridges connected electrically about 25 % of the total number of the bars.

On a growler test (performed at 50 Hz), the magnetic flux lines do not penetrate deeply into the rotor iron core, so the rotor will pass the tests.

Starting performances were satisfactory due to the fact that there were no failures on the rounded topside of the bars (starting cage). Due to lack of rotor bars, the motor performed a higher slip, but still in standard tolerances. The winding ran hotter and the motor was rewound several times.

The failure was discovered when customer decided to discard the motor because of frequent uneconomical repair costs and down-time production as a result of unplanned motor stoppage. When the rotor was cut off, interbars bridges were found.

4.4.4 Rotor broken bars (hidden defects)

Even a thermo-graphic picture of a hot rotor may not reveal these "hidden defects".

These specific failures may occur during different phases in the rotor lifetime.

Photo 4.13 shows such hidden defects that weren't detected for about 1.5 years of the rotor lifetime. This is called "partial rotor broken bars".

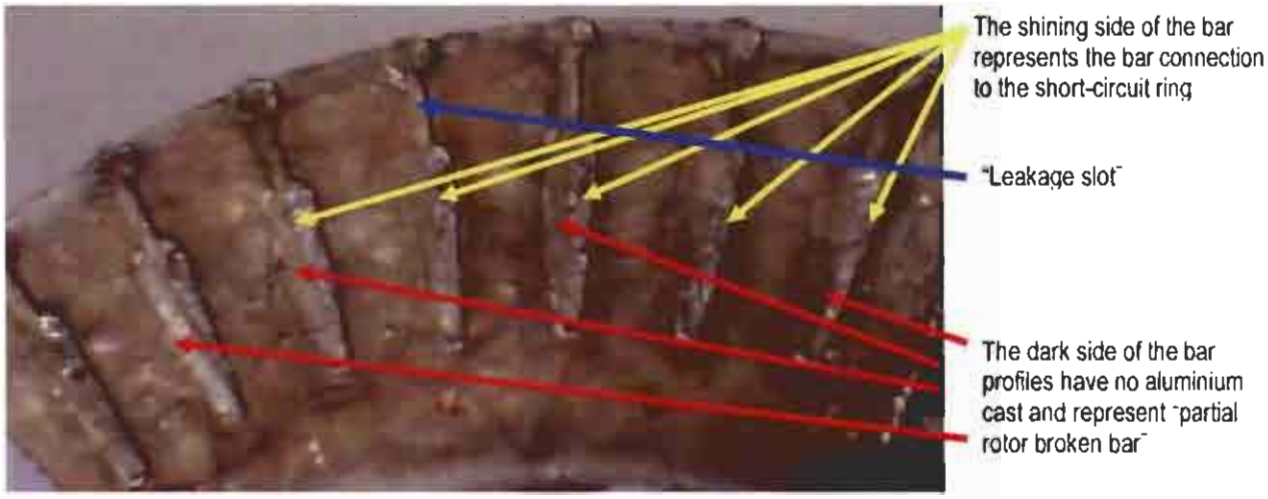

Photo 4.13 "Partial rotor broken bars" on a short-circuit ring of a die cast aluminium rotor

The rotor passed the manufacturer quality assurance system and also the motor repairer specific rotor tests. The motor was rewound twice in 1.5 years; the warranty was rejected as the winding showed overload conditions. It was found that the motor tripped on thermistors overload and the mine by-passed these electronics.

Using a magnifying glass, minuscule holes were found at the bar joints to the short-circuit rings. These indicated the possibility of hidden defects. Tested at vibrations when rings are excited by knocks, hidden defects existence was confirmed.

This type of failure will persist until the rotor structure deteriorates further in such way that the rotor is regarded as the main reason for collateral damage on the motor.

The failure can advance to such an extent that it reaches the situation shown in photo 4.14 where the rotor broken bar can be seen.

Initially the casting did not ensure a complete connection (bonds) between the short-circuit ring and rotor bars. This is one of the characteristic hidden defects that are difficult to detect using existing techniques.

During work time, cyclic thermal stresses acted bi-directionally moving the short-circuit ring axially and weakening the structure of the bonds. As a result, the gap between the short-circuit

ring and rotor iron core increased, this being further detrimental to the electrical connection of the casting between the bars and the short-circuit ring.

When the weakening bonds of the bars to short-circuit rings were destroyed, the rotor revealed a broken bar failure.

Photo 4.14 Short-circuit ring expelled from the rotor body causing a rotor broken bar situation

4.4.5 Rotor broken bars as a result of rotor rubbing against stator

The rotor rubbing against the rotor bore leads to complete damage of the rotor, winding deterioration and further possible damage to the stator core. It in fact leads to the complete destruction of the electromagnetic part of the motor. Photo 4.15 shows a rotor broken bar situation after rubbing process against stator bore.

Photo 4.15 A "rotor broken bar" situation as a result of rotor rubbing against the stator bore

The bars are still connected via a smaller than normal rotor bar cross-section area.

This will result in the rotor overheating locally with heat radiation onto the stator bore. The insulation ageing consequences have already been discussed.

4.4.6 "Bow" rotor, locally overheated rotor

Even though the rotor is centered in the stator (shaft is in perfect concentricity to stator ID), it may be not perfectly round. This can occur as a result of a local thermal vector developed leading to active material leaking from the rotor slots, as shown in photo 4.16.

Photo 4.16 Incipient rotor failure as the aluminium tends to leak from the slots

Presence of a local thermal vector is a good indication of uneven heating of the rotor, which may be caused by:

- Rotor (partial) broken bar
- Previous old rubbing
- Casting problems as voids, interbars bridges or variation in material composition

A rotor concentricity check in "cold" and possible "hot" conditions is mandatory. Uneven heating of the rotor always causes rotor rubbing, as shown in photo 4.17.

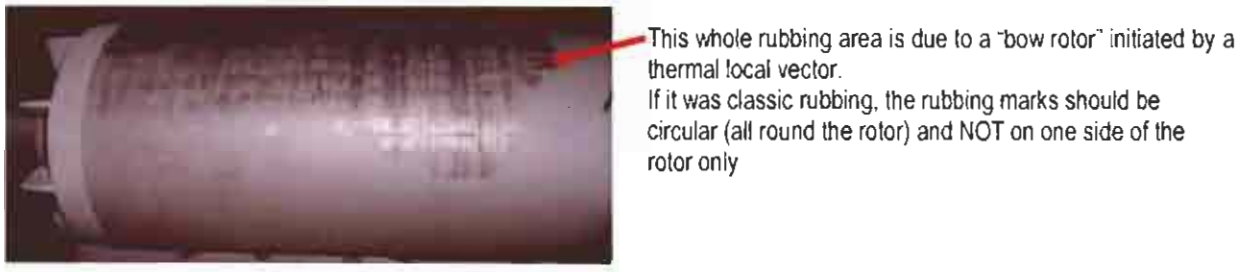

Photo 4.17 "Bow" rotor on a die cast aluminium

In a "bow rotor" caused by local thermal vectors, active material leaks into the motor air gap unevenly. The failure is further extended to rotor rubbing against the stator.

The best prevention of a "bow rotor" is a careful investigation of the rotor "hot spots" by using a classic core test (SABS 0242) or simulating rotor thermal conditions on load, as shown in figure 4.1.

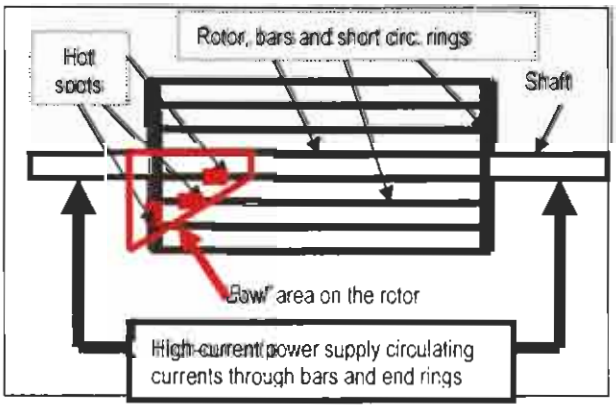

Figure 4.1 Simulating rotor load thermal conditions in order to detect a local thermal vector

Many times a shaft is bent because of rotor distortion as a result of uneven local thermal vectors on the load and the heat being transferred to the shaft, as shown in figure 4.2.

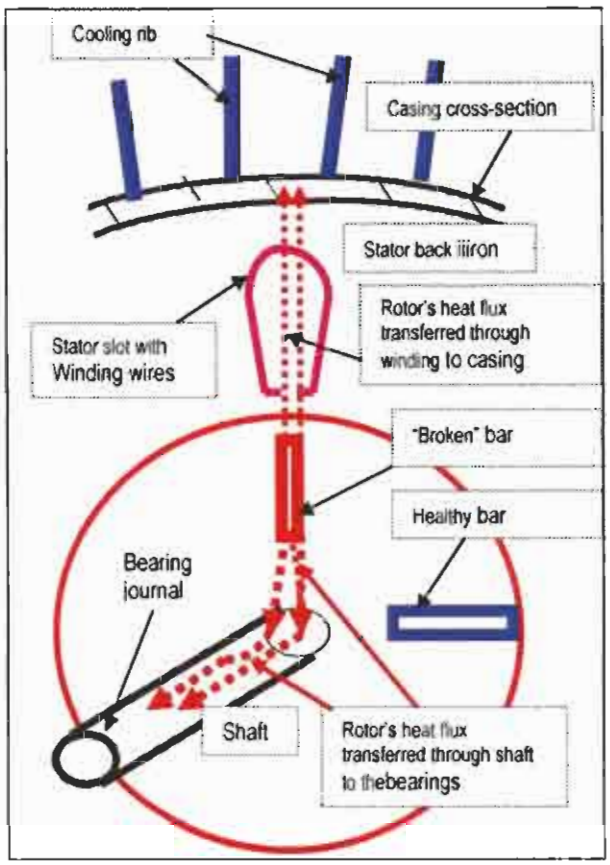

Figure 4.2 Sketch of heat flux transferred unevenly from the rotor to the shaft and to the winding

Thermo-mechanical distortions will vary with temperature, load or other conditions and the vibrations will vary accordingly (often as an unbalanced rotor!).

The non-linear forces caused by the shaft (rotor) run out are the same as those for radial misalignment. This will cause a significant amount of unbalance.

The motor vibration spectrum will be a combination of spectrums similar to radial misalignment and an unbalanced rotor.

On load, these "hot spots" generate so-called "fire circles" thermally stressing the stator core and winding insulation on a specific circumference.

Note 4.3: *Many repairers will "repair" a discolored rotor by "skimming a face". Rotor discoloration may first be an indication of motor overload, and this must be addressed first. Sometimes the rotor discoloration may be due to air gap harmonics developed in a smaller than normal air gap.*

4.4.7 The die cast aluminium rotors rubbing process

Die cast aluminium rotor rubbing represents the end of the rotor life. If rubbing starts, this is an indication of the rotor developing a local thermal vector.

Initially, the vector will develop a local "hot spot". The aluminium will expand unevenly producing permanent micro-fractures of the internal structure.

After a number of cycles the micro-fractures will develop further as cracks that will affect the cast material integrity. Now, the "hot spot" temperature will modify the local rotor OD consistently. A "bow rotor" situation and a "high spot" will be present in the area.

The combined effect of thermal stress and vibrations will produce an emission of aluminium particles from fractures and cracks in the surrounding air gap area.

The rotor now rotates in this "cloud of aluminium particles" present in the air gap.

Continuous friction between this "cloud of aluminium particles" and the high spot will result in a further increase of the "high spot" temperature, thus causing the spot to become hotter. Internal structure damage by cracks and fractures will be accelerated.

As a result of increased electrical resistance in the area and friction to the particles in the area, the local temperature will increase beyond 400 to 500°C.

The "hot/high spot" sizes will increase further, until the high spot sizes will become comparable with air gap sizes. This is the moment when the rubbing process between the rotor and stator bore is ready to start.

4.4.8 Consequences and collateral damages of the rotor rubbing

The rubbing process will escalate in a snowball effect with collateral damages, as shown in photo 4.18.

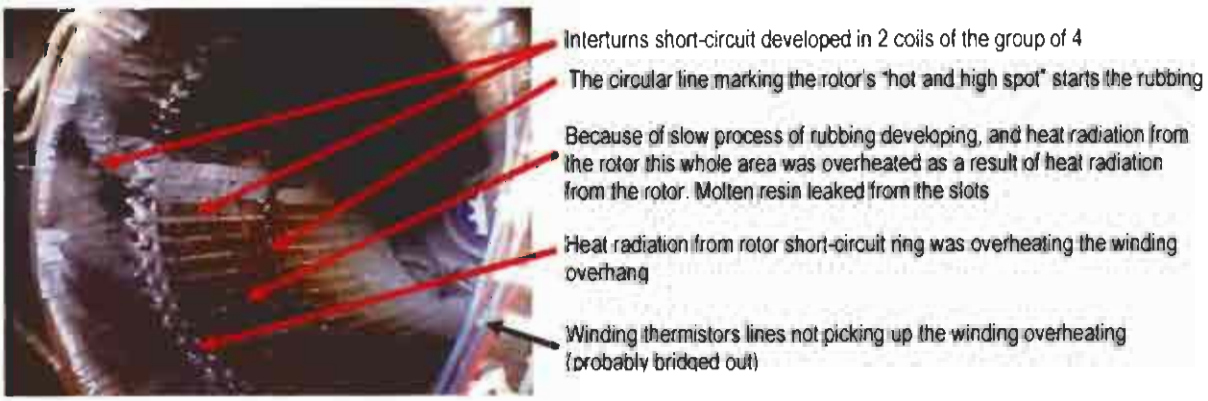

Photo 4.18 Collateral damage of an aluminium rotor rubbing against the stator bore

- Complete rotor failure (aluminium out of the slot)
- Winding contamination and winding failure in the slot (as interturns short-circuit)
- Stator core failure as a result of aluminium penetration by rubbing within laminations
- Stator iron core failure as a result of burnt out iron in the slot, where the interturns short-circuit may be locally developed

4.4.9 Cast material composition

Cast material composition not complying with design requirements is another reason for rotor failure. If the chemical composition of cast material is not controlled properly, there are major consequences related to the five essentials of application engineering.

- **Motor performance alterations due to material conductivity** result in thermo-mechanical stress of the rotor electric circuit, as shown in photo 4.19.

Photo 4.19 Degradation of the electric circuit of the die cast aluminium rotor

- **Cast material corrosion due to material composition** in a hostile environment, as shown in photo 4.20, will also result in the deterioration of rotor performance.

Photo 4.20 Corrosion of rotor electric circuit cast material

4.4.10 Rotor design problems

The rotor design is very important in matching the load requirements (essential one).

An unusual small air gap value will lead to rotor overheating due to air-gap harmonics. The expansion of die cast aluminium rotors may lead to rotor rubbing if a local thermal vector is present. That is why many motor manufacturers using die cast aluminium rotors indicate air gap values in "cold" and "hot" situations.

Another "weak point"* of the die cast aluminium rotor is "the leakage slot" between the upper and bottom bar, as indicated in photo 4.13. Due to the casting process, this slit always contains cast aluminium. There is another probability of casting non-compliance. When the rotor accelerates from standstill to a rated speed, the bar currents circulate through "the leakage slot". Because of this slit-reduced size, the current density reaches very high values. The appearance

of local thermal vectors in these leakage slots overheats the cast pushing the aluminium out of the slot by thermal expansion.

A die cast aluminium rotor designed for a specific application is always a sensitive compromise between performance and manufacturing costs.

4.5 Manufacturing costs or outsourcing (imported rotor) cost of a dedicated die cast aluminium rotor

4.5.1 Cost of a locally manufactured die cast aluminium rotor for a mega cutter motor

A medium-sized South African motor manufacturer decided to challenge Joy Harnishphegger USA in manufacturing the mega cutter 170 kW, 950 Volts, 4-poles motor locally. The motor requires a high starting torque, i.e. high impedance rotor. Initially it was decided to manufacture by reverse engineering a die cast aluminium rotor. Having no facilities for die cast rotors, an enquiry was submitted to a reputable South African die cast rotor manufacturer.

An example of the manufacturing cost structure (excluding VAT) for a new 170 kW, 4-poles, cutter motor using die cast aluminium rotor is presented in Annexure 4.3.

The following briefly presents the answer given by the reputable manufacturer to this enquiry:

Tooling:	Laminations slot & crop punch and die	R7 000
	Die cast tooling	R128 000
Die cast rotor as such (including the gross margins)		R15 000 each
Payment:	in full with order for tooling and cash on delivery for rotor	

Delivery time is 13 to 17 weeks from the date of order, which is totally unacceptable for the customer. The rotor slot design costs are not included.

The rotor cost is about 11% of the tooling costs.

Recapitulation of the costs indicates a **total cost of R150 000** for the rotor.

The price of a new imported motor was at that time R220 000.

These prices, related to the market demand volume, are not acceptable. The repairer must be a big organization with expertise in this field, able to absorb the R&D costs.

Conclusion: Because of the restrictive rotor price, the project failed.

The market requires another type of rotor with similar performances but with higher reliability indicators – longer lifetime and, if possible, cheaper than imported rotors.

4.5.2 Cost of a frequent imported die cast aluminium rotor

Voest Alpine Mining and Tunneling, South Africa are using continuous miners powered by 4 (four) 36 kW, 1 000 V, 4-poles motors (gathering arms and conveyors). They are performing a very high starting torque (2.5 to 2.8 p.u. x FLTq).

Overseas manufacturers, such as Loher, Germany and Damel, Poland, supply these motors and rotors.

Due to very high and complex thermal and mechanical stresses (specific South African conditions), the rotors age and deteriorate at a rate of 1.25 to 2 years.

Continuous miners operating in South Africa only = 80

Total of 36 kW on the machinery = 320

Stock 20% = 64

Total replacement @ 1.8 years average rotor life = 350

Total annually replacement of the rotors = 190 rotors

Estimated annual cost of the replaced rotors = R5 million

Calculations are based on imported rotor costs paid in RSA at Jo-burg custom: R26 000 for a Damel 36 kW or R 22,000 for a Loher 30 kW.

The price structure for this imported rotor estimated according to international rates and related to market indicators is presented in table 4.2.

Table 4.2 Price structure for a 36 kW imported die cast aluminium rotor

No	Item	Price [Rand]	% of pos.11	Notes
1	Magnetic steel core	3 500	25.3	
2	Aluminium cast	500	3.6	
3	Shaft	600	4.3	
4	Key, circlips, etc.	50	0.3	
5	Labor @ R 500/h	1 200	8.7	
6	Overheads	4 000	29.0	
7	Machinery amortissment	520	3.8	
8	Handling & transport	1 000	7.3	
9	Insurance	450	3.3	
10	Taxes paid by manufacturer	1 980	14.4	
11	Total rotor cost	13 800	100%	
13	Gross margin to exporter	9 000	**65.2 %**	**Net Profit**
12	Rotor price before custom	22 800		
14	Customs paid by importer	3 200		
15	Total cost paid by importer	26 000		

Conclusion: The exporter profit is 65.2%! Including customs duty, the user is paying nearly double the rotor! An indigene rotor with similar performances is required.

The patent is offering such rotor as MCFR, with higher reliability indicators (longer lifetime) and cheaper than imported rotors.

4.6 Estimations of economical implications of die cast aluminium rotor failures

As discussed before, the die cast aluminium rotors are sometimes used in specific applications far above the initial design requirements. As a result, performance deterioration and rotor failures generate financial losses recorded by the customer in down-time production, importing rotors, repairing and refurbishing motors.

Estimations of financial losses have been done on a 36 kW gathering arm (spinner) motor and conveyor motors. These motors run with die cast aluminium rotors. They power Voest Alpine Mining and Tunneling continuous miners.

The calculations presented in table 4.3 estimate financial losses, which occur when unplanned stoppage takes place.

Table 4.3 Financial losses estimation for a specific motor fitted with die cast aluminium rotor

Item	Cost rate	Magnitude	Financial loss (Rand)
Average production	R3 000 / hour		
Down time production	(10–15) x R3 000 / hour	7–9 hours*	210 000–405 000
New motor	R65 000		
Average repair cost	R45 000 / motor	Max 70% of new	R45 000**
New rotor cost	R24 000 / new rotor***		
Repairer warranty costs		R20 000	R20 000
Repairer production loss		R10 000	R10 000
TOTAL financial loss			**285 000–480 000**

* From previous experience and according to customer planning, the following activities (with time duration) take place:

Spare motor availability = 3 to 5 hours

Replacing motor and commissioning = 4 hours

** Including rotor replacement @ success rate of 50%

*** Imported cast rotor price was ranging R22 000–R26 000

Conclusion: The financial losses generated by unplanned stoppage as a result of die cast aluminium rotor failure of a 36 kW motor are estimated at R382 500.

Other indirect losses regarding logistics, marketing and repairer image are not taken into consideration.

4.7 General conclusions regarding economical losses

Following are general conclusions regarding economical losses on high impedance dedicated rotors with reference to South African operational conditions.

As a result of failure investigations and motor testing activities, it became obvious that the original design did not match the five stringent South African essentials of application engineering (presented in Chapter 2).

The financial losses generated by unplanned stoppage as a result of double cage rotor failure of a 200 kW motor are estimated at R1, 2 million (paragraph 4.3).

In the South African industrial environment 20% to 25% of the repaired squirrel cage electric motors require rotor replacement.

For old squirrel cage aluminium rotors, replacement becomes a problem, especially when manufacturers ceased rotor production (motors could be scrapped).

When no spare rotors are available on the market, rotors re-design or re-manufacturing in reduced quantities is prohibited because of the price per rotor.

Re-manufacturing cost of a die cast aluminium rotor represents 65–70% of the price of a new imported motor (paragraph 4.5.1).

A rotor importer pays double the rotor price. The exporter profit is around 65%!

A reputable mining house annually pays only in South Africa R5 million for replacement of 36 kW die cast aluminium rotors (paragraph 4.5.2).

The financial losses generated by unplanned stoppage as a result of die cast aluminium rotor failure of a 36 kW motor are estimated at R382 500 (paragraph 4.6).

The total ownership costs of a motor are influenced by some economical components:

- High cost of the new rotors for replacement
- Down-time production, as a result of unplanned motor failure
- Motor repair activities
- Logistic activities

4.8 Common characteristics of "P" family of motors

The author has been investigating numerous causes of Voest Alpine South Africa motor failures for more than a decade.

These dedicated electric motors have been designed and manufactured in Europe. However, it was found that the motors couldn't withstand the harsh South African mining conditions, contravening to some of the essentials of application engineering.

The approach was to identify the motor's "weak points" and to define a specific South African model suitable for indigenous conditions.

By designing these electric motors according to specific conditions, the "P" VOEST family was born.

Table 4.4 indicates the common characteristics of the new manufactured "P" motors.

Table 4.4 Identification of VAMT motors "weak points"

No.	Item	"P" family	"P" Properties	Existent fleet
1.	**Rotors**	**Copper bars fitted in one cylindrical shell Bars in one cylindrical shell**	**Low thermal level, Starting torque according to IEC 600034 tolerances schedule**	**Starting cage:** • **"Fuse" effect** • **Distortions (re-closure)**
2.	**Rotors**	**Copper or MCFR**	**See separate presentations**	**Aluminium with rapid degradation**
3.	Bearings	Clearance and type according to load, less sensitive to heat transfer from rotor's shaft		C3, subject to heat transfer from rotor via shaft
4.	Water jacket	Longitudinal ribs	P nom = 0.5 Barr, High efficiency (85%) Blockages & bypass free	P nom = 1 Barr, High hydrodynamic resistance
5.	Frame & metallic structure	Fabricated, forged, stress-relieved Isotropic, Weld ability, $\sigma = f(\varepsilon)$ in linear range, misalignment free		Composite, an isotropic, $\sigma = f(\varepsilon)$ at the top limit, remnant distortions
6.	Sealing	2^{nd} seal working on compression		Seal on spigot can be shaved
7.	Winding	Round wire trending to diamond coils	Inverter grade, tapped coils, re-design to diamond coils	C 220, Mush
8.	Voltage supply	950 V ±15%	Withstands low voltages	1 000 Volts ±10%

By applying statistic-probabilistic methods as "Fault tree method" and "Policy on motor repair documents", the following "weak points" of Voest Alpine motors have been identified:

- Rotors
- Bearings, lubrication and sealing
- Water jacket
- Frame and metallic structures
- Windings
- Rated voltage supply

The rotor failures were classified as one of the first reasons for motor failures being highlighted in bold letters. Bearing failures was the next reason (influenced by the rotor condition.

A new family of "P" motors was designed and manufactured with new rotor designs being part thereof.

In the invention of the Mixed Conductivity Fabricated Rotor, special reference to has to be made to replacing die cast aluminium rotors.

In this "P" family, the MCFR represents one of the major solutions in improving the efficiency of the mining process with all other consequences already presented in Chapter 1.

CHAPTER 5: A NOVEL SOLUTION: MIXED CONDUCTIVITY FABRICATED ROTOR

This chapter presents a new type of rotor, the Mixed Conductivity Fabricated Rotor – MCFR [1], [2].

A chain of events resulted in the need for an MCFR. Financial losses experienced by the South African mining industry by using only double cage and aluminium rotors represent the biggest portion of the production costs (see also paragraph 4.7).

The invention principle of the MCFR is totally different than that which currently exists on the market and no references and similar manufactured types could be found. After exhaustive bibliographical research, the author found no bibliographical reference to another principle used in designing and manufacturing rotors [3] to [7].

South African and foreign motor manufacturer specialists and academics attending the author's presentations [8], [9] acknowledged the novelty of the invention principle (also see Annexure 5.1).

The answers and other comments received resulting from articles published in specialised magazines [10], [11], [12] also confirmed the MCFR as a novelty.

It was theoretically demonstrated that the resistance variation with frequency function of bar conductivity and/or bar profile is the solution to achieve the invention. Based on theoretical results, the MCFR design uses a "deep bar effect" of various bar conductivities, profiles and sizes.

Calculations on resistance/reactance ratio are confirmed by experimental results.

A summary of the invention aspects and description of preferred embodiments of the patent was done for two main types, the MCFR1 and MCFR2, followed by a description of the basic technological manufacturing process, the operating principle and mathematical equations applied to the MCFR1 design.

According to various customers, the MCFR has definite advantages during operational processes.

5.1 Previous trials in replacing GAM and CM on VAMT machinery

As an alternative to Joy Mining Machinery monopoly in South Africa, Voest Alpine Mining and Tunneling (VAMT), GmbH Austria, started mining operations in our country in 1988.

VAMT effectively penetrated the South African market by using overseas designed high-efficiency continuous miners. Typically, VAMT continuous miners (see Annexure 4.1) are equipped with the following motors:

- Cutter motor (200 kW, 270 kW or 315 kW)
- Hydraulic pump motors (50 kW or 132 kW)
- Gathering arm motors (GAM) – (2 x 36 kW), and conveyor motors (CM) – (2 x 36 kW), each group of two motors working in tandem. Requiring very high starting torque, these motors use high impedance rotors, i.e. die cast aluminium rotors.

Loher – Germany, initially supplied GAM and CM for VAMT continuous miners as 30 kW motors.

Because of the dramatic productivity increase in the South African mining industry, GAM and CM become overloaded and Loher decided to upgrade the existing motor (referred to as "spinner") from **30 kW to 36 kW.**

The following changes had to be made on the 30 kW Loher motor in order to upgrade the motor power **"P"**:

- Reduce the number of turns **"T"** in the stator winding according to:

$$P_{new}\, T^2_{new} = P_{old}\, T^2_{old} \qquad (5.1)$$

- Change the motor thermal protection.
- Increase the motor air gap size from 0.6 mm to 0.7 mm to avoid increasing additional stray losses activity on the rotor surface.

The overall sizes, core length, rotor and bearings of the motor were kept the same because of the space restrictions on the continuous miner.

It was clear that, according to equation 3.9, the motor output coefficient $G = kW/D^2\, L\, n$ was increased by 120%. As a result, motor performances have been changed with some important consequences:

- Motor temperature rise increased with winding burning more frequently.
- Motor rated speed dropped about 20 r/m (rotor was overloaded).
- The rotor temperature rise as well as its heat flux radiation increased.
- Bearing temperature rise increased (heat flux transfer from the rotor was shown in figure 4.2) generating more than expected mechanical failures.

Loher released some rotors with half key only, resulting in "rotor twisting", especially during starting (increasing rate failures).

Increased financial losses related to TOC (repairing activities and down-time production costs) jeopardised Voest's position in the South African market (in competing with JOY Mining Machinery).

In the last attempt to adjust the existing Loher motor to the special South African conditions, VAMT Austria made some additional technical decisions:

- To further increase the air gap sizes to 0.8 mm (decreasing motor stray losses and trying to reduce rotor to stator rubbing probability and improving starting torque)
- To change thermal motor protection: replace winding thermistors – from 160°C to 140°C
- Special heat treatment for rotors

Because of the unchanged high rate of rotors failures, for more than a decade, VAMT tried to find an alternative to replacing GAM and CM (30/36 kW) Loher-manufactured motors.

Custom Electric Motors design: During 1992 to1996, GAM and CM with copper rotors were used. Custom Electric Motors (former Cullinan) designed a copper rotor with the same outside diameter as original, which was able to keep the existing Loher stator in place. The rotor was used with the same Loher stator and winding specification.

The rotor performances were different than the original Loher changing STC motor performances as shown in figure 5.1.

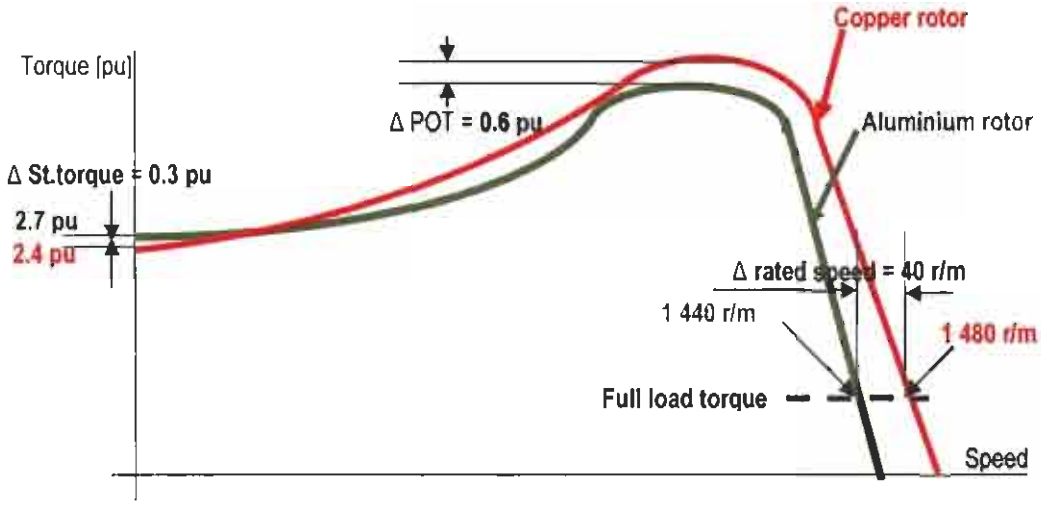

Figure 5.1 Speed-Torque curves of 36 kW, fitted with an aluminium and a copper rotor

Some comments can be made regarding the graph shown in figure 5.1.

- Copper rotor motors do not have enough starting torque, but have a higher rated speed.
- The motors could not work in tandem if one was fitted with aluminium and one with copper.
- Motors fitted with a copper rotor lagged at starting and lead on load.
- This combination increased the failure rate of the motors.

TECO design: During 1994 to 1996 Transvaal Electric (TECO) designed a complete spinner motor fitted with a double cage rotor with a similar STC performance as the Loher motor. The technical solution was abandoned for various reasons:

- Overall sizes of motors were bigger than the Loher to accommodate the space on the continuous miner.
- Replacement of the complete Loher motor was required.

- Starting cage of the rotor was proven to be a "weak point" of the rotor (breaking on starting and stall conditions as shown in paragraph 4.2).
- Manufacturing price was restrictive.

DAMEL design: In the late 1990s, Voest started importing a very cheap 36 kW motor from Damel (Poland). When the rotor lost its performance, it would be possible to discard the entire motor.

The Damel motor also performed better than the Loher. However, the Damel motors have some shortcomings related to the die cast aluminium rotor (as shown in paragraph 4.4).

- Because of the way it is manufactured, the aluminium rotor has a higher failure rate (voids, interbars bridges in casting, other hidden defects characteristic to cast rotors).
- A hot aluminium rotor transfers heat to the bearings via the shaft (see figure 4.2).
- The casing structure does not allow rewind activity inside the casing, pressing out rewind and then and pressing in the stator core generating additional costs, stator damages, electromagnetic misalignment, etc.
- By entering the European Community, Damel motors from Poland became more expensive (in line with the Occidental market), i.e. for aluminium rotors only, the price increasing to R26 000.

Financial losses still occur as a result of rotors failures presented in paragraph 4.5.2 and paragraph 4.6.

Luck & King design: In the last 3 to 4 years VAMT has experienced heavy financial losses related to the failure rate of 36 kW aluminium rotors. Strict dependence on only one motor supplier deciding unilaterally on price, i.e. DAMEL, was a concern, too. Another South African electric motor manufacturer proposed a special brass rotor.

Luck & King introduced brass bars with a specific conductivity by using the same Damel rotor iron core from existing die cast aluminium rotors. Bars joints to short-circuit endrings were done by a partial brazing procedure.

The technological process was, however, detrimental to the rotor shape and performances as shown in photo 5.1.

Photo 5.1 Brass rotor specially manufactured for the VAMT 36 kW spinner motor

- Overall sizes were modified unequally, the rotor changing shape (known as "bow" rotor).
- Slot "openings" become unequal, producing a variation of rotor reactances.
- On load, the rotor was proven to heat up unequally (as a result of local thermal vectors developing in some parts of the rotor) producing rotor rubbing against the stator.
- Motor performances were changed resulting in the performance not complying with accepted tolerances: much higher starting torque and slip than original motors.

5.2 Defining requirements for a new model of a specific type of rotor

The author decided to challenge the VAMT request.

Based on facts presented in Chapter 4, some conditions in defining a new type of rotor have to be mentioned. A proposed complex model was created initially, as presented in table 5.1.

Table 5.1 Conditions imposed on a new rotor replacing die cast imported aluminium rotors

Existing conditions	New proposals	Comments, notes
Die cast aluminium rotors	Fabricated rotors	Only a new principle can be applied
Imported product	Locally manufactured	Reduce economic dependence
High price & price fluctuation of exchange rate	Use indigenous components	Competitive price. Low cost presented in Annexure 6.1.
Rotor manufacturing becomes a monopoly of the big organisations, deciding market prices, too	Medium-sized organisations may be able to become rotor and motor manufacturers.	Offer an alternative option to the market by presenting sound competition
Huge investments for cast process machinery are required	No special investments processes required	Ensure no price monopoly of a specific manufacturer or supplier
Special quality assurance system required	Normal quality assurance system	Advantage of a fabricated rotor
Even on series production, it needs a load test of every motor to prove rotor quality	Load test only for prototype No hidden defects on the product	Advantage of a fabricated rotor
It needs the market to demand high quantities to become economically viable	Can be produced in any quantities without excessive financial expenses	Mass production to be replaced with custom made
Special training and expertise of the personnel required	Normal expertise required	Enables job creation
Consistent performances required	Same performances as original	Offers interchangeability with existing products
Has "weak points" *	Homogenous reliability	Eliminating "weak points"
Rapid performances degradation	Performance stability	Ensure planned stoppage. Cut down-time production losses
Life time is 1.25 to 2 years	Minimum 10 years	Ensure business sustainability
Non-reparable	Repair possibilities	Ownership reduced costs
Hidden defects	No hidden defects	Easy quality inspection
Shaft replacement success rate of 50%	100% success rate on shaft replacement	Easy maintenance and repair activity on refurbishment

Note 5.1: ** "Weak points" mentioned in table 5.1 are components with highest failure intensity indicators (λ_i) and major weight in increasing value of motor failure intensity λ_{motor}.*

5.3 Existing principles in building rotors

A common characteristic in all existing rotors is that the bars in a specific squirrel cage are situated in the same cylindrical shell and have the same profile and the same conductivity. At present, the following principles are applied when constructing rotors:

Principle 1: For a single cage rotor bar configuration as shown in figure 5.2, for both the fabricated and the cast rotor moving around the rotor in the circumferential direction indicated by the red dashed arrow, the rotor bars have the same shape and conductivity.

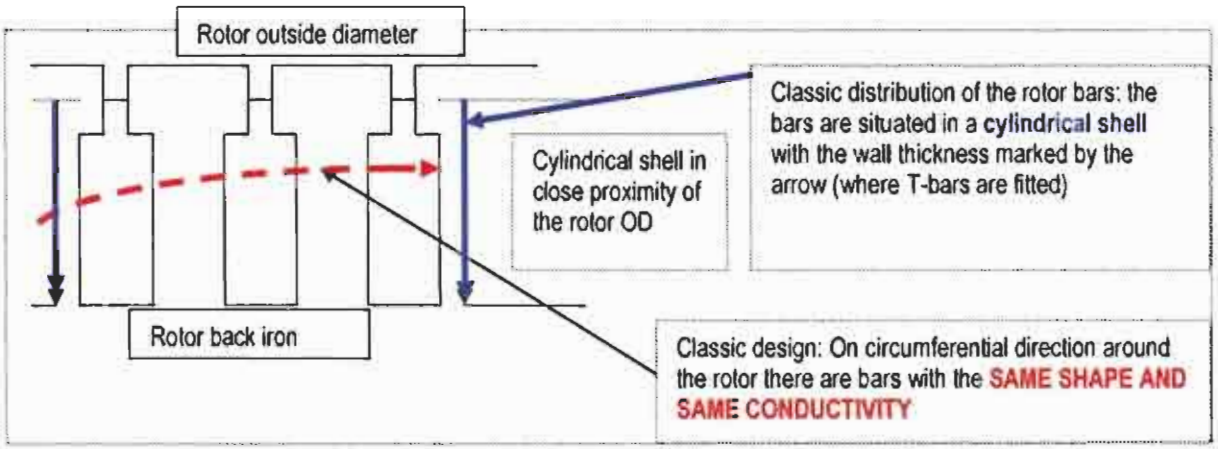

Figure 5.2 Illustration to classic principle no. 1 of the rotor construction

Principle 2: For a double cage rotor bar configuration as shown in figure 5.3, moving around the rotor in a circumferential direction, indicated by the red, dashed arrow, the rotor bars have the same shape and conductivity. However, in the radial direction, indicated by the solid, red arrow, the bars have different shapes and typically different conductivities too.

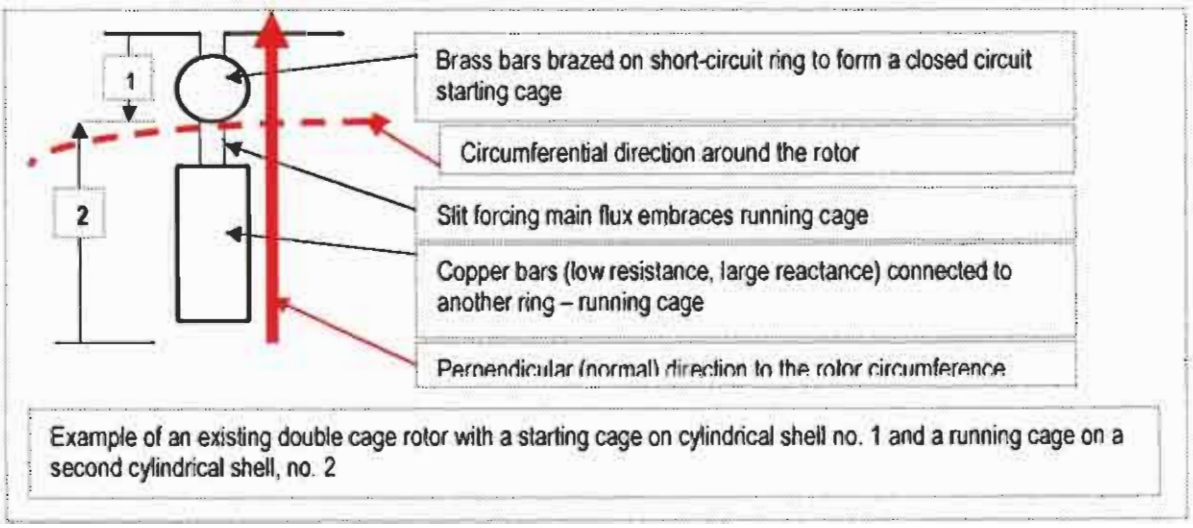

Figure 5.3 Illustration to classic principle no. 2 of the rotor construction

Constructions with deep bars, i.e. rectangular or flat bars, taper bars or sash bars (named T bars), had an increase of effective resistance due to eddy currents. In deep bars, development of eddy loss in bars is proportional to the fourth power of the bar depth, with a considerable increase in resistance being reached at starting when the rotor frequency was high (as presented in paragraph 5.6).

However, the increased slot leakage (an essential factor in the loss of eddy current) adversely affects the power factor and efficiency (lower than that of plain cage).

It would, however, be desirable to be able to provide fabricated rotors with circumferentially different conductivities and/or different profiles.

5.4 Summary of the invention aspects

5.4.1 Main principle of the invention

In broad terms, the present invention provides a rotor for accommodating a plurality of fabricated rotor bars. This plurality of rotor bars together is defining a rotor having **circumferentially different conductivities**. In addition, the rotor bars in the rotor can have the same or different profiles. The invention provides this type of mixed conductivity fabricated rotor.

5.4.2 First aspect of the invention

A rotor is provided with a number of circumferentially spaced slots for receiving rotor bars, wherein circumferentially spaced rotor bars have different conductivities. Preferably, the rotor bars in the rotor have similar cross-sectional profiles.

Alternatively, the rotor bars in the rotor may have different cross-sectional profiles.

Typically, adjacent rotor bars or another periodic combination of rotor bars have different conductivities. Conveniently, the circumferentially spaced rotor bars comprise at least two different conductivities.

5.4.3 Second aspect of the invention

A rotor is provided with a number of circumferentially spaced slots for receiving rotor bars, wherein circumferentially spaced rotor bars have different profiles. Preferably, the rotor bars in the rotor have different conductivities.

Typically, adjacent rotor bars or another periodic combination of rotor bars have different conductivities. Conveniently, the circumferentially spaced rotor bars comprise at least two different conductivities.

5.4.4 Third aspect of the invention

A kit of the parts for the rotor is provided, the rotor having a number of circumferentially spaced slots for receiving bars, and the kit comprising a number of rotor bars with different conductivities.

5.4.5 Fourth aspect of the invention

A kit of the parts for a rotor is provided, the rotor having a number of circumferentially spaced slots for receiving rotor bars, and the kit comprising a number of rotor bars with different profiles.

5.5 Description of preferred versions of the patent

Currently, adjacent, circumferential rotor bars situated in the same cylindrical shell of the rotor have different conductivities; typically at least two conductivities. In addition, the rotor bars can have either the same or different profiles.

5.5.1 Description of the first version – MCFR 1

In the MCFR 1 the MCFR has rotor bars with the same profile, but with different conductivities, resulting in a rotor with circumferentially varying rotor bars.

The fitted bars in the rotor slots have the same shape, but are manufactured from materials with different conductivities.

The bars are fitted either alternatively or in any other periodic combination, for example one bar of material with conductivity c1, one bar of material with conductivity c2, one bar of material with conductivity c3, etc., or: a number of bars with conductivity c1 and then a number of bars with conductivity c2, etc., repeating the sequence periodically.

In this version, there are two, three or more cages in the same cylindrical shell of the rotor with the same bar profile, but with different conductivities.

Typically, the bar with the highest conductivity would be used for the "running" cage, as described above in the double cage rotor; bars with the lowest conductivity would be used for the "starting" cage, and other, intermediate conductivities will be used in the intermediate period between starting and running.

The simplest version of the MCFR 1 has bars with the same shape but two different conductivities fitted in an alternative sequence, as shown in figure 5.4.

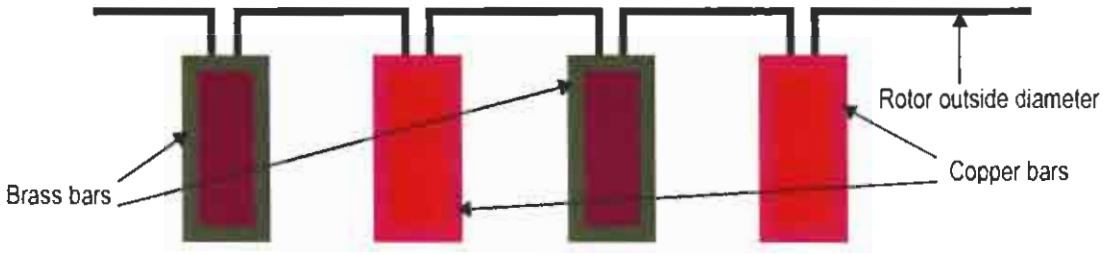

Figure 5.4 Schematic diagram of one of the simplest versions of the MCFR1

This will create a "mixed conductivity" accepted by the stator as an average conductivity of copper and brass bars.

5.5.2 Description of the second version – MCFR 2

In the MCFR 2, the embodied rotor bars have different profiles and different conductivities.

Thus, in this version, in the same cylindrical shell slots are stamped alternatively or periodically with different profiles in which bars with different conductivities are fitted. There are also two or more cages in the same cylindrical shell with different slot profiles and different conductivities.

5.6 Mathematical expressions of flux density and current density variation in "deep bars"

The ideal motor should have a varying secondary (rotor) resistance, which is large at standstill, and decreases as the speed rises [13].

The MCFR was designed to perform such resistance variations. Standard components are used with preference for deep and narrow bars with various conductivities.

If a squirrel cage bar is made very deep and narrow, as shown in figure 5.5, the bar current will have different densities, function of induced voltage frequency, at different bar levels [3], [14].

The main flux path that saturates is the tooth-tip slot leakage, particularly in the case of semi-closed slots and open slots with magnetic wedges [15] (see also paragraph 3.5.2).

Differential leakage flux is a higher space harmonic flux that does not involve torque, producing flux linkages and therefore contributes to the overall leakage flux [16]. In a cage rotor, the currents can balance the stator currents at every point without restrain, so that differential leakage vanishes except for those space harmonics whose wavelength is comparable with the slot-pitch [4]. This property was used by the MCFR invention. Most sources define belt leakage and zigzag leakage as the main differential leakage components, but it is important to appreciate that zigzag leakage is effectively of the same frequency as the fundamental [17].

In a rough calculation we assumed that the current in the bar was producing a leakage flux considered to have a path straight across the slot and around the iron at the bottom of the slot.

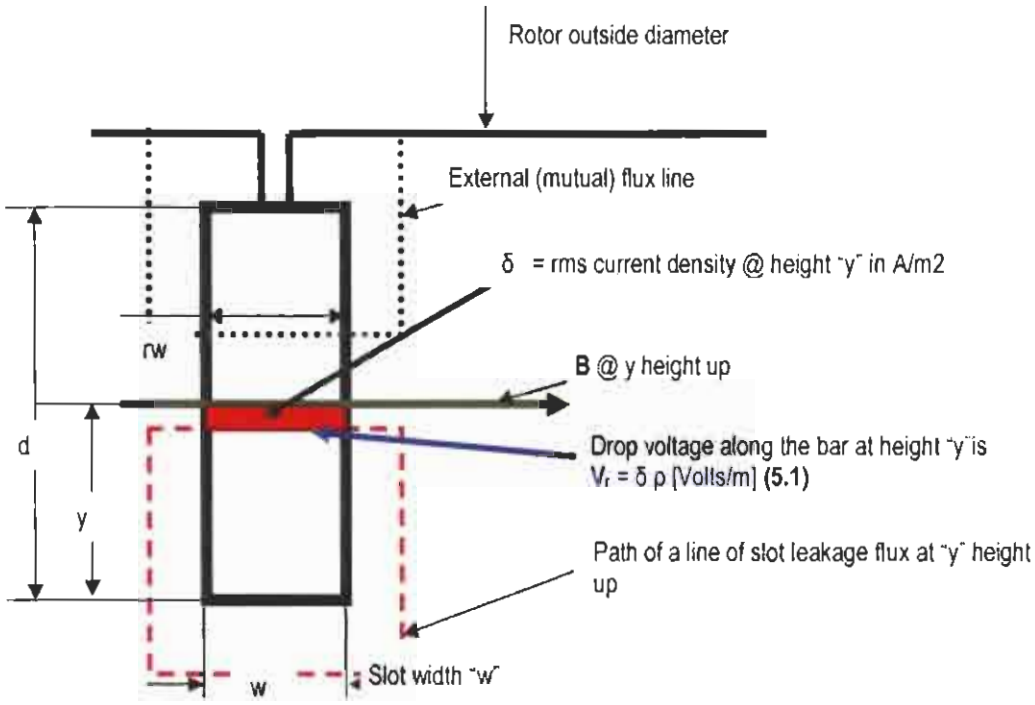

Figure 5.5 Cross-section of a deep bar linked by a leakage flux

The flux, at height "y", only links the lower part of the conductor and contributes to the induction of that part only. It is obvious that such a flux has a lower density than in the tooth lips area, as only a fraction (y/d) of the current is available to provide the mmf necessary for this flux.

Consider the following:

d = depth of the bar in meters

w = width of the slot in meters

r = ratio of the bar width to the slot width

f = frequency in Hertz

ρ = resistance of the bar material in Ohm - meters

$I_b = \sqrt{2}\, I \sin 2 \Pi f t$ = total current in the bar in A

y = distance up from the bottom of the bar in meters

B = rms flux density across the slot at height "y", in Webers/m2 [Tesla]

$\mu o = 4 \Pi (10^{-7})$ permeability of free space in H/m

δ = rms current density at height "y" in Amperes/m2

R_{dc} = ρ/wd Ohms/meter of axial length

E = Induced voltage in Volts/meters of bar axial length

In this specific case, the current density at the height y is the net voltage (impressed voltage V minus induced voltage E) divided by bar resistance:

$$\delta = \frac{V - E}{\rho} \quad [A/m2] \qquad (5.2.a)$$

or:

$$V = \delta \rho + E \qquad (5.2.b)$$

The rms voltage induced by rms flux linking the bar filament at the height y can be calculated by supposing a sinusoidal variation of this flux Φ:

$$\Phi = \Phi_m \sin 2 \Pi f t$$

According to Lenz's law (as shown in figure 5.6)

$$E = - [d \Phi/dt] = - 2 \Pi f \cos 2 \Pi f t = 2 \Pi f \sin [2 \Pi f t - \Pi/2]$$

$$E = - j 2 \Pi f \Phi \qquad (5.3)$$

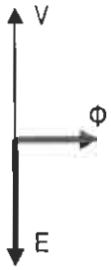

Figure 5.6 Phasor diagram of the mutual flux and induced voltage

The flux linking the bar is:

$$\Phi = \int_y^d B \, dy \qquad (5.4)$$

Where, the rms flux density B across the slot at the height y is:

$$B = \frac{4 \Pi r}{10^7} \int_0^y \delta \, dy \qquad (5.5)$$

Introducing equation 5.4 in equation 5.3, the result is:

$$E = - j 2 \Pi f \Phi = - j 2 \Pi f \int_y^d B \, dy \qquad (5.6)$$

The first derivative of equation 5.2.a gives:

$$d \delta / d y = - [d E / d y] / \rho$$

By using the relation between induced voltage E and flux density B according to equation 5.6, the result is:

$$\mathbf{d\,\delta / d\,y = j\,2\,\Pi\,f\,B / \rho} \qquad (5.7)$$

The first derivative of equation 5.5 with respect to "y" is:

$$d\,B / dy = 4\,\Pi\,r\,\delta / 10^7 \qquad (5.8)$$

The second derivative of equation 5.8 is:

$$d^2\,B / d\,y^2 = [4\,\Pi\,r / 10^7\,] \,.\, [d\,\delta / d\,y]$$

By substituting $d\,\delta / d\,y$ from equation 5.7, the expression of flux density along the slot is:

$$\frac{\mathbf{d^2\,B}}{\mathbf{d\,y^2}} = \frac{4\,\Pi\,r}{10^7} \times \frac{j\,2\,\Pi\,f\,B}{\rho} = \mathbf{2\,j\,\alpha^2\,B} \qquad (5.9)$$

Where $\mathbf{\alpha^2 = [4\,\Pi^2\,r\,f\,] / \rho\,10^7}$

The general solution of equation 5.9 is:

$$\mathbf{B} = P \cosh (1+j)\,\alpha\,y + Q \sinh (1+j)\,\alpha\,y \qquad (5.10)$$

The constants P and Q in equation 5.10 will be determined from the limit conditions [18].

When y = 0 (at the bottom of the slot), there is no flux density linking the bar, so B = 0

The result is P = 0

When y = d (at the top of the slot), according to $B = 4\,\Pi\,I / w\,10^7$, where:

$$4\,\Pi\,I / w\,10^7 = Q \sinh (1+j)\,\alpha\,d$$

$$Q = [4\,\Pi\,I / w\,10^7] / [\sinh (1+j)\,\alpha\,d]$$

The general solution of flux density variation along the slot in a "deep bar" is:

$$\mathbf{B} = \frac{\mathbf{4\,\Pi\,I}}{\mathbf{w\,10^7}} \times \frac{\mathbf{\sinh (1+j)\,\alpha\,y}}{\mathbf{\sinh (1+j)\,\alpha\,d}} \quad \mathbf{[Wb / m^2]} \qquad (5.11)$$

By substituting equation 5.11 in equation 5.7: $d\,\delta / d\,y = j\,2\,\Pi\,f\,\mathbf{B} / \rho$

The result:

$$d\,\delta / d\,y = \frac{j\,2\,\Pi\,f}{\rho} \times \frac{\mathbf{4\,\Pi\,I}}{\mathbf{w\,10^7}} \times \frac{\mathbf{\sinh (1+j)\,\alpha\,y}}{\mathbf{\sinh (1+j)\,\alpha\,d}}$$

Integrating in both members of the equation:

$$\delta = \frac{j\,2\,\Pi\,f\,4\,\Pi\,I}{\rho\,w\,10^{7}} \times \frac{1}{\sinh(1+j)\,\alpha\,d} \times \frac{\cosh(1+j)\,\alpha\,y}{(1+j)\,\alpha} \quad [A/m^2]$$

The general solution of current density variation along the slot in a "deep bar" is:

$$\boldsymbol{\delta = \frac{(1+j)\,\alpha\,I}{r\,w} \times \frac{\cosh(1+j)\,\alpha\,y}{\sinh(1+j)\,\alpha\,d}} \quad [A/m^2] \qquad (5.12)$$

According to equation 5.12, the current density in a "deep bar" is function of:

- Frequency of induced voltage (current), f in Hz
- Bar resistance, ρ in Ohm - m
- Bar depth, d, in m
- Distance up from the bottom of the bar, y in m
- Average bar current, I in A
- Ratio of the bar width to slot width, r (0.91 to 0.925); if r < 0.91, there is a "slack" rotor bar.

The current density given by equation 5.12 may be regarded as the superposition on the uniform (average) current density of a circulating current flowing:

- Additively along the top of the bar
- Subtractive along the bottom of the bar, in such a way that it opposes the cross slot-leakage flux

At full frequency, the current will be crowded toward the top of the bar, increasing the effective resistance.

At full speed, when the slip frequency is very low, the current will be uniformly distributed, giving low resistance.

This could be explained by the fact that the bottom filament of the bar is linked by all the slot leakage flux, whereas the top filament of the bar is linked only by external (mutual) flux.

The additional reactance of the bottom filament causes its current to be smaller and lagging more in time phase than the current in the top filament of the bar.

Equation 5.12 resembles in form the well-known formulae of transmission-line propagation from top to the bottom of the slot [19].

It is possible to build up a formula for the circulating current in the bar by successive approximations.

Step 1: Assume the circulating current is limited solely by bar resistance, i.e. it is too small to reduce the flux crossing the slot significantly.

Step 2: Calculate the cross flux that would be produced by the circulating current (acting alone) calculated in step 1. As a result, a corresponding additional amount of circulating current will be determined.

This process leads to an infinite series of terms, from which the additional RI^2 loss, reduced reactance, etc., can be obtained [5].

A general solution for the effects of the eddy currents on RI^2 loss and reactance can be obtained more directly.

We may assume that the total voltage drop along the bar is a sum of the voltages due to the RI drop and to the linkages produced by the cross-slot flux.

The real component of this total voltage drop along the bar will give the effective resistance of the bar on alternating currents.

The imaginary (j) component of the total voltage drop will give the effective reactance.

As confirmation of the assumptions and previous calculations, let us calculate the RI drop voltage along the bar at any height "y": $\mathbf{V_r = \delta\, \rho}$ in Volts/m (equation 5.1 in figure 5.5).

The average drop over the entire bar is:

$$V_r = \frac{\rho}{d} \int_0^d \delta \, dy \qquad (5.13)$$

By introducing equation 5.12 into equation 5.13, the expression of average drop voltage along the rotor bar is as would be expected:

$$V_r = \frac{(1+j)\,\alpha\,\rho\, I}{rwd} \int_0^d \frac{\cosh (1+j)\,\alpha\, y}{\sinh (1+j)\,\alpha\, d}\, dy$$

$$\mathbf{V_r} = \frac{\rho\, I \sinh (1+j)\,\alpha\, d}{rwd \sinh (1+j)\,\alpha\, d} = \frac{\rho\, I}{rwd} = I\, R_{dc} \qquad (5.14)$$

DC bar resistance in Ohm/length unit: $\mathbf{R_{dc}} = \frac{\rho}{rwd}$ (5.15)

According to equation 5.2.a in which equation 5.3 has been introduced, the total voltage applied to the bar at the height "y" is:

$$\mathbf{V = \rho\, \delta - j\, 2\, \Pi\, f\, \Phi} \qquad (5.16)$$

Introducing in equation 5.4 (relation between the flux linking a circuit and flux density)

$$\Phi = \int_{Y}^{d} B\, dy$$

the general solution of flux density as presented in equation 5.11, the total rms flux crossing the slot above the height y, and, therefore linking the current below y is:

$$\Phi = \int_{y}^{d} \frac{4\,\Pi\, I}{w\, 10^7} \times \frac{\sinh (1 + j)\,\alpha\, y}{\sinh (1 + j)\,\alpha\, d}\, dy$$

$$\Phi = \frac{4\,\Pi\, I}{(1 + j)\,\alpha\, w\, 10^7} \times \frac{\cosh (1 + j)\,\alpha\, d - \cosh (1 + j)\,\alpha\, y}{\sinh (1 + j)\,\alpha\, d} \qquad (5.17)$$

Substituting equations 5.12 (current density) and 5.17 (flux) in equation 5.16:

$$V = \frac{(1 + j)\,\alpha\, I\, \rho \cosh (1 + j)\,\alpha\, y}{rw \sinh (1 + j)\,\alpha\, d} + j\, 2\,\Pi\, f \frac{4\,\Pi\, I \cosh (1 + j)\,\alpha\, d - \cosh (1 + j)\,\alpha\, y}{(1 + j)\,\alpha\, w\, 10^7 \sinh (1 + j)\,\alpha\, d}$$

In the second member of the equation two substitutions can be done:

$$2j / (1 + j) = (1 + j) \quad \text{and} \quad \frac{\alpha^2 \rho}{r} = \frac{4\,\Pi^2 f}{10^7} \qquad (5.18)$$

These relations allowed the cancellation of terms containing cosh (1 + j) α y

The result:
$$V = \frac{j\, 2\,\Pi\, f\, (4\,\Pi\, I) \cosh (1 + j)\,\alpha\, d}{(1 + j)\,\alpha\, w\, 10^7 \sinh (1 + j)\,\alpha\, d}$$

Using substitutions according to equations 5.15 (R_{dc}) and 5.18, it results **expression of the total voltage applied to one rotor bar:**

$$\mathbf{V = I\, R_{dc} \frac{(1 + j)\,\alpha\, d \cosh (1 + j)\,\alpha\, d}{\sinh (1 + j)\,\alpha\, d}} \qquad (5.19)$$

The real portion of equation 5.19 represents the active drop voltage, and therefore the active loss component of the voltage is:

$$\mathbf{V_{real} = I\, R_{dc}} \frac{\alpha\, d\, [\sinh 2\,\alpha\, d + \sin 2\,\alpha\, d]}{\cosh 2\,\alpha\, d - \cos 2\,\alpha\, d} \qquad (5.20)$$

The imaginary "j" part of equation 5.19, representing the reactive component of voltage is:

$$V_{reactive} = j\, I\, R_{dc} \frac{\alpha\, d\, [\sinh 2\,\alpha\, d - \sin 2\,\alpha\, d]}{\cosh 2\,\alpha\, d - \cos 2\,\alpha\, d} \quad (5.21)$$

Consider the product (α d) <1.5 (most probably for low conductivities and low frequencies).

Equation 5.20 will be approximated as [20]:

$$V_{real} = I\, R_{dc}\, \{1 + [4\, (\alpha\, d)^4] / 45 - [16\, (\alpha\, d)^8] / 4.725 + \ldots.\} \quad (5.22)$$

Equation 5.21 will be approximated as:

$$V_{reactive} = j\, I\, R_{dc}\, [2\, (\alpha\, d)^2 / 3] \times \{1 - [8\, (\alpha\, d)^4] / 315 + [32\, (\alpha\, d)^8] / 31.185 + \ldots\} \quad (5.23)$$

Consider the product (α d) >2 (most probably for high frequencies, as 50 to 40 Hz, regardless of conductivity values).

Equation 5.20 will be approximated as:

$$V_{real} = I\, R_{dc}\, (\alpha\, d) \quad (5.24)$$

Equation 5.21 will be calculated as:

$$V_{reactive} = j\, I\, R_{dc}\, (\alpha\, d) \quad (5.25)$$

The last two equations prove that at frequency values of 40 to 50 Hz, the resistance and reactance of deep bar approach the equality.

This is due to the general law of "skin effect": the redistribution of current in a deep bar forced by eddy currents causes R to approach equality with X asymptotically as the frequency increases.

The increase in starting resistance is caused by the reactive voltage that forces the current into a higher-resistance path when the frequency is high.

When the rotor speeds up and the secondary frequency decreases, this voltage declines, and the current assumes its normal path of lower resistance and higher inductance.

In the MCFR, the voltages decline in inverse ratio to the resistance of the bars. This was obtained by computer simulation [21] and was experimentally confirmed by monitoring the rotor's reactance and resistance ratio evolution during the starting period for a 36 kW - MCFR1.

Two sets (identical profile and equal number) of standard bars were fitted into the rotor (copper with conductivity c1= 100 % IACS and brass with conductivity C2 = 27 % IACS). It result a resistance ratio Rbr/Rco = 3.77, for an equivalent conductivity of 63.5% IACS with 50/50 bars weight contribution (N1=N2). The bar length ratio is RL = 1.12, as presented in figure 5.7. From this graph it results the currents distribution between the bars with different conductivities fitted in MCFR1 type.

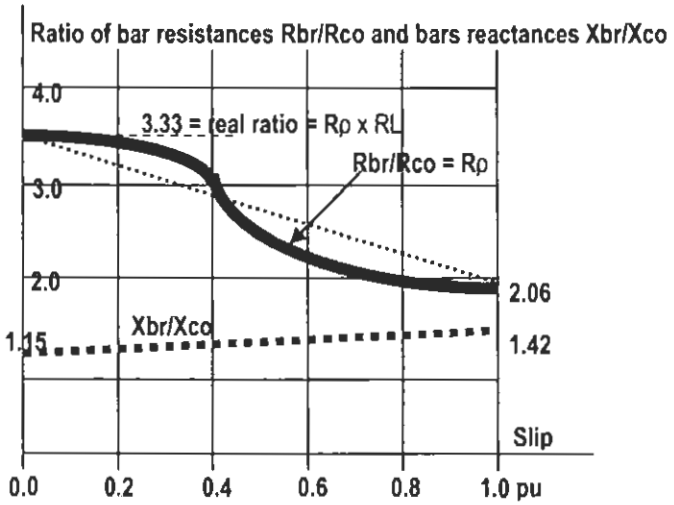

Figure 5.7 MCFR1 reactance and resistance ratio evolution during motor starting

Various authors indicate practical relations to estimate bar current I necessary to be introduced in equations 5.12 and 5.19 to 5.25.

An estimation proposed the bar current calculation as "phase" current of the rotor [22]:

$$I = K_I \left[(2\, N_1\, T_1\, K_{w1}) / Z_2\right] I_{Nom} \qquad (5.26)$$

Where:
- I_{Nom} = Motor rated current
- Z_2 = Rotor bars number
- K_{w1} = Stator winding factor
- T_1 = Stator turns per phase in series
- N_1 = 3-phases of the stator
- K_I = 0.8125 (cos φ) + 0.203125

K_I is a factor with an estimated value function of the motor power factor. It takes into consideration the influence of the magnetization current of the motor because the stator and the rotor ampere-turns are perfectly equal.

Another bar current estimation was proposed by considering motor shaft mechanical power P_{Nom} [23]:

$$I = K_{rot} \left[(P_{Nom} / T_2\, E_2\right] \qquad (5.27)$$

Where K_{rot} = 1.08...1.14 is a coefficient taking in account all the approximations, function of the motor rated power (for medium and large machines K_{rot} = 1.1)

The rotor e.m.f $E_2 = 4.44\, K_{w2}\, s\, f\, T_2\, \Phi$

Where:
- T_2 = Rotor bars number
- K_{w2} = 1 (for squirrel cage rotors)
- Φ = Mutual flux of the machine
- s = slip
- f = frequency

5.7 The MCFR's operating principle

The explanation is based on the supposition that deep rectangular bars are used (as shown in figure 5.4). The preference for standardised "deep bars" types and standard materials has been justified by the required rotor, motor performances and cost price, especially

At starting and very low speeds, because of the skin effect, the current in the rotor bars is confined to the top of the bars, and distributed between the high conductivity and low conductivity bars in proportion to the conductivity of these bars (see equation 5.12 of current distribution in a deep bar). As a result, high currents are expected on the high conductivity bars, thereby increasing their temperatures and their resistance in order to reach the resistances of the low conductivity bars.

All rotor bars will perform high resistances and at the high frequencies the rotor will be regarded as a high impedance rotor type, with a very solid "starting cage" (made of rectangular bars).

The high conductivity bars are more thermally stressed, with their temperature increasing at a much higher rate than the temperature of the lower conductivity bars. Their resistance tends to reach the low conductivity bars' resistance during motor's stall conditions

Taking this principle into consideration, adjustable starting torque and starting current values can be obtained in relation to the conductivity ratio of the bars.

At the normal running speed, the rotor current frequency is low and, in accordance with Ohm's law, the bars will carry the rotor current.

The rotor behaviour therefore simulates an arrangement in which high conductivity bars "short-circuit" the low conductivity bars.

At low frequencies, the rotor will be regarded as an energy efficiency rotor type.

The high conductivity bars tend to raise asymptotically their temperature faster, in order to reach the resistances of the low conductivity bars (tending to equalize brass bars resistance). This is depending by general thermal constant of the rotor. When bars resistances are equalised, the rotor presents a balanced electric circuit (when the motor is rated continuous – S_1). If the motor runs intermittently, the electric circuit of the rotor will still have bars of different resistances.

Thus, by using different bar conductivities, shapes and lengths, the starting torque, pull-up torque, pull-out (breakdown) torque and full-load torque (in conjunction with corresponding speeds) can be adjusted to meet load requirements.

Consider again two sets of standard bars (copper with conductivity c1= 100 % IACS and brass with conductivity C2 = 27 % IACS) with resistance ratio **Rbr/ Rco = Rp = 3.77** fitted into MCFR1 as mentioned in figure 5.7. The copper bars number is equal to brass bars number (**N1 = N2**). The bars length ratio is **RL = 1.12.**

During the starting period (higher frequencies), the current distribution in the rotor bars will be influenced by the leakage reactance.

At full speed, current distribution in the rotor bars will be in inverse proportion to the bar resistances and in various cross-sections. That means:

- During starting period, brass bars will have a major contribution towards rising the starting torque due to I^2R losses;
- At full load, the rotor currents will circulate mainly through copper bars in order to bring their resistance value closer to that of brass bars (distribution in inverse proportion to bar resistances), while the ratio of the current values in brass bars will be estimated as:

$$\mathbf{1: \{½\,[c1 + c2] \times R\rho \times RL\}}$$

When the **motor re-starts**, the brass bars will be available again at a lower temperature (low values of I^2R losses during full load). As a result, the rotor comportment will be close to a denominated **"cold rotor" situation**.

That is why this rotor can keep the starting torque very constant even after the motor reaches its thermal stabilised "HOT" condition!

5.8 Mathematical equations of the MCFR1 model

5.8.1 Slip equation

It has been found that the full load speed of an MCFR1 is closer to the speed of a normal copper rotor and, as a result, efficiency is slightly higher than expected for this type of "composite" rotor.

However, the root average rule on slips applies.

$$S^2_{mcfr} = S_{copper} \times S_{brass} \tag{5.28}$$

Where:

S_{mcfr} = MCFR slip [r/m]

S_{copper} = Copper rotor slip [r/m]

S_{brass} = Brass rotor slip

For example [11]:

- For copper bars, the rotor configuration Nnom = 1490 r/m, S_{copper} = 10 [r/m]
- For a brass bars, the rotor configuration Nnom =1462 r/m, S_{brass} = 38 [r/m]

By applying equation 5.28, the result is S_{mcfr} = 19.5 [r/m]

The MCFR version presented above will have Nnom = 1480.5 r/m

5.8.2 Starting torque equation

The starting torque value on the MCFR configuration (St. Tq.) can be calculated as:

$$\textbf{St.Tq.} = [\Sigma\ \textbf{St.Tq.i x Ni}] / \Sigma\ \textbf{Ni} \qquad (5.29)$$

In this specific case

$$\text{St. Tq.} = [\text{St.Tq. co} + \text{St.Tq. br}] / 2$$

Where:

St.Tq.co = starting torque in a copper rotor configuration

St.Tq.br =starting torque in a brass rotor configuration

5.8.3 Starting current equation

The starting current for this configuration can be calculated as an average of the starting currents of a copper rotor and a brass rotor respectively:

$$\textbf{St.Crt} = [\Sigma\ (\textbf{St.Crt.i x Ni})] / \Sigma\ \textbf{Ni} \qquad (5.30)$$

In this specific case [11], with N1 = N2 and RL = 1.12, the values are:

- Starting current for a brass rotor is 6.60 x Inom
- Starting current for a copper rotor is 8.20 x Inom
- According to equation 5.30, starting current for a MCFR1 will result 7.40 x Inom

5.8.4 Breakdown torque (POT) and slip value equations

The breakdown torque or pull-out torque (POT) value is related to the rotor design. For example [11], by using deep trapezoidal bars configuration in a specific position and slot profile, POT values are above 3.05 pu x FLTq.

The slip value where the pull-out torque occurs can be calculated according to equation 5.28 as well:

- POT for a brass rotor = 3.1 pu @ 0.213 slip value
- POT for a copper rotor = 3.1 pu @ 0.045 slip value
- POT for an MCFR = 3.1 pu @ 0.098 slip value

5.8.5 Run up time equation

Motor run up time (Rut) on the MCFR1 configuration is approximately the arithmetic average of the run up time values of a brass and a copper rotor, respectively.

$$Rut_{mcfr} = [Rut_{copper} + R_{brass}] / 2 \qquad (5.31)$$

Where:

Rut_{mcfr} = motor run up time in an MCFR1 configuration

Rut_{copper} = motor run up time in a copper rotor configuration

R_{brass} = motor run up time in a brass rotor configuration

5.8.6 Maximum stall time equation

Duration of the maximum stall time (Mst) is an average value between the stall time of a copper rotor and a brass rotor, respectively.

$$Mst_{mcfr} = [Mst_{copper} + Mst_{brass}] \quad (5.32)$$

Where:

Mst_{mcfr} = Duration of motor stall time in the MCFR1

Mst_{copper} = Duration of motor stall time in a copper rotor

Mst_{brass} = Duration of motor stall time in a brass rotor

5.8.7 Rotor bars temperature rise during starting, equation

During the starting time period, the **bars temperature rise Tb** for the **MCFR1 N1=N2, Rρ = 3.77, RL = 1.12** [11] can be calculated as:

$$\frac{1}{Tb} = \frac{1}{Tco} + \frac{1}{Tbr} \quad (5.33)$$

Where:

Tco = Temperature rise of rotor bars when copper rotor bars are fitted only

Tbr = Temperature rise of rotor bars when brass rotor bars are fitted only

5.9 References

1. Pitis C.D.; Provisional patent registered as "Mixed Conductivity Fabricated Rotors – MCFR" patent registration no. 6886, Spoor and Fisher, Johannesburg, August 2004.
2. Pitis, C.D.; "Mixed Conductivity Fabricated Rotor", South African Patent No. 2005/07280, Johannesburg, Sept. 2005.
3. Alger, P.L.; "Induction machines – Their Behavior and Uses", 2nd Edition, Gordon & Breach Science Publishers, N.Y. USA, pp. 261–286.
4. Say, M.G.; "Performance and design of alternating current machines", 3rd Edition, Isaac Pitman & Sons, London, 1983, pp 300–320.
5. Gheorghiu, I.S.; "Electric Machinery – Problems and industrial uses", 2nd Edition, Volume I and II, Technical Publishers, Romania, 1966.
6. Richter, R.; "Electric Machinery – Asynchronous motor", Vol. IV, Translation from German, Technical Publishers, Romania, 1960.

7. Piotrovsky, L.M.; "Electric Machinery", Translation from Russian, Electroenergetics Publishers, Romania, 1953.
8. Pitis, C.D.; "Mixed Conductivity Fabricated Rotor" presented as "Alternative method of squirrel cage design and replacement", South African Rotating Machinery Working Group, L.H. Marthinunsen, Johannesburg, 15th June 2005 (see also Annexure 5.1).
9. Pitis, C.D.; "Electric Motors Life Extension by Renewal of Squirrel Cage Rotors", Proceedings of International Conference: "Industrial & Commercial Use of Energy", Cape Town, 2005, pp 87–3.
10. Pitis, C.D.; "Alternative method of squirrel cage design and replacement", Electricity + Control, Sept. 2005, pp 4–7.
11. Pitis, C.D.; "A consideration of how to adjust the performance of MV squirrel cage motors during rebuilding", Electricity + Control, January 2006, pp 22–24.
12. Pitis, C.D.; "Method of adjusting direct-on-line starting performances of squirrel cage induction motors", Vector, August 2005, pp 22–27.
13. Lloyd, T.C., Giusti, V.F., Chang, S.L.; "Reactances of Squirrel-Cage Induction Motors", A.I.E.E. Transactions, Vol. 66, 1947, pp 1 349–1 355.
14. Adams, C.A.; "The Leakage Reactance of Induction Motors", Transactions of International Electrical Congress, St. Louis, USA, 1904, Vol. I, 1905, pp 706–724.
15. Veinott, C.G.; "Performance calculations on Induction Motors", A.I.E.E. Transactions, Vol. 51, Sept. 1932, pp 743–754.
16. Norman, H.; "Induction motor locked saturation curves", Transactions AIEE, 53, 1934, pp 536–541.
17. Hellmund, R.E.; "Zigzag leakage of Induction Motors", A.I.E.E. Transactions, Vol. 26, Part II, 1907, pp 1 504–1 524.
18. Stroud, K.A.; "Engineering Mathematics – Programs and Problems" 10th Edition, Chapter 21 to 24, Macmillan Press Ltd, London, 1981.
19. Say, M.G.; "Alternating Current Machines", Chapter 8, 5th Edition, Longman Scientific and Technical, Singapore Publishers, 1995.
20. Davies, H.G., Hicks, G.A.; "Mathematics for Scientific and Technical Students", 4th Edition, Chapter 10 to 12, Longman Group Ltd., London, 1978.
21. Landy, C.F., Meyer, A.; "Squirrel cage motors design program – SCDES2", Witwatersrand University, Johannesburg, 1998.
22. Cioc, I., Nica, C.; "Design of Electric Machines", Chapter 10, Didactic and Pedagogic Publishers, Bucharest, Romania, 1994.
23. Fransua, Al. S., Magureanu, R., Tocaci, M.; "Electric machines and drives, with solved problems", Chapter 6, Didactic and Pedagogic Publishers, Bucharest, 1980.

CHAPTER 6: DESIGN AND MANUFACTURING PROCESS OF THE MCFR

The design and manufacturing process of the MCFR is based on a registered patent [1], [2].

Over the years, a 36 kW spinner motor used by Voest Alpine Mining and Tunneling was a challenge for various manufacturers. Only in South Africa VAMT spent R5 million annually in periodically (1.5 to 2 years) replacing die cast aluminium rotors for this specific motor.

Main steps in designing the MCFR1 for new motors and re-designing an aluminium rotor to become an MCFR1 are based on theoretical notes presented in Chapter 5. A complete design of the MCFR1 is presented with drawings and photos taken during the manufacturing process.

Investigations regarding the MCFR1's condition after 1.8 years' continuous running underground are part of the project-design validation and verification. It was confirmed that, as a novel rotor solution, the MCFR has a sound design, representing a reliable long-term solution.

6.1 Basic conditions and inputs for new the design

For more than a decade, a specific motor used in the coal-mining industry was a challenge for repairers, manufacturers and mines, mainly because of the rotor's reliability and performance in harsh mining conditions (quality of power supply, user's unusual operating conditions, etc.).

One of the general requirements was that a new locally designed motor was to have equal or better performances under starting conditions than the original motor.

The design and manufacturing of the MCFR1 is based on a customer's request to replace an imported aluminium rotor with a local, more reliable fabricated rotor, for a 36 kW, 1000 V, 4-poles gathering arm motor (GAM) and conveyor motor (CM) powering the continuous miner in the coal-mining industry.

A new 36 kW spinner motor, the MCFR1, was designed that challenged the price as well (see Annexure 6.1).

Spinner motors work in tandem, for example, if a motor with a copper rotor is fitted with a motor with an aluminium rotor, there will always be a shift on either the starting or the running conditions, as presented in figure 5.1.

Eventually, one of the motors will burn out, depending on the predominant working conditions (continuous running or frequent starting) imposed by the operator.

Keeping the motor performance in as close range as possible to that of the original aluminium rotor is a very important condition for this specific application.

An electric squirrel cage motor design program was used for electromagnetic design calculations [3]. The program enabled simulating the various states of the motor:

- No load, cold and hot
- Normal running conditions on various loads
- Starting conditions on saturated and unsaturated voltages
- Temperature rise assessment on the motor's active materials

The electric motor's geometrical sizes were kept the same (stator outside and inside diameter, core length, air gap, stator and rotor slot combination).

The design competed successfully against five other different rotor manufacturers using various materials for the rotor bars.

- Aluminium rotor, manufactured by Loher, Germany as shown in photo 6.1
- Aluminium rotor, manufactured by DAMEL, Poland, as shown in photo 6.2

Photo 6.1 Rotor manufactured by Loher (Flender), Germany

Photo 6.2 Rotor manufactured by DAMEL, Poland

- Copper rotor, manufactured by Custom Electric Motors (Cullinan Electric)
- Double cage rotor, manufactured by TECO
- Brass cage rotor, manufactured by Luck & King, South Africa, as shown in photo 6.3

Photo 6.3 Rotor manufactured by Luck & King, RSA

The design approach in manufacturing the MCFR1 was to obtain a complete spinner motor fitted with an MCFR1. The project serial number was FMM 0072 [4].

6.2 Initial data required for the MCFR

The optimum MCFR1 can be obtained by a number of iterations.

Initial data is introduced based on a resistance evaluation of rotor bars that is determined by:

- Bars length **(L)**
- **Cross-section and profiles** of the rotor bars
- Material **conductivities**

The **bars length (L)** is determined by:

- Core length related to output power coefficient $G = kW/D^2Ln$ where D = air gap diameter, L = core length, n = motor speed.
- Overhang of rotor bars (used for fine adjustments of starting and running conditions)
- Specific motor requirements (speed torque curve of existing rotor to be replaced)

The cross-sectional area and profiles of rotors bars and short-circuit rings necessary to obtain acceptable performances of the motor in different states are determined by:

- Required motor performances (speed-torque curve) including starting, running, pull-out torque and pull-in torque
- Motor's specific magnetic and electrical loading
- Motor and rotor temperature rises
- Current densities in rotor bars and short-circuit rings

Material conductivities are decided by a number of iterations starting from high conductivity (IACS 99%) to the lowest conductivity (IACS 7%) corresponding to ISO normalised values.

The concept of the rotor bar average conductivity $C_{av.b}$ indicator was introduced as a result of the mixed conductivities number as an integer divider number of rotor bars number as presented in table 6.1.

Table 6.1 Initial estimations of $C_{av.b}$ used in new design situations

No.	Bars profile	Conductivities	C.av.b =
1	Same	2 different	= [C1 + C2} / 2, where C1 (C2) = conductivity of bar no. 1 (2)
2	Same	N different	= [Σ Ci] / N, where i = 1...N and Ci is conductivity of bar "i"
3	Different	2 different	= [C1 x S1 + C2 x S2] / 2 where S1(S2) = cross-section of bar no. 1 (2)
4	Different	N different	= [Σ (Ci x Si)] / N, where i = 1...N and Ci is conductivity of bar "i" Si is cross-section of bar "i"

First assessment of the existing rotors must be referred to: slots number (N_{Rotor}), aluminium rotor bars cross-section or profile (S_{al}) and conductivity, motor duty and special customer requirements.

6.3 Main steps in designing the MCFR

Suppose a die cast aluminium rotor with 38 slots with a slot shape as no. 6 (shown in figure 3.4 and figure 6.1) to be replaced with a MCFR having new bars made of brass/copper or other materials, with a rectangular shape (using "deep-bar" effect).

The following main steps in designing the MCFR1 must be considered:

Step 1: Determine the number of bars of the aluminium rotor: N_{Rotor} = 38. The rotor slots number is divisible by 1, 2, and 19. Number 1 cannot be considered because there's no sense in replacing (it seeing that it is a classic replacement already on the market).

Number 2 is to be considered. There will thus be two different conductivities in the new MCFR: C1 and C2.

Step 2: Determine the old bar conductivity of the aluminium rotor C_{al} by direct measurement or by analyzing material composition.

Step 3: Determine the new bar width W:

$$W = \frac{\Sigma_i Wi}{N} \qquad (6.1)$$

Where i = 1 to 4, the different widths of the original aluminium bar shape, and N = 4

Step 4: Determine the new bar depth from using the cross-section equation and ratio conditions of deep bar sizes:

$$S_{new} = W \times D = S_{al} \qquad (6.2)$$

where S_{new} is the cross-section of the new bar, W is the bar width and D is the bar depth.

Step 5: Determine the new bar conductivities using equation 6.3 derived from table 6.1:

$$[C1 + C2] / 2 = C_{al} \quad (6.3)$$

For the first iteration C1 = C_{copper} existing on the market.

For example if C_{al} = 63% IACS is given, and choose C_{copper} = C1 = 99% (existing on the market).

According to equation 6.3, C_{brass} = C2 = 27% (existing on the market).

Conclusion: When replacing a 38-bars die cast aluminium rotor of 63 % IACS conductivity, with a MCFR rotor with two set of bars, there will be a combination of two conductivities: brass bars 27% IACS conductivity, 19 off and copper bars 99% IACS conductivity, 19 off.

However, based on current densities and flux densities conditions, it was decided that the new designed motor, FMM 0072, would have a rotor slot number = 58 slots.

As a result, in designing the MCFR1 a combination of two conductivities was chosen: brass bars 27% IACS conductivity, 29 off, and copper bars 99% IACS conductivity, 29 off. These bars will be alternatively inserted into the rotor (as shown in figure 5.4 and photo 6.5). This will create a "mixed conductivity" accepted by the stator as an average conductivity.

The new bars may be a rectangular with the width W according to equation 6.1 and depth D according to equation 6.2. The simplest 3 x 25 mm rectangular bars available on the market were used for the MCFR1 – as per rotor slot profile no. 1, shown in figure 3.4.

Evaluation of the effects of the eddy currents on Joule loss and reactance of the "deep bars" were discussed in paragraph 5.6.

Step 6: The diameter of the short-circuit rings is decided by:

- Bars depth D
- Cross-section S_{shc} to achieve a required current density = $\frac{I_{shc\ (calculated\ by\ program)}}{S_{shc}}$

From experience and recommendations in literature [5], [6], for the first iteration, current density in the short-circuit rings = 0.75 x current density in the bars.

Step 7: Verification of thermal elongation applies for different types of material used to manufacture the rotor bars:

$$L = Lo\,[1 + \alpha\,\Delta\,T] \quad (6.4)$$

Where:

L is bar length @ final temperature T

Lo is the bar length @ ambient temperature T_0

α is the elongation coefficient

$\Delta T = T - T_o$

The difference in the elongation of the different conductivity bars can be calculated:

$$\Delta L = L_{copper} - L_{brass}$$

A condition for a unique short-circuit ring is that ΔL is smaller than 0.1–0.2 mm

Step 8: Verification of resistance variation:

$$R = Ro\,[1 + \delta\,\Delta T] \tag{6.5}$$

This applies for different types of material, say, copper and brass, where

$$R = \rho\, l / s \tag{6.6}$$

R = bar resistance at temperature T

Ro = bar resistance at temperature T_0

ρ = material resistivity

l = bar length

s = bar cross-section

δ = coefficient of resistance variation with temperature

$\Delta T = T - T_0$

By running the entire motor design on a computer for old and new designs, the following results have parameters have to be monitored for the different states of the motor:

- Torque, speed and current
- Magnetic and electric loadings
- Motor and rotor temperature rise
- Thermal elongation of the rotor bars and conductivity variation with temperature
- Motor efficiencies and power factors
- Performance deviation on specified ranges

The slot opening and lips will be an adjusted in further iterations, function of the required motor performance and strength of material (withstanding to centrifugal forces).

6.4 Main steps in re-designing an aluminium rotor

Based on previous experience, an aluminium rotor has been redesigned [7] to create an MCFR1.

The customer regarded replacing the rotor with a manufactured rotor (with identical performances) as a cheap technical, reliable and economical solution.

- New, fabricated rotors must run in existing stators with no alteration of rated motor performances.
- The cost of the new rotor must compare to the up-dated price of cast aluminium rotors.
- New rotors must have an extended life expectancy with no alteration of the major performances.

In addressing these requirements, it was found that the main problems reside in adjusting the motor breakdown torque (POT) and DOL starting performances to the given rated values. Calculations followed compulsory steps:

Step 1: The reference data was obtained by simulating, on computer, the running condition of old squirrel cage motors fitted with aluminium cast rotors [3].

Step 2: Keeping the same slot combinations (60/50) and using standard copper bars (100% IACS conductivity), the program must simulate the motor systems with different fabricated rotor slot profiles (and position) until the optimum solution is found (as shown in figure 6.1). Motor pull-out torque is decided during this process.

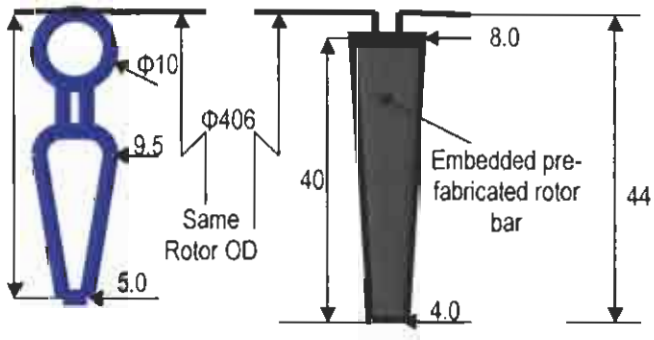

Blue: Aluminium rotor slot profile
Green: Fabricated bar rotor slot profile

Figure 6.1 Initial cast aluminium and fabricated bar rotor slot profiles

Step 3: The rotor core slots number **Nr** and profiles have to be designed according to general conditions and specific customer enquiries.

The proposed MCFR1 type to be used must have the following characteristics:

- Number of bars with different conductivities (N1/N2/N3/.), **Σ Ni = Nr** = 50 bars
- Ratio of conductivities **Rρ** (ρ1/ ρ2)
- Ratio of homogenous groups bars length **RL** (L1/L2)
- Short-circuit rings sizes (2 x 700 sq.mm) and conductivities based on current densities.

Step 4: By using different ratios of N1/N2 = constant, the conductivity ratio **Rp** can vary in steps, according to values already on the market.

Step 5: The rotor bars length ratio **RL** is used for fine adjustment of rated speed.

Equations 6.1 to 6.6 shall apply.

It is obvious that steps 3, 4 and 5 will be repeated in different sequences in a continuous step-by-step iteration process to reach the optimum solution.

Step 6: The running conditions of the motor will be simulated with different MCFR1s until the perfect match to the required motor performances is achieved. By concept, the MCFR allows a large range of alterations to motor performance.

For this specific application, an MCFR1 type was chosen in three repetitions with equivalent conductivities of 85%, 71% and 63% IACS. In Annexure 6.2 comparative rated values and other calculated values for major steps taken during rotor re-design are presented:

- No.1 = initial aluminium cast rotor
- No.2 = fabricated rotor with embedded standard copper bar (100% IACS conductivity); design chosen on pull-out torque conditions
- No. 3a = MCFR equivalent conductivity of 85%
- No. 3b = MCFR equivalent conductivity of 71%
- No. 3c = MCFR equivalent conductivity of 63% – final

The comparative table presented in Annexure 6.2 indicates that only electric motors fitted with an MCFR1 performs just as well when compared to the performance of the original cast aluminium rotor (speed, efficiency, power factor and starting conditions).

6.5 MCFR1 design for a new 36 kW spinner motor

6.5.1 Stator lamination design

The stator lamination design is shown in figure 6.2.

The bottom slot profile is characteristic for high-torque motors. It also represents a balance between magnetic loading and electric loading.

Tolerances on stator OD sizes are essential in order to ensure good heat transfer from the stator core to the water jacket.

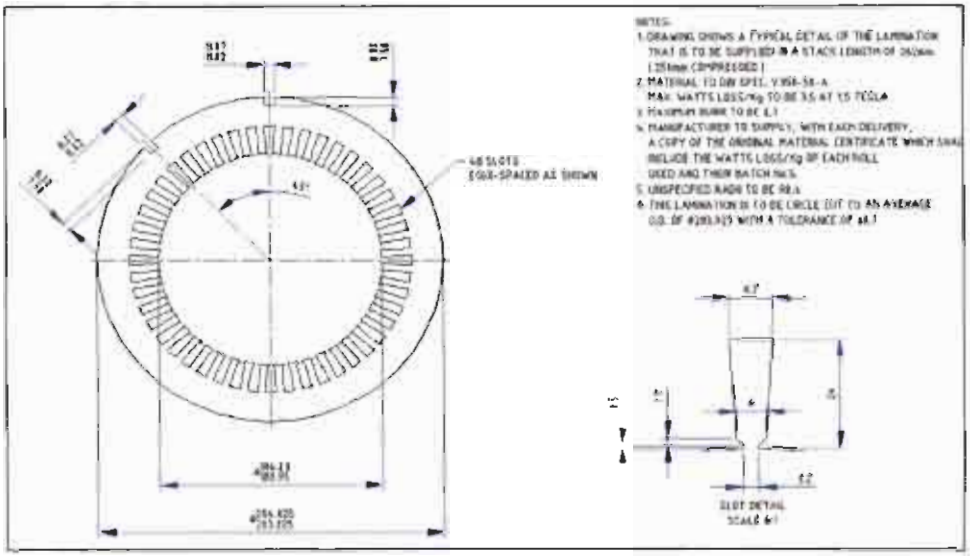

Figure 6.2 Stator lamination design for 36 kW spinner motor

6.5.2 Rotor lamination design

The rotor lamination design for the MCFR1 is shown in figure 6.3.

The preference for "deep bars" has been theoretically justified in Chapter 5.

Throughout the electric design, the production of eddy currents is only encouraged partially in deep solid bars with width = rw, and depth = d situated in the same cylindrical shell. The bars participate with different torques function of their conductivities and motor states [8].

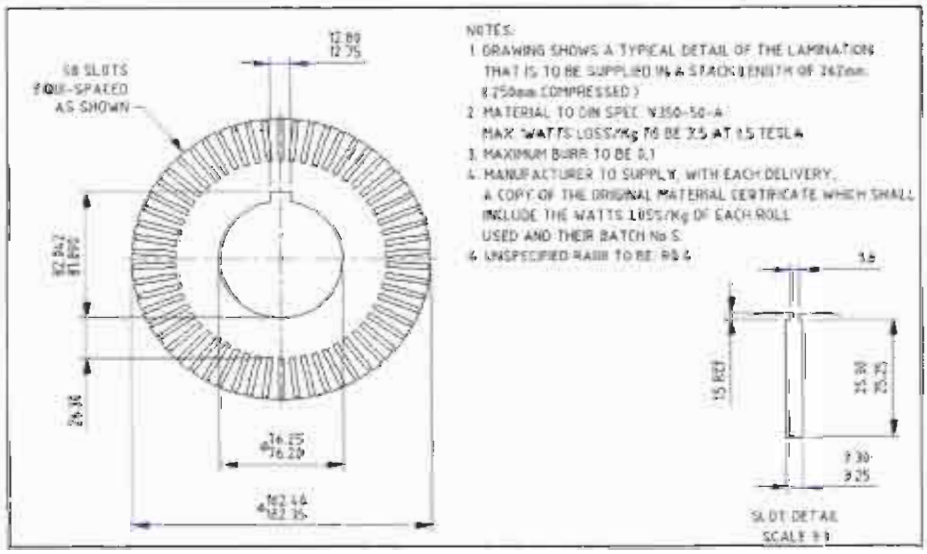

Figure 6.3 Design of the rotor lamination for a 36 kW spinner motor fitted with the MCFR1

Although current distribution in the bars can be described by the classic hyperbolic functions of (rw x d) and bars conductivities as per equation 5.12, there is a difference when compared to classic rotors: the torque contribution of the bars in different motor states is different in the principal functioning of their conductivity (as presented in paragraph 5.7). This is advantageous when starting from HOT conditions as was described in paragraph 5.7.

The slot tolerances are essential in avoiding a "slack" bar situation. It has a major influence on flux density (equation 5.11) and current density (equation 5.12) as presented before.

For a slot width w = 3.25 to 3.30 mm with a bar width of 3.00 mm, it results r = 0.91 to 0.923 (see also equation 5.12). The marginal value of r = 0.91 has been chosen based on:

- Punch and die tolerances influencing the tooling costs
- Artisans and operators medium qualification influencing the labour costs

6.5.3 Manufacturing of the magnetic circuit

The rotor laminations are stacked onto the shaft in a pack, as shown in photo 6.4.

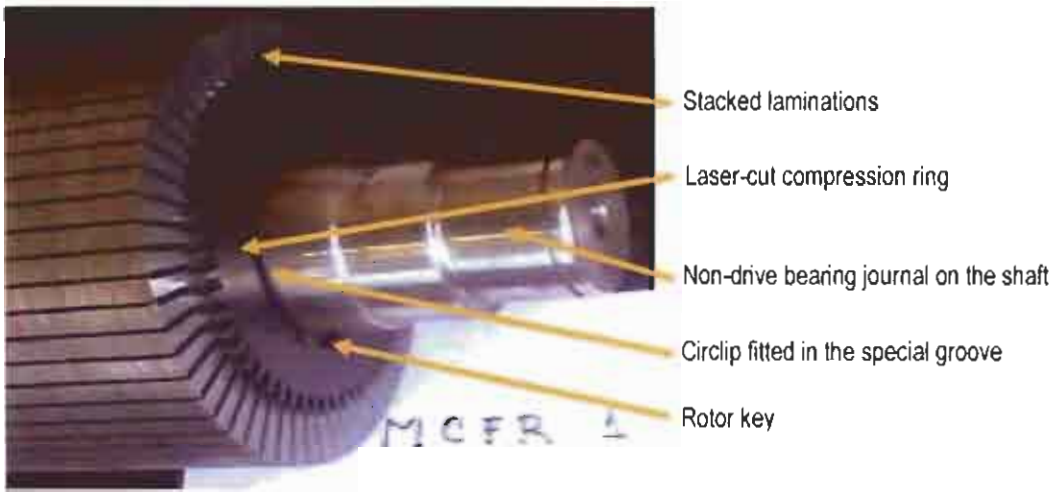

Photo 6.4 Rotor iron core pack build-up on the shaft for the MCFR1, 36 kW spinner motor

Laminations are compressed (by 30 tons press) on the shaft at the required core length.

Stacking factor = 0.93 to 0.95.

Compression rings with profiled laser cut teeth are fitted at the both sides of the core pack in order to prevent lamination splitting. A circlip fitted in a groove holds all the packs in position.

6.5.4 Manufacturing of the electric circuit

The manufacturing instructions for the MCFR1 electric circuit are presented graphically in figure 7.4. Low conductivity bars **(lcb)** BA can be shorter and high conductivity bars (**hcb**) EC can be longer. If the bars are cut off the other way around, then the DOL starting torque will reach maximum values because the equivalent bar resistances will have the maximum value.

The bars are fitted into the rotor core before starting the brazing process. For the MCFR1, 36 kW motor, the bars sequence is shown in photo 6.5.

Because the bar materials are different (different thermal expansion), the short-circuit rings will be different – one at the bottom of the bars (for low conductivity bars) and one at the end of the bars (for high conductivity bars) or vice versa.

The bars to be connected to the lower short-circuit ring (under the bars), i.e., **low conductivity bars** are fitted first in slots with uneven numbers, with a suitable projection per side in order to ensure the brazing process.

High conductivity bars have to be fitted in slots with even numbers, with a projection longer than that of the **low conductivity bars**.

Bars with the same conductivity must be connected to different short-circuit rings because of different thermal expansion calculated according to equation 6.4.

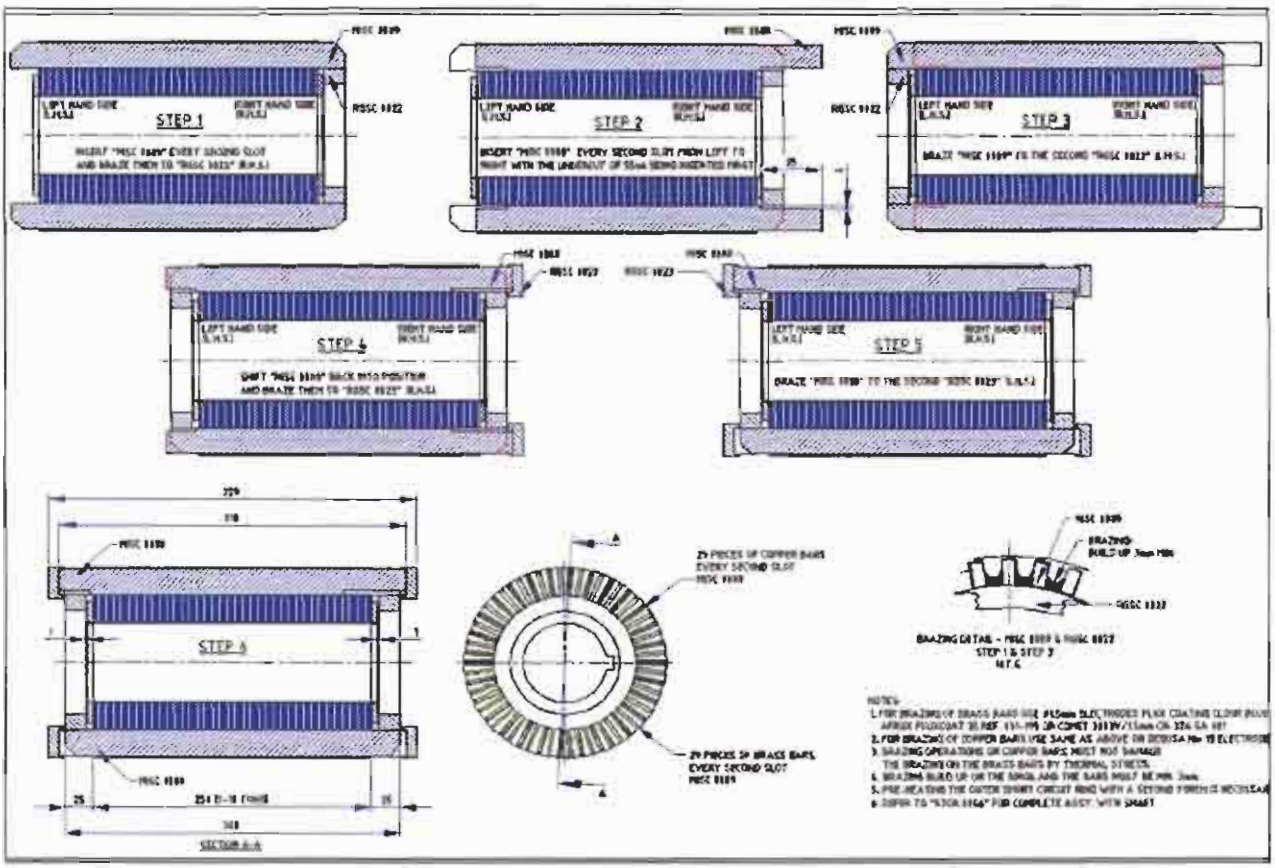

Figure 6.4 Manufacturing instructions for the electric circuit of the MCFR1

The material and conductivities for short-circuit rings could be different, or the same as the conductivity of the bars. This is decided by the motor required performances.

The short-circuit rings with a cross-section area for an acceptable current density have to have an outside diameter 0.5 mm smaller than the distance between the opposite bottom slots. This is required by the thermal radiation towards winding overhang and assembly of the rotor in the stator bore conditions.

The short-circuit rings can be copper or any other material (according to the required rotor performance) and the cross-section profile has to be with a circular slot ± 0.5 mm per side wider than the width of the copper bars and 3 to 5 mm deep. This is to enable good conditions of the brazing bath joining the rotor bars.

At the both ends, the short-circuit ring (copper or same brass material as Icb) has to be brazed to the **low conductivity bars**. Brazing has to be done with the rotor axle in a horizontal position using suitable brazing rods (according to the material to be brazed). The brazing joint cross-area has to be at least equal to the brass cross-section area (in order to eliminate hot connections). Brazing has to be done with the rotor axle in vertical position in order to create a brazing bath in the short-circuit ring slot. Brazing quality is enhanced when the components are pre-heated to 80 to 120°C using a second torch. An alternative brazing process is the special induction brazing technique.

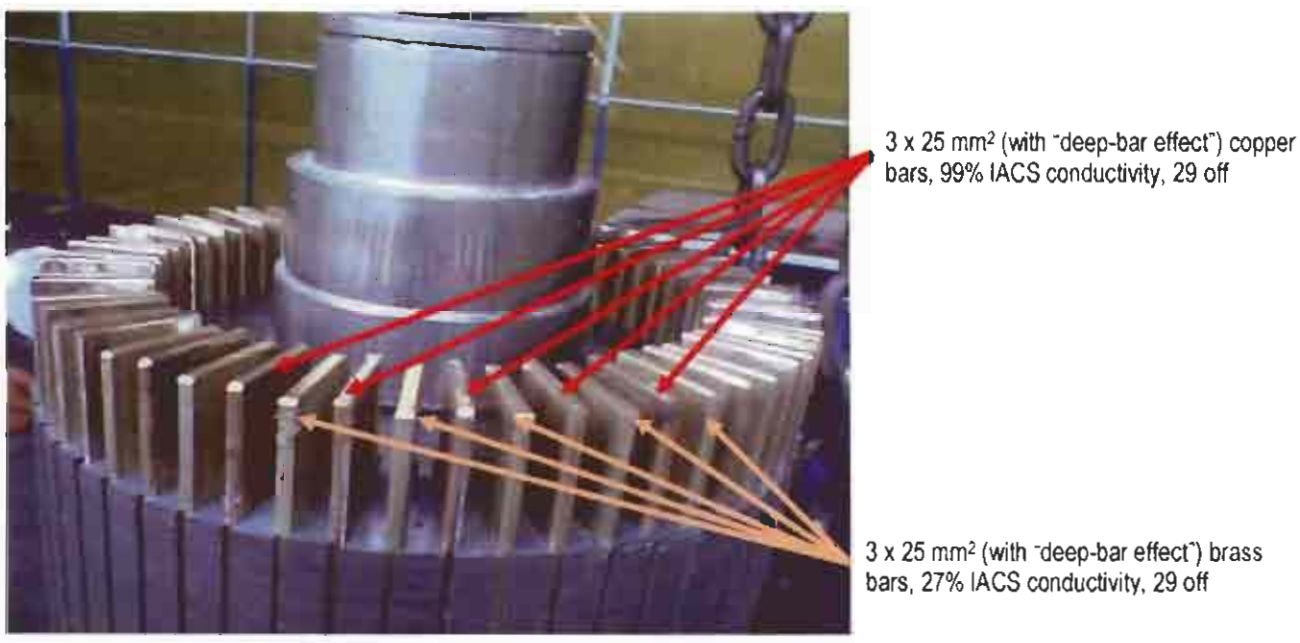

Photo 6.5 Sequence of different bar conductivities fitted in an MCFR1

Because of a very low rotor temperature rise, the short-circuit ring pair is unique, as shown in photo 6.6. This ring connects all the bars, regardless of the conductivity.

This rotor performs a very low temperature rise (T_{rotor} = 100 °C) and, as a result, there is no difference between the thermal elongations of the bars. Coefficients of linear expansion are:

- For copper α_{Co} = 0.0000168 [1/°C]
- For brass α_{Br} = 0.0000185 [1/°C]

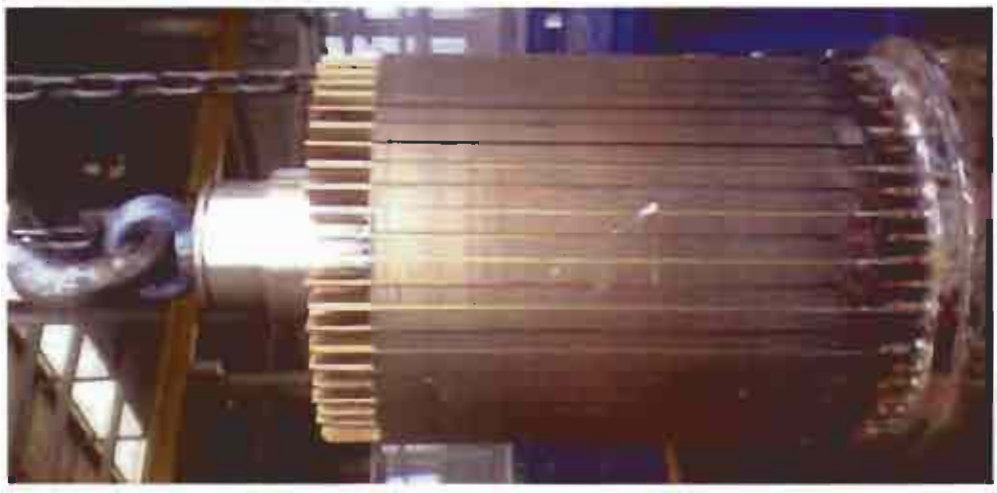

Photo 6.6 The MCFR1 fitted with a unique short-circuit ring
(The photo was rotated 90 degrees)

The initial length of the rotor bar, Lo = 280 mm. According to equation 6.4, the thermal elongation for T_{rotor} = 100°C will be:

- For copper bars: L – Lo = 0.420 mm
- For brass bars: L – Lo = 0.462 mm

That means, because of the low level of thermo-mechanical stress during the working process, micro-fractures in the brazing area are not possible.

6.5.5 Completing manufacturing process

A complete MCFR1 assembly drawing is shown in figure 6.5.

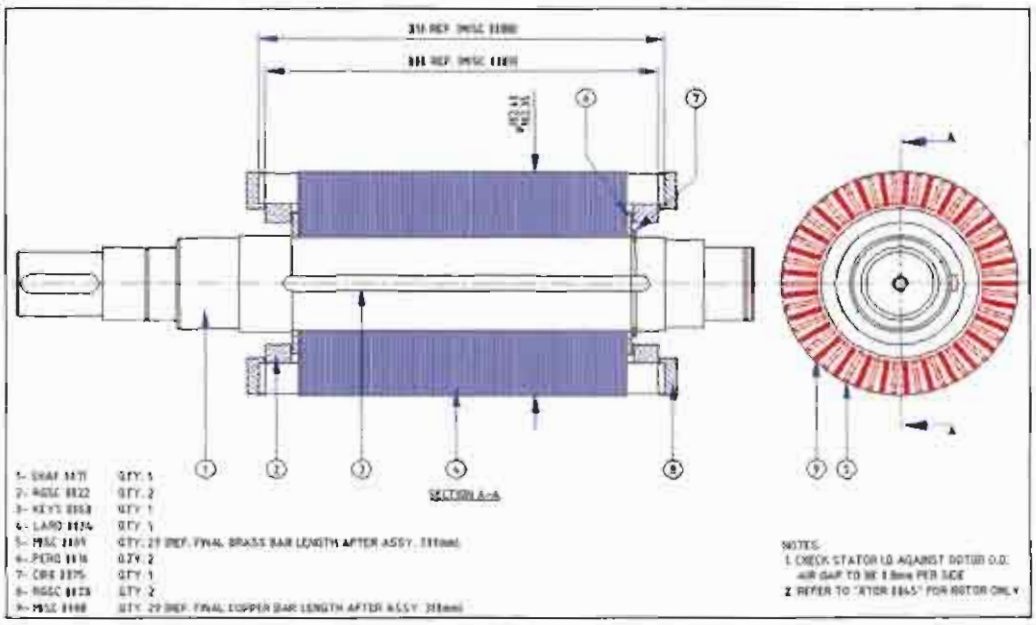

Figure 6.5 Assembly drawing of the MCFR1

Photo 6.7 shows a complete MCFR1 manufactured according to the technological instructions presented above.

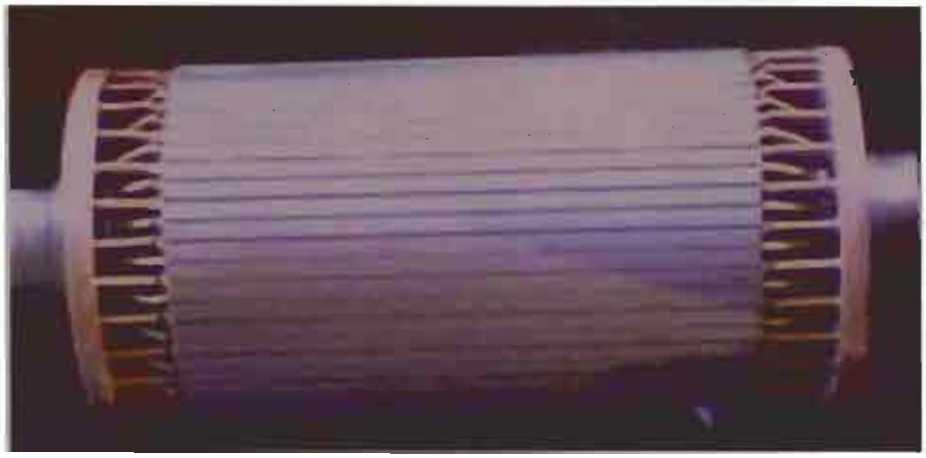

Photo 6.7 MCFR1 manufactured with two pairs of short-circuit rings

The performance of this rotor is the same as that of an aluminium die cast rotor.

6.6 Investigations on the MCFR after 1.8 years' continuous running underground

Photos 6.8 shows a 36 kW motor fitted with an MCFR1 returned after 1.8 years of running underground.

Photo 6.8 A spinner motor fitted with an MCFR returned after 1,8 years running underground

The dark mark represents the mixture of the coal duff and water accumulated at the lowest level (the motor is fitted in a position rotated 35 degrees from its normal vertical plan). The top of the drive end shield is free of coal duff.

Photo 6.9 shows the same MCFR1 after 1.8 years of running underground. The rust on the rotor iron core is due to water ingress.

Photo 6.9 The MCFR1 after 1.8 years of running underground

After inspection of the rotor, no signs of overloading, hot spots or discoloration areas were found, indicating no presence of local thermal vector on the rotor magnetic circuit.

The absence of any local thermal stress on the rotor iron core proved that no harmonics activities were present during the motor life.

The absence of any rotor core discoloration proved that the flux density values have been in accordance with design and patent calculations.

The rotor bars and short-circuit rings performed no discoloration, proving that the current densities values have been in accordance with design and patent calculations.

The rotor bars and short-circuit rings present no distortions proving that the rotor was able to withstand harsh South African specific conditions.

No oxidation or micro-fractures were found on the joints of the rotor bars to the short-circuit rings proving the design resilience to the thermo-mechanical stresses.

When the motor was dismantled, an amount of 0.25 to 0.3 litres of water emerged from it. However, from the rusted watermarks found on the end shields (as shown in photo 6.10), it was obvious that there was more water than that in the motor.

The water leaking from water jacket was excluded based on results of the test performed (40 bars, 1 minute indicates no pressure decay).

Water penetration via motor spigots was also excluded seeing that inspection of the rubber compression "O"-ring revealed no damages.

Further investigations revealed the following situations:

- The motor was not stored properly at ground level (not under cover, e.g. a roof) and after preliminary inspection, at receiving, the box connection lid was left open.

- The waiting period before being assembled on the continuous miner was about 10 to 15 days.
- During this time period rainwater penetrated the motor enclosure via the power leads orifice.
- The first watermark with higher level indicates the amount of rainwater that penetrated the motor enclosure when the motor was stored on the pallet in a vertical position; the amount has been estimated at 0.5 litres of water.
- After being fitted on a continuous miner, the motor ran underground with this amount of water previously collected. The second watermark in photo 6.10 indicates the typical position of the motor on the machine.
- The amount of water was reduced by evaporation. However, during the working period the water penetrated through a 0.2–0.3 mm gap between the bearing cap spigot and shaft contaminating the bearing grease.
- When the contaminated bearing grease ceased its greasing function, the bearing temperature increased beyond the acceptable values of temperature-sensor.
- The bearing temperature sensor fitted onto the bearing house tripped the protection and the motor stopped.

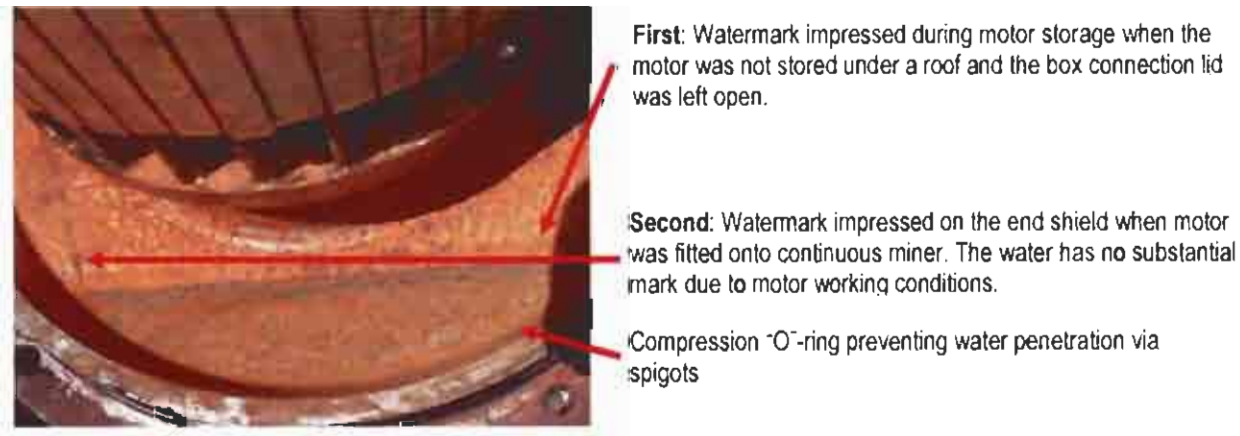

Photo 6.10 Water ingress into the motor during storage

Photo 6.11 shows the rusted watermarks inside the motor enclosure. These rusted watermarks prove the initial existence of water (before the motor was commissioned) confirming the investigations.

This investigation was part of the validation and verification regarding the FMM0072 project and confirmation of the MCFR patent.

Photo 6.11 The stator was rusted due to water in the motor enclosure

6.7 Advantages of the MCFR

During manufacturing and operational processes and as a result of extensive experience in dealing with various customers, some relevant advantages of the MCFR have been claimed:

- Improved rotor capability and ability to withstand higher thermal, electro-dynamic and mechanical stresses (frequent starting, overload, re-closure, prolonged stall conditions, misalignment, vibrations, rubbing, etc.), when compared to other high impedance rotors.
- As a result of the design, the proposed new MCFR patent has **higher reliability indicators** compared to aluminium rotors and double cage rotors:
  - Preservation of motor performances, with reference to alteration or rapid deterioration of performance during its life time
  - Elimination of the starting cage as a "weak point"
  - Increase in the general life span of the motor
- Adjustable running characteristics, including power factor, speed and efficiency.
- Adjustable starting characteristics, including starting torque and starting current.
- Adjustable pull-up and breakdown (pull-out) torque.
- The current MCFR can be designed and manufactured to keep the same characteristics as the original motor with an aluminium rotor (i.e. starting current, starting torque, breakdown torque, speed, temperature rise, etc.).
- Lower investment expenses related to the **re-capitalisation process** resulting from the fact that the entire old motor had to be discarded in some of the following situations:
  - Their damaged rotors cannot be replaced if rotor production is ceased (cast aluminium especially).
  - Restrictive prices when new rotors (especially when imported) are purchased.
  - Motors dedicated to a specific application always require the same performance when rotors have to be replaced.

  - Motor's application becomes redundant and the motor cannot be used for another application because of its very specific performances.
- Using standard tooling, materials and bar profiles, the MCFR can be manufactured without major supplementary expenses. In particular, the manufacturing cost is relatively low, regardless of the production volume.
- In the double cage MCFR, the running cage, using high conductivity bars, does not need to be placed deep into the rotor as with conventional double cage rotors, and the resulting motor using the current MCFR has a slightly improved power factor.
- The starting cage of a double cage rotor has been proven to be a "weak point" of the rotor. In the current MCFR, low conductivity bars with the same mechanical strength as the running cage and which can cope better with very frequent starts, re-closure, reverse and prolonged stall conditions are used.
- The design of the current invention provides easy visual inspection for detecting cracks and/or broken rotor bars.
- The current invention offers low **ownership expenses**.
  - Relaxed maintenance plan because of increased rotor's MTBF
  - Lower cost to repair the rotor or replace bars because the rotor iron core and short-circuit rings are saved (rotor can be repaired)
  - Reduced down-time production costs

Finally, the current invention is able to provide higher or at least equal starting torque values when hot, which is contrary to the behaviour of existing motors (the heating process developed during motor running only selectively increases the bars' resistivity, thereby improving motor starting torque from HOT.

6.8 References

1. Pitis C.D.; Provisional patent registered as "Mixed Conductivity Fabricated Rotors – MCFR" patent registration no. 6886, Spoor and Fisher, Johannesburg, August 2004.
2. Pitis, C.D.; "Mixed Conductivity Fabricated Rotor", South African Patent No. 2005/07280, Johannesburg, Sept. 2005.
3. Landy, C.F., Meyer, A.; "Squirrel cage motors design program – SCDES2", Witwatersrand University, Johannesburg, 1998.
4. FEMCO Mining Motors; "Spinner Motor for Voest Alpine Continuous Miner – FMM 0072", Johannesburg/Brits, November 2003 to July 2004.
5. Alger, P.L.; "Induction machines – Their Behavior and Uses", 2nd edition Gordon & Breach Science Publishers, N.Y. USA, pp 261–286.
6. Say, M.G.; "Performance and design of alternating current machines", 3rd Edition, Isaac Pitman & Sons, London, 1983, pp 300–320.

7. Pitis, C.D.; "A consideration of how to adjust the performance of MV squirrel cage motors during rebuilding", Electricity + Control, January 2006, pp 22–24.
8. Pitis C.D.; "Electric Motors Life Extension by Renewal of Squirrel cage Rotors", ICUE Proceedings, Cape Town, 25–27 May 2005, pp 87–93.

CHAPTER 7: EXPERIMENTAL RESULTS, VALIDATION AND VERIFICATION

Typical tests according to SABS regulations were performed to obtain product approval.

Special tests performed on the MCFR portrayed the performances of the rotor during starting conditions. The following main parameters of the MCFR1 were assessed, confirming the design and new principle of invention:

- Assessment of inrush current
- Assessment of possible dips on transient speed-torque curve
- Assessment of breakdown (pull-out) torque
- Assessment of estimation of the surge factor
- Presence of harmonic induction torques and harmonic synchronous torques

Thermal assessment of the MCFR formed another part of the investigations:

- Heat radiation on the radial direction towards stator winding
- Heat transmission on the axial directions towards bearings
- Rotor temperature rise on load and per start (in DOL, starting from HOT conditions).
- The presence of local thermal vectors on the rotor iron core and rotor core discoloration

These tests enabled comparing the product's performance to that of similar products on the market.

It was confirmed that the MCFR offers reliable torques with no major parasitic torques during the start-up sequence. No parasitic harmonics are present during steady state or transient conditions.

Based on this experimental data, the MCFR life span has been estimated to be net superior to existing rotors on the market.

On-site validation and verification confirmed the life span estimation and project soundness.

Economical assessments related to savings obtained by using the MCFR were estimated at R150 000 per year, per 36 kW spinner motor. On a continuous miner machine there are 4 (four) 36 kW motors, while the number of VAMT continuous miners operating in the world are:

- In Africa: about 140 machines (80 in RSA)
- In Europe: about 2 200 machines
- In the USA: about 1 200 machines
- In Russia and Australasian regions: about 2 000 machines

7.1 Test conditions

Tests were performed in FEMCO's test bay. A functional block diagram is shown in figure 7.1.

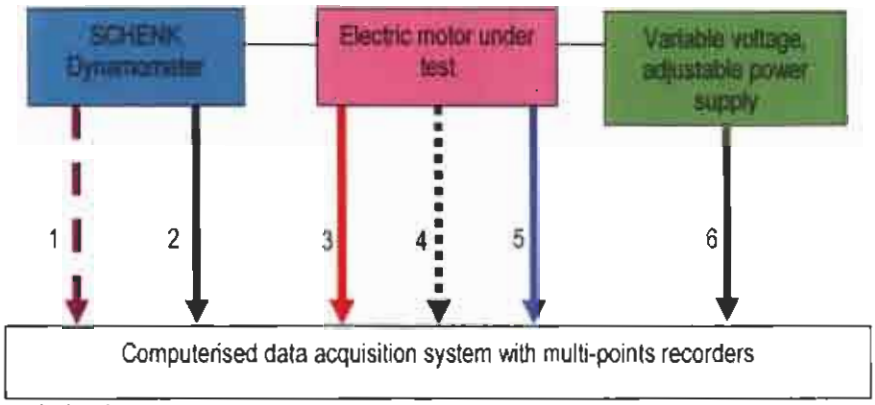

Legend for data transmission lines:

1. Motor speed
2. Motor output (shaft) torque
3. Temperature sensors on windings, bearings, casing, water, ambient including transmission lines
4. Motor vibrations
5. Hydraulic parameters (pressure, flow)
6. Electrical parameters of the supply (voltages, currents, power factor, input power)

Figure 7.1 Functional block diagram of the testing bay

A calibrated Schenk dynamometer with a computerised acquisition data system was used to confirm the motor performances and the new-patented design of the rotor.

The test procedure was done according to the following standards:

- IEEE Std 112 – 1996: Standard Test Procedure for Polyphase Induction Motors
- SANS IEC 60034 – 2001: Rotating electrical machines
- SABS 1804-2 – 1998: Low voltage, three-phase standard motors
- SABS IEC 60079-1 – 2001: Electrical apparatus for explosive gas atmospheres
- SABS 1561 – 1998: Rewinding and refurbishing of rotating electric machines
- DIN 57 530 – 1994: Specification for rotating electrical machines – Methods for determining losses and efficiency, VDE Verlag GmbH, Berlin 1997
- VDE 530 – 2003: Bestimmungen fur umlaufende elektrische Maschinen, VDE Verlag, GmbH Berlin
- SABS, Test House: Test Reports procedure

***Note 7.1**: Estimated uncertainty of calculations: ± 0.75% for a confidence level of max. 95%.*

***Note 7.2**: Voest Alpine Mining and Tunneling and Anglo Americans Field Services representatives have witnessed the tests.*

***Note 7.3**: Performed tests were intended to confirm spinner motor performances by using the MCFR patent, according to application and customer requirements.*

***Note 7.4:** Test results were presented to Voest Alpine Mining and Tunneling GmbH Austria, Herr Gerhardt Neuper – Technical Director.*

A 3D picture of the spinner motor is shown in figure 7.2.

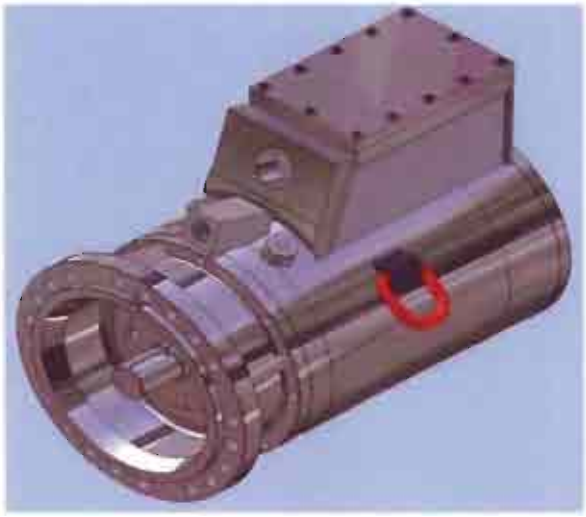

Figure 7.2 3D picture of a spinner motor used for confirmation of MCFR1 performances

7.2 Typical tests performed for SABS approval

Comprehensive tests according to standards [1] to [6] were done on the newly designed spinner motor fitted with the MCFR.

These tests were required to confirm the motor and rotor rated performances in order to obtain SABS approval. The tests performed were:

- No load test cold
- Locked rotor cold
- Temperature rise test at rated power and 100% voltage with vibrations assessment
- Temperature rise test at rated power and 90% voltage with vibrations assessment
- Temperature rise test at rated power and 110% voltage with vibrations assessment
- Locked rotor hot
- Stall test – breakdown torque
- Winding insulation assessment in hot conditions
- No load test HOT
- Vibrations assessment and shaft rotation free
- Calculation of losses separation @ full load and rated voltage

Temperature rise tests were performed at various voltages until all motor components reached complete stabilised temperatures.

Conditions during load tests were: water flow = 10 litres/minute and test site altitude = 1 350 m

A locked rotor test was done as discussed in paragraph 3.5.2.

Other special tests were performed to confirm the rotor design as well.

7.2.1 No Load test cold

Volts [V] = 1000,3

Current [A] I1 = 15.4; I2 = 15.8; I3 = 16.1(av. = 15.77)

Input power [kW] = 2.26

Line resistance [Ohms] = 0.947/**0.948**/0.949

Ambient T1 [Celsius] = 22

Copper losses [kW] = 0.353

7.2.2 Locked rotor test cold

Volts [V]	= 200	350	500
Current [A]	= 41.9	76.1	110
Input power [kW]	= 6.58	21.4	46.2
Power factor	= 0.453	0.464	0.485
Torque [Nm]	= 21	69	151

DOL Starting current [A] **= 226 (7.7 x FLCrt)**

DOL Starting torque [Nm] **= 636 (2.7 x FLTq)**

7.2.3 Temperature rise test at rated power and 100 % voltage

Average voltage [V] = 999

Current [A] I1 = 29.1; **I2 = 29.3**; I3 = 29.5

Input power [kW] = 41.9

Power factor = 0.826

Torque [Nm] = 237

Speed [rpm] = 1 457

Output power @ Dyna [kW] = 36.16

Efficiency [%] = 86.3 %

Vibrations measurements in mm/sec rms:

	Axial	Vertical	Horizontal
Drive end bearing	0.6	1.2	1.3
Non Drive bearing	0.6	1.1	1.1

Line resistance of stator winding:

Cold [Ohms] = 0.948

Hot [Ohms] = 1.24

Winding temperature, cold [degrees] = 22

Average temperature of cooling medium [degrees] = 13.5

Temperature rise of stator winding = 87.5 degrees

Specified maximum temperature rise for H class = 125 degrees

Stabilised temperatures recorded at the end of the test:

Temperature water inlet [degrees] = 13.5

Temperature water outlet [degrees] = 19

Ambient air [degrees] = 25

Winding temperature in the overhang [degrees] = 117

Drive end bearing temperature [degrees] = 70

Non-drive bearing temperature [degrees] = 65

Frame average temperature [degrees] = 49 (maximum 74 degrees)

Test duration = 3.75 hours

7.2.4 Temperature rise test at rated power and 90% voltage

Average voltage [V] = 903

Current [A] I1 = 29.3; I2 = 29.8; I3 = 29.7

Input power [kW] = 41.7

Power factor = 0.89

Torque [Nm] = 239

Speed [rpm] = 1 444

Output power @ Dyna [kW] = 36.14

Efficiency [%] = 86.66 %

Vibrations measurements in mm/sec rms:

	Axial	Vertical	Horizontal
Drive end bearing	0.6	1.2	1.3
Non Drive bearing	0.6	1.1	1.1

Line resistance of stator winding:

Cold [Ohms] = 0.948

Hot [Ohms] = 1.29

Winding temperature, cold [degrees] = 22

Average temperature of cooling medium [degrees] = 12

Temperature rise of stator winding = 102.5 degrees

Specified maximum Temperature rise for H class = 125 degrees

Stabilised temperatures recorded at the end of the test:

Temperature water inlet [degrees] = 12

Temperature water outlet [degrees] = 18

Ambient air [degrees] = 26

Winding temperature in the overhang [degrees] = 127

Drive end bearing temperature [degrees] = 74

Non-drive bearing temperature [degrees] = 75

Frame average temperature [degrees] = 50 (maximum 75 degrees)

Test duration = 1 hour (after temperature rise test 3.75 h)

7.2.5 Temperature rise test at rated power and 110% voltage

Average voltage [V] = 1100

Current [A] I1 = 31.8; **I2 = 32.1**; I3 = 32.6

Input power [kW] = 41.5

Power factor = 0.683

Torque [Nm] = 234

Speed [rpm] = 1 461

Output power @ Dyna [kW] = 35.8

Efficiency [%] = 87.2%

Vibrations measurements in mm/sec rms:

	Axial	Vertical	Horizontal
Drive end bearing	0.6	1.3	1.3
Non-drive bearing	0.6	1.1	1.2

Line resistance of stator winding:

Cold [Ohms] = 0.948

Hot [Ohms] = 1.33

Winding temperature, cold [degrees] = 22

Average temperature of cooling medium [degrees] = 12

Temperature rise of stator winding = 113 degrees

Specified maximum temperature rise for H class = 125 degrees

Stabilized temperatures recorded at the end of the test:

Temperature water inlet [degrees] = 12

Temperature water outlet [degrees] = 19

Ambient air [degrees] = 27

Winding temperature in the overhang [degrees] = 137

Drive end bearing temperature [degrees] = 77

Non-drive bearing temperature [degrees] = 79

Frame average temperature [degrees] = 60 (maximum 79 degrees)

Test duration = 1.45 h (after load test at 90 % voltage)

7.2.6 Locked rotor test in HOT conditions

Locked rotor test (unsaturated at reduced voltage):

Volts [V]	= 200	350	500
Current [A]	= 38.4	68.7	100
Input power [kW]	= 6.7	21.9	46.9
Power factor	= 0.503	0.526	0.541
Torque [Nm]	= 19	70	160

DOL starting current [A] = **205 (7 x FLCrt)**

DOL starting torque [Nm] = **670 (2.83 FLTq)**

7.2.7 Stall test – breakdown torque (pull-out torque)

Pull-out torque (POT) @ test voltage		Rated voltage converted
Voltage	= 495 V	1 000 V
Current	= 71 Amps	150 Amps
Input power	= 34.5 kW	141 kW
Output (Dyna)	= 23.5 kW	96 kW
Torque	= 196 Nm	**800 Nm (3.385 x FLTq)**
Speed	= 1 146 rpm	1 146 rpm

7.2.8 Winding insulation assessment in hot conditions

Test voltage of 1 000 V DC was applied between winding terminals and earth.

Winding average temperature, 70 degrees. Insulation resistance values were converted at 40°C

Insulation resistance @ o seconds	20 MOhms
Insulation resistance @ 1 minute	30 MOhms
Insulation resistance @ 3 minutes	50 MOhms
Insulation resistance @ 10 minutes	60 MOhms
Dielectric absorption	**DA = 1.66**
Polarization index	**PI = 2.0**

7.2.9 No load test – HOT

Volts [V]	= 1001
Currents [Amps]	I1 =14.6; **I2 = 14.9**; I3 = 15.3
Input power [kW]	= 2.12
Power factor	= 0.081
Line resistance of stator winding @ ambient	= 1.24 Ohms
Stator copper losses at no-load [kW]	= 0.413
Iron, friction, windage losses [kW]	= 1.710
Friction, windage losses [kW]	= 0.410
Iron losses [kW]	= 1.300

7.2.10 Vibrations assessment

Vibrations measurements on no load hot conditions in mm/sec rms:

	Axial	Vertical	Horizontal
Drive end bearing	0.4	0.7	0.8
Non-drive bearing	0.4	0.7	0.8

Shaft rotation free = 45 seconds

The motor vibration state differences between no load (hot conditions) and load in mm/sec rms are as follows:

Axial: from 0.4 to 0.6 mm/sec = 0.2 mm/sec

Vertical: from 0.7 to 1.2 mm/sec = 0.5 mm/sec

Horizontal: from 0.8 to 1.3 mm/sec = 0.5 mm/sec

These vibration levels differences of maximum 0.5-mm/sec rms and vibrations level on a load of maximum 1.3 mm/sec rms are far below the standard acceptance [7] of 2.5 mm/sec rms proving that no parasitic harmonics or torques are present during no load or full load states of the motor.

7.2.11 Losses separation calculation at full load and rated voltage

Input power		**41.9 = kW**
Stator copper losses		= 1.6 kW
Iron losses		= 1.3 kW
Stray losses		= 0.18 kW
Air gap power		= 38.82 kW
Rotor losses		=1.13 kW
Friction, windage losses		= 0.41 kW
Output power		**= 37.29 kW**
Calculated efficiency	**@ 1000 V, 36 kW**	**= 89%**

7.2.12 Calculation of stator and rotor temperature rises

Based on experimental results, real output power was calculated from dynamometer test measurements. As a result, the following temperature rises are calculated:

Corrected temperature rise @ 100% voltage = 81.5 degrees

Corrected temperature rise @ 90% voltage = 95.5 degrees

Corrected temperature rise @ 110% voltage = 106 degrees

Rotor temperature rise per one DOL start	= 12 degrees Celsius
Winding temperature rise per one DOL start	= 14 degrees Celsius
Permissible number of stop-start DOL from HOT	= 8 (eight) in row

7.3 Declared nameplate rated values

The nameplate details have to be declared in order to allow comparison of the motor to other similar motors.

Motor power	36 kW
Duty cycle	S1 (continuous running)
Insulation class	H
Temperature rise	80 °C
Voltage/frequency	1000 V/50 Hz
Current	28.5 Amps
Power factor	0.83
Speed	1460 rpm
Nominal torque	237 Nm
Pull-out torque	800 Nm
Efficiency	89 %
Rotor type	Mixed Conductivity Fabricated Rotor type 1
Moment of inertia	0.16 kgm2
Type of protection	IP 65
Flameproof enclosure	Ex d I 150°C
Flameproof approval	IA SABS M/04-194
Cooling	Water-cooled

7.4 Comparison of performance to products on the market

Basic performances were taken into consideration in comparing performances of different 36 kW spinner motors manufactured over the years (as presented in paragraph 5.1).

- Full-load (rated) torque
- Full-load (rated) speed

- Starting torque
- Breakdown torque
- Starting current
- Rotor temperature rise on continuous running
- Winding temperature rise on continuous running
- Bearings temperature rise on continuous running
- Allowed DOL starts from HOT conditions (rotor temperature rise per start)
- Estimated rotor life span

Table 7.1 Comparison of performances of various spinner motors

Performances	"P" series with MCFR1	Loher die cast aluminium rotor	DAMEL die cast aluminium rotor	Cullinan El. copper rotor	Luck & King brass rotor	TECO, Double cage rotor
Power [kW]	36 (43)	36 (30)	36	36	36	36
Efficiency [%]	89	87	88	90	82	88.5
St. Tq. [Nm]	235.5	238.75	235.5	232.3	242.1	235
Start. torque [p.u.]	**2.7–2.8**	2.4–2.6 (Lagging)	**2.6–2.8**	2.1–2.3 (Lagging)	3.2–3.4 (Leading)	2.6–2.8
Pull-out torque [p.u.]	**3.45**	1.94	**2.76**	2.6	4.5	3.4
Start. Current [p.u.]	**7–7.5**	7–7.5	**7–7.5**	8–9	5.5–.6	6.8–7.3
Full-load speed [rpm]	**1 460**	1 440	**1 460**	1 480	1 420 (Lagging)	1 465
Temp. rise wind. [°C]	75–85	100–115 (Overheating)	90–105	85–90	110–125 (Overheat)	80–100
DE/NDE Brg. temp.rise[°C]	45/40	65/75	45/60	48/50	75/75	Unknown
Rotor construction	Patent MCFR 1	Aluminium 30 kW design	**Aluminium**	Copper rotor	Brass rotor	Double cage rotor
Rotor temp. rise [°C]	**150–160**	245–265	**210–220**	180–200	280–320	180–200
DOL starts hot	**8 (eight)**	1–2	**2–3**	2–3	1 (one)	3–4
Est. rotor life span (MTBF)	**20 years**	1.1–1.4 years	**1.6–2 years**	8–10 years	5–7 years	Unknown
Est. motor life	10 years	1.5–2 years	3–4 years	5–8 years	Unknown	Unknown

Conclusion: Table 7.1 reveals net superiority of the MCFR patent and design.

7.5 Special tests performed in DOL starting conditions

7.5.1 Recording starting current in DOL conditions

The motor was connected DOL and the saturated stator current transient evolution was recorded during a time period of 0.5 seconds.

Inrush current and saturated starting current increase will enable the investigation of motor performances when fitted with the MCFR. The oscillogram is shown in figure 7.3.

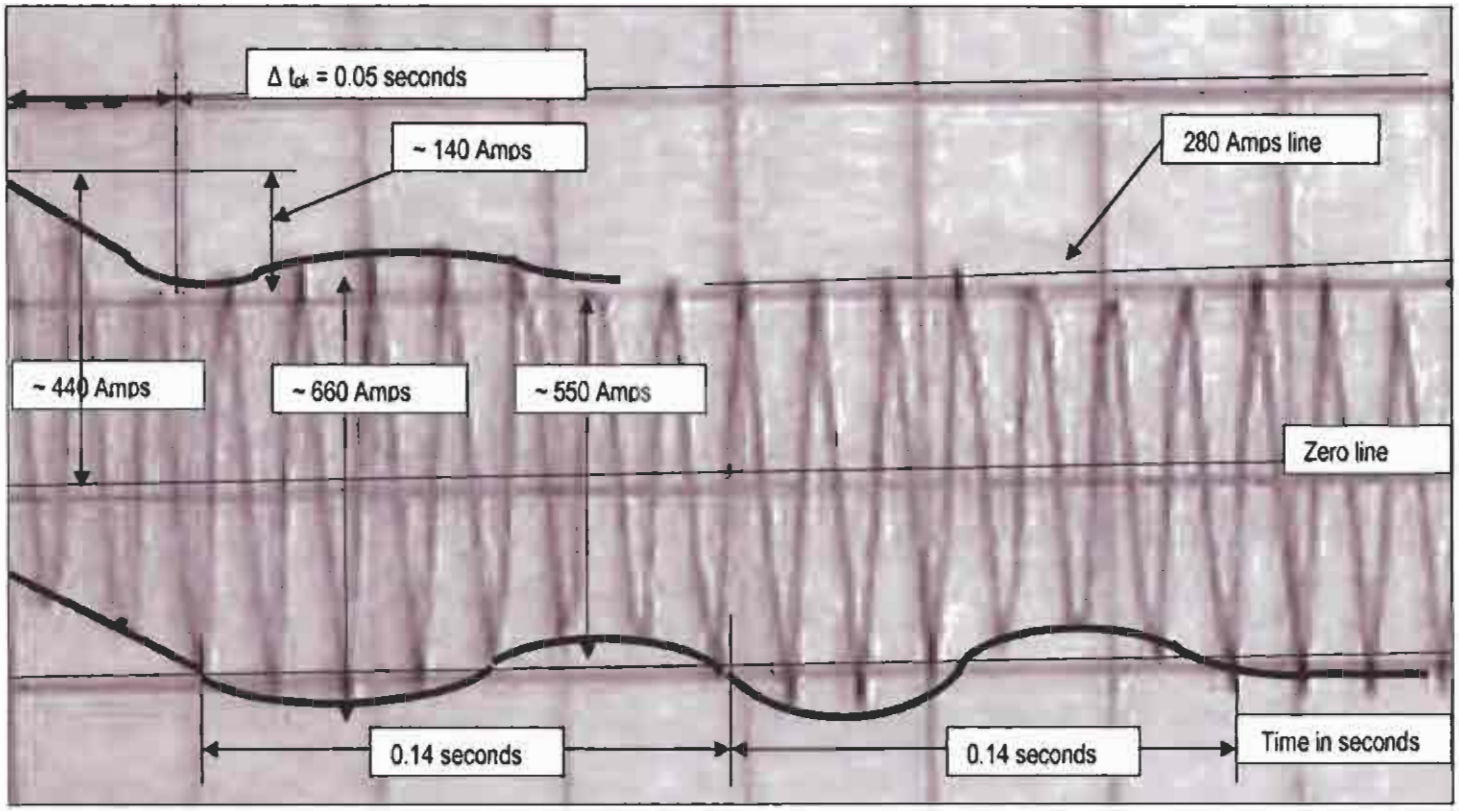

Figure 7.3 Oscillogram of DOL starting current for a 36 kW fitted with MCFR

Vertical scale: 1 division = 280 Amps

Time is measured on horizontal scale in seconds: 1 division = 0.05 seconds

From the oscillogram it results that:

- Starting current $I_{rms\ st}$ = 200 Amps rms
- Inrush current I_{pk} = 440 A
- The inrush current decay period is Δ t_{pk} = 0.05 seconds

Inrush current is the current that is required in the motor electromagnetic circuit to restore it to the state in which the e.m.f across the coil terminals is proportional to the time derivative of the flux linked by the coil (Faraday's law).

7.5.2 Assessment of the inrush current

Due to the relatively large air gap, the ratio of inrush current to rated current is significantly lower than that experienced with low-leakage transformers. Because of relatively high leakage reactance of this specific design, the peak current value is limited to 420 Amps. The relation to saturated starting current $I_{rms\ st}$ = 220 Amps rms is:

$$I_{pk} = 1.91 \text{ x.} I_{rms.st} \qquad (7.1)$$

Equation 7.1 and Δt_{pk} = 0.05 seconds indicate that according to standards [6], [8], [9], the **inrush current of this specific design does not affect power system components and protection equipment (there will be no spurious tripping of protection devices).**

7.5.3 Assessment of possible dips on transient speed-torque curve

A DC component of 140 A is present in the measured current during starting.

The current "swinging" characteristic is due to the DC current component that is induced in the rotor cage by the currents flowing in the stator winding. The oscillation is a function of the interaction between the two currents as the motor accelerates.

Noticeably (close to the zero-speed point on the graph), there is no reduction or variations in the slope of current oscillations when DC offset occurs.

That means no "dip" in the transient speed-torque curve (as shown in figure 7.3.) occurs for this specific design.

Note 7.5: *This mentioned torque "dip" is only relevant to transient speed-torque curves derived from low-inertia starts on strong supplies at the rated motor voltage. Should a motor happen to "crawl" due this torque dip, it would recover quickly as soon as the transient condition subsides. Despite the dip being a transient effect, as well as the fact that its magnitude is difficult to predict very accurately, the phenomenon affects the acceleration time and it should therefore be taken into account during run-up time calculations, particularly where a critical application is concerned [10].*

7.5.4 Assessment on breakdown (pull-out) torque

The same transient phenomena that affect the current and the torque during the initial part of the start have an associated effect on the dynamic torque during the remainder of the DOL start.

Since there are distinct time-constants limiting the rate at which the flux in any part of the motor may change (or reach a particular steady state), there is a corresponding delay before the motor pull-out torque (POT) reaches its steady-state value.

If the run-up time of the motor is sufficiently long, then the relevant DOL speed-torque curve will be very similar to the steady-state characteristic. On the other hand, if the run-up time is relatively quick, the difference between the dynamic and steady state pull-out torque characteristics will be different (as shown in paragraph 3.6.4). This effect should also be taken into account when calculating the starting time for a critical low-inertia application with an expected run-up time that is short enough to warrant assuming transient conditions [11].

In this specific design the pull-out torque (POT) reaches the value after a 0.5 second interval, meaning that dynamic (transient) POT reaches the steady state calculated value.

7.5.5 Estimation of surge factor

Instantaneous peak inrush current indicates a DC component of 140 Amps.

The ratio between total asymmetrical current I_{pk} = 420 A and starting current, peak value I_{st} = 220 √2 = 310 A is:

$$I_{pk} / I_{st} = 1.36$$

According to Underwriters Laboratories, UL Specification 845, February 1995:

$$I_{pk} = I_{st} \times \sqrt{2} \times \chi \qquad (7.2)$$

It results in a very good value of surge factor **χ = 0.97 < 1.25**

The value of the surge factor χ =1.25 is stipulated by UL Specification 845 – Table 26.2, as a function of the DOL starting power factor. In this case the power factor = 0.55

Other authors **[8]**, **[10]** indicate a maximum surge factor value of **χ = 1.40 to 1.56**

That means the MCFR offers a good value of surge factor, as referred to in paragraph 2.6.

7.5.6 Estimation of harmonic induction torques and harmonic synchronous torques

The oscillogram depicts a modulation of starting current. The modulation has the following data:

- Amplitude A = [660 – 550] / 2 = 55 A
- Wave length λ = 0.14 sec, indicating the seventh harmonic n = **7**
- Total periods number = 2

This means that during the start-up period, two torque oscillations will occur in the interval of 0.05 to 0.35 seconds, as shown in figure 7.3.

Using the relationship between starting current Ist = 7.7 pu and starting torque Mst = 2.7 pu, we can calculate the amplitude of these oscillations.

$$(55 \text{ A} / 310\text{A}) \times (2.7 \text{ pu} / 7.7 \text{ pu}) = 0.0584 \qquad (7.3)$$

That means the parasitic torque values are maximum ± 5.84% of the actual dynamic torque values recorded during starting.

Taking into account the maximum run-up time period T_r = 1 sec and the motor speed torque curve (presented in Annexure 7.1), it results that the parasitic torques of the 7^{th} harmonic are imposed on the speed torque curve in a range of 75 r/m to 450 r/m speed. The speed-torque curves of the motor and the load (countertorque) are shown in figure 7.4 (informative and not to scale).

The minimum value of acceleration torques A Tq = Tq_d – Tl = 680 Nm – 330 Nm = 350 Nm excludes any possibility of a "crawling" situation of the application. There is no pull-up torque. A reserve value of starting torque Δ T = F.L.Tq = 235 Nm ensures a very good and reliable

starting. High breakdown torque (POT = 800 Nm) excludes any appearance of the stall conditions.

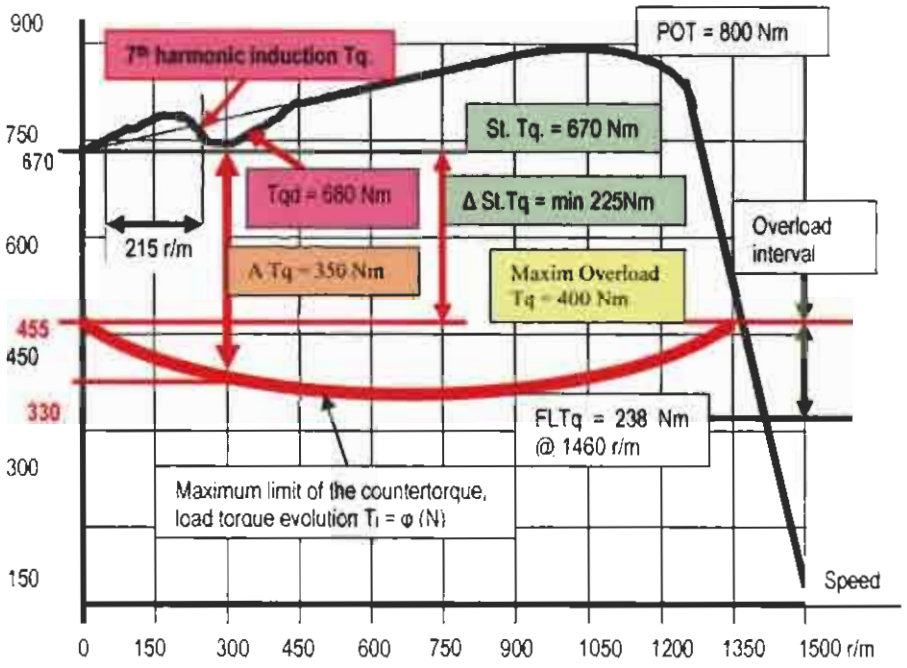

Figure 7.4 Speed-torque curve of the 36 kW prototype (informative and not to scale)
(For reference see also figure 2.1)

For this speed range, the counter-torque maximum values are in the range of 320 to 400 Nm.

The parasitic torques will have the deep momentary torque Tq_d = 680 Nm and the top momentary torque of Tq_t = 730 Nm. However, both values are below 10% of the actual momentary torques as accepted by standards and literature [6], [8], [9], [10].

The momentary torque is also 140% to 150% bigger than actual torques developed by aluminium cast rotors [12].

This means that the MCFR offers a reliable torque with no major parasitic torques during the start-up sequence.

7.6 Thermal assessment of the MCFR

7.6.1 Directions of investigations

A complete thermal assessment can be done for the MCFR using the following data:

- Experimental results obtained from dynamometer temperature rise tests
- Investigations were made on a returned motor after running on the application for 1.8 years

The assessment is based on possible directions of heat transfer from the rotor, discussed in paragraph 4.4.6 and shown in figure 4.2. The following investigations will be made:

- Radial direction towards stator winding
- Axial directions towards bearings
- Rotor temperature rise on load and DOL per start
- Investigations of the presence of local thermal vectors on the rotor iron core and rotor core discoloration

7.6.2 Assessment on heat radiated on radial direction

As discussed in paragraph 4.4.6 and shown in figure 4.2, an overheated rotor should radiate heat towards the winding.

As a result, the stator winding temperature rise will increase artificially beyond the electromagnetic design estimations.

From tests performed on a dynamometer, comparative results of various windings temperature rise are available in table 7.2.

Table 7.2 Comparison of windings temperature rise

Performances	"P" series with MCFR1	Loher alum. rotor	DAMEL alum. rotor	Cullinan El. copper rotor	Luck & King brass rotor	TECO, dbl. cage rotor
Temp. rise wind. [°C]	75–85	100–115 (Overheating)	90–105	85–90	110–125	80–100

These results confirm that the **MCFR does not radiate heat towards the stator winding.**

7.6.3 Assessment on heat transferred in axial directions

As discussed in paragraph 4.4.6 and shown in figure 4.2, an overheated rotor should transfer heat by conductivity through the shaft towards the bearings. As a result, the bearing temperature rise will increase artificially beyond the estimated calculations.

From tests performed on a dynamometer, comparative results of the temperature rise of the bearings are available in table 7.3.

Table 7.3 Comparison of the temperature rise of bearings

Performances	"P" series with MCFR1	Loher alum. rotor	DAMEL alum. rotor	Cullinan El. copper rotor	Luck & King brass rotor	TECO, dbl. cage rotor
DE/NDE Brg. Temp.rise[°C]	45/40	65 /75	45/60	48/50	75/75	Unknown

These results confirm that the **MCFR does not transfer heat by conductivity via the shaft towards the bearings.**

7.6.4 Assessment on rotor temperature rise on load and per DOL start

Direct measurements performed on the rotors at the end of the temperature rise test allowed assessment of the MCFR performance in comparison with other rotors.

The low temperature of the rotor enables the rotor to support numerous DOL starts from hot conditions.

Experimental results and estimations made over the years made it possible to compare MCFR performances with other rotors, as shown in table 7.4.

Table 7.4 Rotor temperature rise and DOL starts

Performances	"P" series with MCFR1	Loher alum. rotor	DAMEL alum. rotor	Cullinan El. copper rotor	Luck & King brass rotor	TECO, dbl. cage rotor
Rotor temp. rise [°C]	150–160	245–265	210–220	180–200	280–320	180–200
DOL starts hot	8 (eight)	1–2	2–3	2–3	1 (one)	3–4

These results confirm that the **MCFR has a low thermal heat level and no parasitic harmonics are present during load or starting procedures**.

7.6.5 Investigations of the existence of local thermal vectors

This investigation was carried out directly on the MCFR after temperature rise tests. Visual inspection revealed no discoloration resulting from parasitic harmonics.

Thermal vectors were detected by investigating rotor "hot spots" [13]. The method of simulating rotor load thermal conditions were described in paragraph 4.4.6 and shown in figure 4.1.

Rotor concentricity in hot conditions was also verified.

The maximum run-out values at 100°C were 0.025 mm. The standard acceptance conditions [14] are maximum 0.08 mm.

This measurement confirmed that no local thermal vectors were present on the rotor iron core.

The same set of tests and inspections were carried out on the MCFR that worked for 1.8 years on the underground application as well. Photo 7.1 shows the rotor condition (after rust was removed).

Photo 7.1 The MCFR iron core in excellent condition after running on load for 1.8 years

Conclusion: The tests and inspections performed on the MCFR revealed no presence of local thermal vectors on the rotor iron core and/or rotor core discoloration.

These measurements confirmed again that the **MCFR does not generate parasitic harmonics or torques during the rotor-working period.**

7.6.6 Estimations regarding the MCFR life span

From the above experimental results it has been demonstrated that MCFR performances are similar or superior to that of an aluminium cast rotor.

By design, the MCFR inherited the features of a fabricated rotor with all the related features, as presented in Chapter 5.

At the low thermal level at which it works, the absence of parasitic torques and harmonics indicate a longer life than similar rotors on the market.

Comparison of the rotor life span is presented in table 7.5. The data confirms that the MCFR is a reliable and economical design.

Table 7.5 Estimations of rotor and motor life span

Performances	"P" series with MCFR1	Loher alum. rotor	DAMEL alum. rotor	Cullinan El. copper rotor	Luck & King brass rotor	TECO, dbl. cage rotor
Est. rotor life span (MTBF)	20 years	1.1–1.4 years	1.6–2 years	8–10 years	5–7 years	Unknown
Est. motor life	10 years	1.5–2 years	3–4 years	5–8 years	Unknown	Unknown

7.7 Technical and economical assessments during validation and verification activity

Estimations on the economic and technical impact of replacing the aluminium rotor with an MCFR were done with reference to the above case study.

Based on the motor's MTBF and rotor life span estimations, specific technical and economical events were predicted for a period of 15 years (as presented in table 7.6).

Table 7.6 Comparison of specific technical and economical performances

Item/Motor	Alum rotor	MCFR
Winding temperature rise	97°C	80°C
DE/NDE bearing temp. rise	45°C /60°C	30°C /45°C
Rotor temperature rise	210°C	155°C
Winding expected life time	9 months	18 months
Bearings expected life time	8 months	15 months
Working load hours/year	4000 h	4000 h
Overload hours/year	1500 h	1500 h
Load/overload efficiency	88% / 87 %	89% / 89%

As discussed in paragraph 4.6, down-time production of 7 to 9 hours is the necessary time to replace a failed 36 kW motor (in the case of an unplanned failure).

Not taken into account are costs savings related to:

- Logistic activities
- Motor's components ageing process as a result of repair activities

Table 7.7 Predicted events on 36 kW spinner motors for a projected 15-year period

Item	Aluminium Rotor	MCFR
Number of motor failures	13	7
Number of rotor replacements	8	None
Down-time production total	104 hours	56 hours
Rotor life span [months]	18	200 (estimated)
Motor MTBF [months]	13 (unplanned.)	Min.24 (estimated)
Motor cost	R55 000	R60 000
Rotor cost	R26 000	R20 000
Motor repair cost	R45 000	R25 000
Av. production loss cost/hour	R35 000	R35 000

However, it was noted that in both situations (aluminium and MCFR) unplanned motor failure occurred before the planned replacement, in spite of the fact that the MCFR had proven its extended life span (this enables the end-user to repair the product based on a maintenance plan).

Year 2005 prices and an electricity cost of 0.15 R/kWh were considered constant for the entire one-year assessment period.

Based on specific technical and economical comparison performances and predicted events in a projected 15-year period, economical indicators and savings are presented in table 7.8.

Table 7.8 Comparison of economical indicators and savings obtained per 36 kW spinner motor

Item	Aluminium rotor	MCFR	Saving
Electricity costs on load [R]	368 200	360 000	6 000
Electricity Cost on Overload [R]	139 650	135 000	4 650
Variable capital (rotors) [R]	208 000	None	208 000
Down time costs [R]	3 640 000	1 680 000	1 960 000
Motor repair costs [R]	285 000	175 000	90 000
Initial capital [R] / per motor	60 000	60 000	nil
TOTAL SAVING [Rand]			**2 270 650**
Savings by using MCFR only [R]			**2 258 000**
Annual savings per rotor [Rand]			**150 000**

These estimations based on experimental data obtained from tests carried out as part of validation and verifications prove the economical impact of using the MCFR in a specific application only.

7.8 References

1. IEEE Std 112 – 1996; "Standard Test Procedure for Polyphase Induction Motors", IEEE, New York, May, 1997.
2. SANS IEC 60034/2 – 2001; "Rotating electrical machines – Methods for determining losses and efficiency of rotating electrical machinery from test", Chapter 5.2, Council of SABS, Pretoria, 2002.
3. SANS 1561-1 – 1998; "Low voltage, three-phase induction motors", Chapter 7, Council of SABS, Pretoria, 1999.
4. SANS IEC 60079-1 – 2004; "Electrical apparatus for explosive gas atmospheres", Chapter 15, Council of SABS, Pretoria, 2004.
5. DIN 57 530 – 1994; Specification for rotating electrical machines – Methods for determining losses and efficiency, VDE Verlag GmbH, Berlin, 1997.
6. VDE 530, Teil – 2003; Bestimmungen fur umlaufende elektrische Maschinen, Anhang X, VDE Verlag, GmbH Berlin.
7. ISO 1940/1-1986; "Mechanical vibrations – Balance quality requirements of rigid rotors", ISO, TC, Switzerland, 1986.
8. Melaia, R., Grayer, I.; "Direct-on-line starting current of cage induction motors", Elektron, June, 1996, pp 25–27.
9. NEMA, MG 1, Part 12 – 1998; "Motors and Generators – Tests and Performances", NEMA Publications Washington, 1998.

10. Norman, H.; "Induction motor locked saturation curves", Transactions AIEE, 53, 1934, pp 536–541.
11. Ostovik, V.; "Computer-aided Analysis of Electric Machines", Prentice-Hall, 1994, pp 307–318.
12. SANS IEC 600034 –12; "Starting performance of single speed three-phase cage induction motors", Council of SABS, Pretoria, February 1993.
13. SANS 0242; "The rewinding and refurbishing of rotating electric machinery – Low voltage three-phase induction motors", Council of SABS, Pretoria, 2002.
14. SANS 1804/2-1998; "Low voltage three-phase induction motors", Chapter 4, Council of SABS, Pretoria, 1999.

CHAPTER 8: CONCLUSIONS AND RECOMMENDATIONS

8.1 Conclusions

In the South African coal-mining industry, overseas-designed high-impedance double cage and die cast aluminium rotors record high rate failures with heavy related financial losses.

As a result, the need for an alternative rotor type appeared on the market which was able to comply with specific basic South African conditions ignored previously.

The problem was addressed by understanding the essentials of application engineering with reference to special conditions imposed by the South African mining industry.

The invention is actually a solution to specific application engineering problems with the motor design in South Africa.

The most significant design variable in squirrel cage motors is the effective resistance of the rotor cage circuits, which was actually the focus of the invention.

Mixed Conductivity Fabricated Rotors (MCFR) are designed and manufactured based on a new principle and are able to withstand harsh South African mining conditions.

The patent offers a large variety of technical and economical advantages, increasing the mining processes efficiency beyond expectations (see also table 7.8).

This thesis emphasises the MCFR's design adaptability, i.e. altering the rotor design to meet the demands of a specific engineering application as a base line of drives design.

By design, as fabricated rotor, the MCFR patent has **high reliability indicators** compared to those of die cast aluminium rotors.

Performance stability, including the fact that the rotor can keep the starting torque value very constant even after motor has reached its thermal stabilised condition, i.e. "hot condition", represents one of the salient performances of invention.

The invention was materialised initially in a set of special rotors powering continuous miners of a reputable coal-mining house. This mining house was spending about R5 million annually in replacing imported 36 kW aluminium rotors only. Losses related to down-time production and repair activities are not included.

Table 8.1 presents projected savings on **total ownership costs** obtained by VAMT when using the MCFR as replacement of die cast aluminium rotors as a result of:

- Relaxing the maintenance plan (increased rotor's MTBF) – reduced repair costs

- Preservation of motor performance, with reference to performance alteration
- Increasing general life span of the motor
- Lower cost of rotor repair or replacement
- Reduced downtime production costs

Table 8.1 Comparison of economical indicators and savings obtained per 36 kW spinner motor (15-year projection)

Item	Aluminium Rotor	MCFR	Saving[R]
Electricity costs on load[R]	368 200	360 000	6 000
Electricity cost on overload [R]	139 650	135 000	4 650
Variable capital (rotors) [R]	208 000	None	208 000
Down-time costs [R]	3 640 000	1 680 000	1 960 000
Motor repair costs [R]	285 000	175 000	90 000
Initial capital [R] / per motor	60 000	60 000	nil
TOTAL SAVING [Rand]			**2 270 650**
Savings by using MCFR only [R]			**2 258 000**
Annually savings per rotor [Rand]			**150 000**

These estimations are based on experimental data obtained from tests carried out as part of validation and verification activities. The estimations prove the economical impact of using the MCFR in a specific application only.

MCFRs represent a viable solution of reducing investments related to the **re-capitalisation** process because old motors have to be discarded in one of the following situations:

- Their damaged rotors cannot be replaced if rotor production ceased (die cast aluminium, especially)
- Restrictive prices when a new rotor (especially when imported) has to be purchased
- Motors dedicated to a specific application always require the same performances when rotors have to be replaced
- The motor's application becomes redundant and it cannot be used for another application because of its very specific performances.

The MCFR patent represents a breakthrough regarding the monopoly of the large manufacturers in deciding market prices. It will enable medium-sized organisations to become rotor and motor manufacturers. Sound competition will offer the market an alternative option.

The patent is part of the new South African trend of increasing the efficiency of processes. It offers the possibility of designing dedicated motors with a positive impact on the South African economy. Some socio-economical advantages are worthy of considerable study.

- Being locally manufactured, the MCFR may reduce the country's economical dependence.
- Requiring no special expertise, the MCFR can be produced in any quantity and size without excessive investment.

- The MCFR offers the market an alternative option (product interchangeability) and sound competition (with export potential).
- The patent ensures business sustainability conditions, which diffuse financial constraints on motor manufacturers and end-users during the re-capitalisation process (very actual in South African economic and industrial environment).

8.2 Recommendations

The invention represents part of the concept of global efficiency by creating new business opportunities. A technical-economical analysis should be welcomed when studying further the patent integration in this global concept.

A very interesting path for further investigations is the medium voltage motors population where the invention may offer large possibilities to improve performances (speed-torque curve) at reduced ownership costs.

The invention offers large possibilities of substituting slip ring motors with more rugged squirrel cage rotors, at the same torques performances.

Supplementary studies and calculations have been done in this thesis regarding heat transfer from the rotor by radiation and conduction. These represent a starting point in designing TE flameproof motors where the heat evacuation determines the motor's flameproof status. These flameproof motors are largely used on JOY mining machinery.

The patent and calculations presented in this thesis set up some base lines for some further researches regarding squirrel cage electric motors:

- Deep-bar cages machines
- Parallel cages machines
- High-torque cages in replacing slip-ring induction motors
- Skewed MCFRs slots.
- MCFRs comportment in re-closure conditions
- Unbalanced magnetic pull
- MCFR in a double cage configuration
- Mathematic models and equivalent circuits
- Monitoring squirrel cage MCFR
- Investigation and study of broken bars phenomenon
- Global concept of efficiency

ANNEXURE 1.1: MCFR PATENT FORMS

SPOOR & FISHER

FORM P.1

REPUBLIC OF SOUTH AFRICA
PATENTS ACT, 1978

APPLICATION FOR A PATENT
AND ACKNOWLEDGEMENT OF RECEIPT
(Section 30 (1) – Regulation 22)

REGISTRAR OF PATENTS DESIGNS TRADE MARKS AND COPYRIGHT
BILLED
2005 -09- 10
SPOOR P
REGISTRATEUR VAN PATENTE MODELLE HANDELSMERKE EN OUTEURSREG

The granting of a patent is hereby requested by the undermentioned applicant on the basis of the present application filed in duplicate

OFFICIAL APPLICATION NO.			
21	01	2005/07280	PA137818/ZA

FULL NAME(S) OF APPLICANT(S)	
71	FEMCO MINING MOTORS (PTY) LTD

ADDRESS(ES) OF APPLICANT(S)	
	33 PIET PRETORIUS STREET, INDUSTRIAL AREA, BRITS, PRETORIA, 0250, GAUTENG, SOUTH AFRICA

TITLE OF INVENTION	
54	MIXED CONDUCTIVITY FABRICATED ROTOR

THE APPLICANT CLAIMS PRIORITY AS SET OUT ON THE ACCOMPANYING FORM P.2, THE EARLIEST PRIORITY CLAIM IS:

COUNTRY:	NUMBER:	DATE:
ZA	2004/6886	30 AUG 2004

~~THIS APPLICATION IS FOR A PATENT OF ADDITION TO PATENT APPLICATION NO.~~

21	01	

~~THIS APPLICATION IS A FRESH APPLICATION IN TERMS OF SECTION 37 AND IS BASED ON APPLICATION NO.~~

21	01	

THIS APPLICATION IS ACCOMPANIED BY:

- ☒ 1. Two copies of a complete specification of 23 pages.
- ☒ 2. Drawings of 3 sheets.
- ☒ 3. Publication particulars and abstract (Form P.8 in duplicate)
- ☒ 4. A copy of Figure 6a of the drawings for the abstract.
- ☐ 5. Assignment of invention.
- ☐ 6. Certified priority document.
- ☐ 7. Translation of the priority document.
- ☐ 8. Assignment of priority rights.
- ☒ 9. A copy of the Form P.2 and the specification of S.A. Patent Application No. 2004/6886
- ☐ 10. Declaration and power of attorney on Form P.3.
- ☐ 11. Request for ante-dating on Form P.4.
- ☐ 12. Request for classification on Form P.9.
- ☒ 13. Form P.2 in duplicate.
- ☐ 14. Other.

74	ADDRESS FOR SERVICE: SPOOR & FISHER

Dated: 9 September 2005

J.D. WHITTAKER

SPOOR & FISHER
PATENT ATTORNEYS FOR THE APPLICANT(S)

RECEIVED
2005 -09- 09
REGISTRAR OF PATENTS

FORM P.2

REPUBLIC OF SOUTH AFRICA	REGISTER OF PATENTS	PATENTS ACT, 1978

OFFICIAL APPLICATION	LODGING DATE: PROVISIONAL	ACCEPTANCE DATE
21 01	22	47
INTERNATIONAL CLASSIFICATION	**LODGING DATE: COMPLETE**	**GRANTED DATE**
51 H02K	23 9 SEP 2005	

FULL NAME(S) OF APPLICANT(S)/PATENTEE(S)

71 FEMCO MINING MOTORS (PTY) LTD

APPLICANTS SUBSTITUTED:	DATE REGISTERED
71	

ASSIGNEE(S)	DATE REGISTERED
71	

FULL NAME(S) OF INVENTOR(S)

72 PITIS, CONSTANTIN DANUT

PRIORITY CLAIMED	COUNTRY	NUMBER	DATE
N.B. Use International abbreviation for country (see Schedule 4)	33 ZA	31 2004/6886	32 30 AUG 2004

TITLE OF INVENTION

54 MIXED CONDUCTIVITY FABRICATED ROTOR

ADDRESS OF APPLICANT(S)/PATENTEE(S)

33 PIET PRETORIUS STREET, INDUSTRIAL AREA, BRITS, PRETORIA, 0250, GAUTENG, SOUTH AFRICA

ADDRESS FOR SERVICE	S & F REF
74 SPOOR & FISHER	PA137818/ZA

PATENT OF ADDITION NO.	DATE OF ANY CHANGE
61	

FRESH APPLICATION BASED ON	DATE OF ANY CHANGE

SPOOR & FISHER

PATENT, TRADE MARK AND COPYRIGHT ATTORNEYS

Femco Mining Motors (Pty) Ltd
P O Box 2218
Brits
0250

Attention: Mr B Penzhorn

Your Ref:
Our Ref: PA137818/ZA
Date: 20 September 2005

Associates
Postal Address
Tel +27 12 676 1111
Fax +27 12 676 1100

Dear Sirs

South Africa - National phase patent application
Applicant : Femco Mining Motors (Pty) Ltd
Inventor : Pitis, Constantin Danut
Title : Mixed Conductivity Fabricated Rotor
Number : 2005/07280
Filing Date : 9 September 2005
National phase entry date: 9 September 2005

We confirm the instructions to file this application and now enclose the following:

1. The official filing receipt for the application;
2. A memorandum explaining the consequences of the filing of the application and advising on further steps to be taken.

We draw your attention to the fact that the following documents are outstanding:

- Declaration and Power of Attorney form P.3. This document must be filed at the Patent Office within six months of the national phase entry date given above.
- Deed of Assignment of Invention. This document must be filed at the Patent Office within twelve months of the national phase entry date given above, but preferably within six months in order to avoid unnecessary costs.

/2...

ANNEXURE 4.1: TYPICAL CONTINUOUS MINER

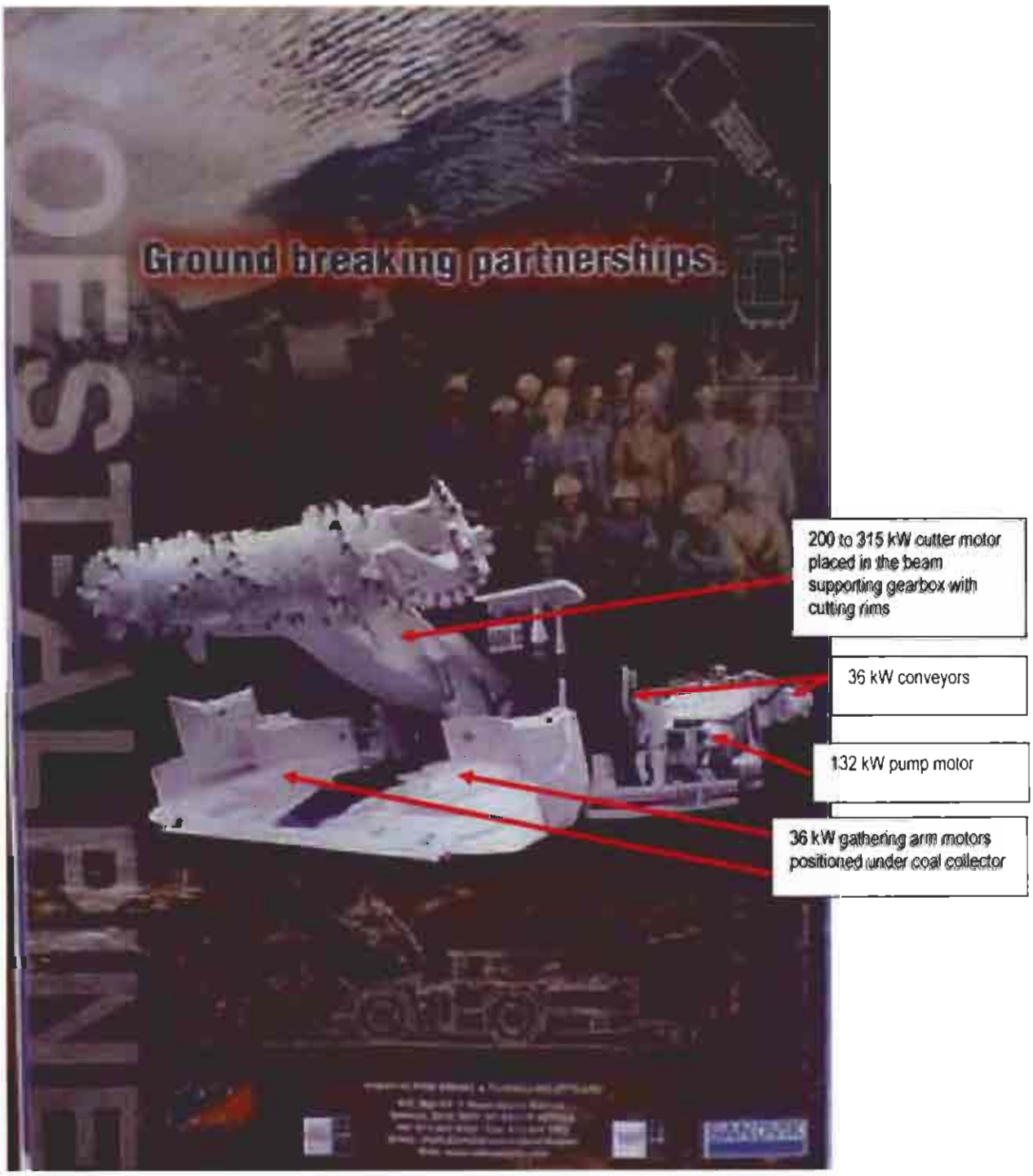

Graphic picture of a typical coal cutter continuous miner

The machine rated values are 40 000 tons coal per month. Currently, in South Africa, this machine is cutting 80 000 to 120 000 tons coal per month.

Voest Alpine Mining and Tunneling GmbH Austria has about 5 550 operating units.

ANNEXURE 4.2: DESIGN LIMITS OF DOUBLE CAGE ROTORS

Bottom limit of the double cage rotor design

For the double cage design, an outside diameter of 200 mm can be considered the bottom limit. It will be very difficult for the designer to fit the bars because of the restriction imposed by the materials and electromagnetic design.

- Minimum sizes are required for the running cage bars.
- Minimum sizes are imposed by the teeth width (at least 5 mm) in order to withstand handling during rotor manufacturing and other mechanical stresses.
- Acceptable values of flux density in the teeth at the bottom of the slot.

An example is a 4-poles rotor with an outside diameter of D = 200 mm.

A core length of L = 250 mm is the closest corresponding figure to the proposed sizes of a 4-poles motor.

If the motor is water-cooled, then, according to equation 3.9, an output coefficient

G = 3.0 kW/m3. r/m, will give a motor power of about 0.22 x 0.25 x 1500 x 3.0 = 50 kW.

For this type of motor, a minimum of 44 rotor slots is recommended. According to figure 4.1, the bottom slot will have a maximum diameter of 169 mm (imposed by the bars minimum requirements for material strength).

That means the tooth width at the bottom of the slot wt will be in the region of wt = 7 mm, which is still acceptable for an electromagnetic design.

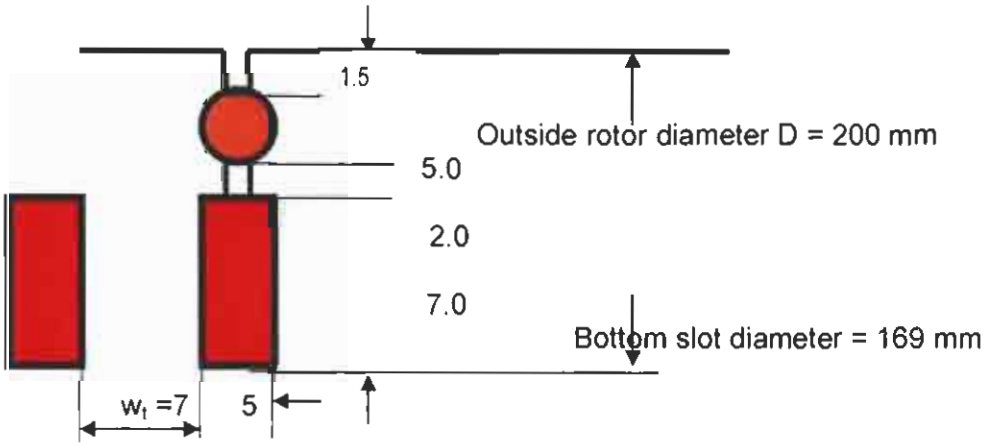

Figure 4.1 Sketch of a minimum design required by double cage slot arrangement for an outside rotor diameter D = 200 mm

This example is confirmed by the double cage motor sizes existent on the market.

Upper limit of double cage rotor design

Above specific diameter sizes, for a specific voltage of 1000 V, the motor power will increase beyond the starting cage capability in order to cope with the absorbed starting current.

Let's consider a 400 kW, 1000 Volts, 290 Amps, 4-poles, water-cooled motor.

According to equation 3.9, for an output coefficient G = 3.5 kW/m^3. r/m and 1500 r/m, it result in the product:

$$D^2 L = 0.0762 \text{ m}^3$$

If L = 0.65 m, the result is a motor with an air gap diameter, or rotor outside diameter, D = 342 mm.

Conductor per slots number = 12 for a 2 // Δ winding internal connection, 48 slots, half basket.

It results in stator turns in series per phase $T_1 = 48$.

For U_1 = 1000 V the e.m.f per phase in one rotor bar U_{20} = 11.4 Volts.

For a rotor bar number Z_2 = 44 bars, from it results in a bar current of I_b = 880 Amps.

Taking a current density of 4.5 A/mm^2 into account, it results in a running bar cross-section of 196 mm^2. From the design, the stator starting current can be approximated as Ist. = 7.0 p.u x Inom = 2030 Amps, while the bar current in the starting cage $I_{bst.}$ = 690 Amps. For a current density of 5 A/mm^2, the result is a round bar of 13.25 mm diameter, say, 14 mm (a possible standard size). The rotor slot configuration for this 400 kW motor is presented in figure 4.2.

The bottom slot will have a diameter of 278 mm. The tooth width at the bottom of the slot, w_t, will be in a region of w_t = 5.8 mm. This is a bottom limit of the tooth width, because of the high values of flux density at the bottom of the slot.

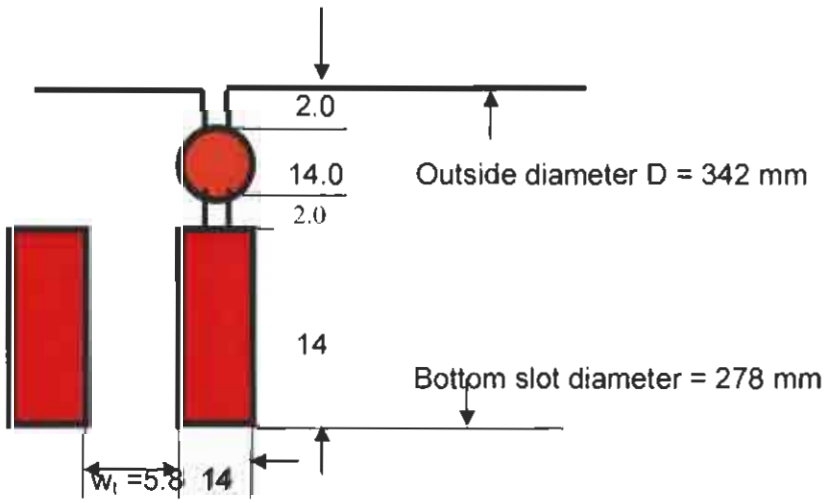

Figure 4.2 Sketch of a rotor slot of a double cage rotor for upper limit of 400 kW, 1 000 V, 4 poles, water-cooled motor

The tooth width, wt =5.8, represents a bottom limit of lamination tooth stamping from a mechanical strength point of view.

Note: *The tooth bottom size width can be increased if the motor core length "L" could be shortened and diameter "D" increased. But, taking into account the special application being used (continuous miner cutter motor always requires small diameters), this option will be unacceptable because of the general outline diameter of the motor.*

Comparison of Cutter Motors – Basic Design Calculations

Item **motor type**	**E 200**	**E 300**	**E 400**
Motor power kW	200	270	400
Core length, mm	570	600	650
Stator core OD, mm	419	449	523
Airgap diameter D, mm	275	293	342
Ratio D / OD	0.656	0.652	0.655
Winding Internal connection	2 // D	4 // D	4 // D
Conductor/slot	17	29	24
Proposed connection	2 //D	2 // D	2 // D
Converted conductor/slot	17	14.5	12
Cond/slot according to PT^2 = const	17	14.6	12
D^2 L n	64.66	77.26	114.04
Output coefficient G = KW / D^2 L n	3.09	3.5	Minimum 3.5
Rated current, A	144	193	290
Starting current, A	920	1300	**2100 very high**
St. current, p.u	6.4	6.73	7.2

ANNEXURE 4.3: QUOTATION OF A NEW DIE CAST ALUMINIUM ROTOR

This quotation indicates a **total cost of R150 000** for the rotor.

At that time the price of a new imported motor was R220 000.

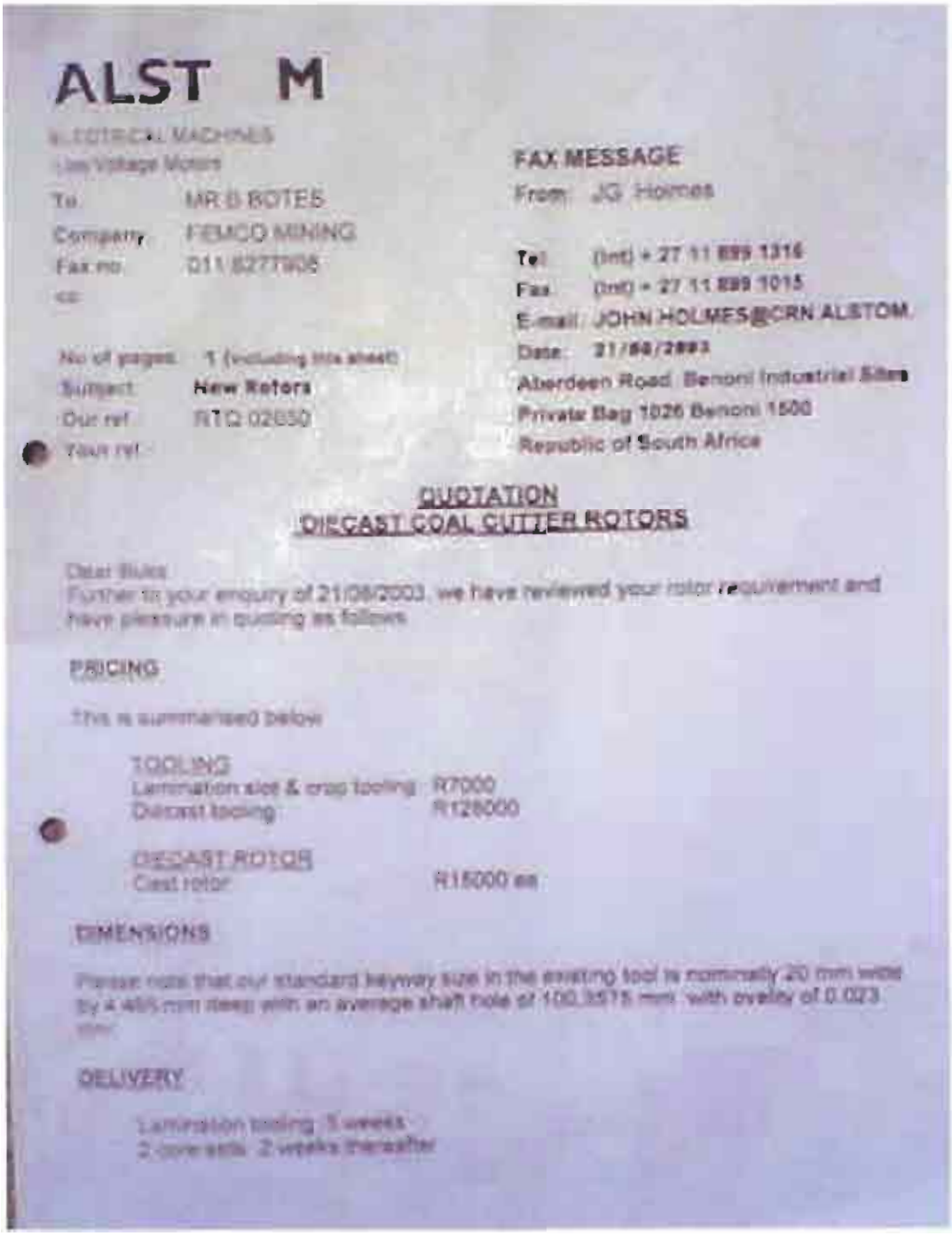

ALST M

ELECTRICAL MACHINES
Low Voltage Motors

To: MR B BOTES
Company: FEMCO MINING
Fax no: 011 8277906
cc:

No of pages: 1 (including this sheet)
Subject: New Rotors
Our ref: RTQ 02650
Your ref:

FAX MESSAGE
From: JG Holmes

Tel: (Int) + 27 11 899 1316
Fax: (Int) + 27 11 899 1015
E-mail: JOHN.HOLMES@CRN.ALSTOM.
Date: 21/08/2003
Aberdeen Road Benoni Industrial Sites
Private Bag 1026 Benoni 1500
Republic of South Africa

QUOTATION
DIECAST COAL CUTTER ROTORS

Dear Bules
Further to your enquiry of 21/08/2003, we have reviewed your rotor requirement and have pleasure in quoting as follows

PRICING

This is summarised below

TOOLING
Lamination slot & crap tooling R7000
Diecast tooling R128000

DIECAST ROTOR
Cast rotor R15000 ea

DIMENSIONS

Please note that our standard keyway size in the existing tool is nominally 20 mm wide by 4.465 mm deep with an average shaft hole of 100.3515 mm with ovality of 0.023 mm

DELIVERY

Lamination tooling 5 weeks
2 core sets 2 weeks thereafter

ANNEXURE 5.1: MCFR PRESENTATION TO THE SOUTH AFRICAN ROTATING MACHINES WORKING GROUP

THE ROTATING MACHINES WORKING GROUP

NOTICE OF MEETING

From: Mark/Pamela [catspen@mweb.co.za]
Sent: Tuesday, May 10, 2005 6:45 AM
To: Thys Botha; Mark Abbott; Willie Cronje; Uresh Naidoo; Tony Phillips; Steve Marshall; Sherwin Jerrier; Ron Scollay; Peter Heim; Paddy Bateman; Nic Grobler; Mo Ahmed; Mike Case; Meyer Naude; Martin Scholtz; Martin Kamper; Mark Spencer; Mark Peters; Mac Hipner; Klaus Kuhn; Johan Nell; Jan de Kock; james@fsatie.techpta.ac.za; James Cowling; J Gieras; Iain Grayer; Herman van der Merwe; Greg Diana; Geoff Howell; Gavin Garland; Frikkie van der Merwe; Flip van Vuuren; Ernie Muller; DuToit Grobler; Dries Wolmarans; Clinton Jones; Chris Tute; At Greyling; Andy McCutcheon; Andre Maritz; Alan Mitchell ; Alan Meyer; Alan Lotter; A. Smith; Vits Maharaj; Rob Melaia; Peter Warner; Pearlie John; Mitch McAllister; Mark McNally; Mario Kuisis; Johan de Lange; Jerry Walker; Henry du Preez; Henk de Swart; Grant Muller; Gerard Donachie; George Jeans; Derek Wood; Dave Braude; Dan Pitis; Charles Morton; Anesh Surendra; Andrzej Tomzynski; Antonio Teixeira; Gary Danes
Subject: Fw: Rotating Machines Working Group.

Regards,
Mark.

----- Original Message -----
From: Mark/Pamela
To: Thys Botha ; Mark Abbott ; Willie Cronje ; Uresh Naidoo ; Tony Phillips ; Steve Marshall ; Sherwin Jerrier ; Ron Scollay ; Peter Heim ; Paddy Bateman ; Nic Grobler ; Mo Ahmed ; Mike Case ; Meyer Naude ; Martin Scholtz ; Martin Kamper ; Mark Spencer ; Mark Peters ; Mac Hipner ; Klaus Kuhn ; Johan Nell ; Jan de Kock ; james@fsatie.techpta.ac.za ; James Cowling ; J Gieras ; Iain Grayer ; Herman van der Merwe ; Greg Diana ; Geoff Howell ; Gavin Garland ; Frikkie van der Merwe ; Flip van Vuuren ; Ernie Muller ; DuToit Grobler ; Dries Wolmarans ; Clinton Jones ; Chris Tute ; At Greyling ; Andy McCutcheon ; Andre Maritz ; Alan Mitchell ; Alan Meyer ; Alan Lotter ; A. Smith ; Vits Maharaj ; Rob Melaia ; Peter Warner ; Pearlie John ; Mitch McAllister ; Mark McNally ; Mario Kuisis ; Johan de Lange ; Jerry Walker ; Henry du Preez ; Henk de Swart ; Grant Muller ; Gerard Donachie ; George Jeans ; Derek Wood ; Dave Braude ; Dan Pitis ; Charles Morton ; Anesh Surendra ; Andrzej Tomzynski ; Antonio Teixeira ; Gary Danes
Sent: Sunday, May 08, 2005 7:32 AM
Subject: Rotating Machines Working Group.

Dear Members,
The Notice of Meeting and the Agenda are attached for the next meeting. Note the slightly earlier starting time.
I hope most of you will attend to ensure a good meeting.

Regards,
Mark Spencer

Chairman, Rotating Machines Working Group.

The next meeting of the RMWG will take place on Wednesday 15 June at ArmCoil Africa, 127 Main Reef Road, corner of Serfontein Road, Technikon, Roodepoort. (Telephone No. 011 474-9551)

The Meeting will start at **14:00** and not 14:15 in order to give us more time for business.

There will be three presentations:

1. Predictive diagnostics for MV & LV machines by Mario Kuisis of Martec,
2. Sasol's history of large motors by Andre Maritz of Sasol
3. Mixed conductivity fabricated rotors by Dan Pitis of FEMCO.

AGENDA

1. Opening
2. Welcome
3. Apologies
4. Acceptance of minutes of the last meeting
5. Matters arising
6. Presentations:
    1. Predictive Diagnostics for MV & LV Machines by Mario Kuisis
    2. Sasol's history of large machines by Andre Maritz
    3. Motor rotors with mixed conductivity metal bars by Dan Pitis
7. Activity Reports/R&D
8. Section Feedback
    Machine insulation Assessment
    IEC/Cigre
    Motor Specification Guide
9. Membership
10. Activity/presentation suggestions for the next meeting
11. Chairman of the Group
12. General
13. Next meeting date and venue
14. Closure.

ANNEXURE 6.1: MCFR ENQUIRIES

FEMCO Mining Motors

A Member of the Pasdec Group

33 Piet Pretorius Street, Brits
PO Box 2218, Brits, 0250
Tel: +27 (012) 250 2101
Fax: +27 (012) 250 3409
Web site: www.pasdec.co.za

17th July 2004
Internal Memo: Kevin Pather
Copy: C.D.Pitis – Project Manager
Tinus Boshoff – Accounting Manager

Bruno Penzhorn – Business Development manger

Request for prototypes manufacture

1. **Mixed Conductivity Fabricated rotor replacement for Damel die cast aluminium rotors - 36 kW spinner motors**

Since 2004, FEMCO's 36 kW "P" spinner motor FMM 0072 fitted with MCFR patent is competing with Damel motors fitted with aluminium rotors.
The aluminium Damel rotors proved to have a limited life span.
Voest Alpine has therefore requested Femco to design and manufacture a MCFR-patent rotor to replace spare rotor imports from overseas. In this way Femco will be able to participate in this South African and overseas market.
Estimated material and labour cost per MCFR = R14 000.
Estimated South African market: 200 motors in the first year.
Estimated World market: 3000...4000 motors

Approved,

Kevin Pather
DIRECTOR

----- Original Message -----
From: bruno
To: Kevin Pather
Sent: Tuesday, December 14, 2004 2:07 PM
Subject: Fw: Pragmatic Solution / Proposal for 36 kW Motors

Kevin,
Voest had a solid brass bar rotor build by Luck & King.
The tests were not satisfactory but we need to prevent them developing ties with third parties.

Our proposal would also make sense for us given our market for 36 kW "P" motors for price fluctuation reasons.
Bruno.

----- Original Message -----
From: bruno
To: George A Filen – Voest Alpine, Sandvik
Cc: Ossie Carstens ; Peter Dresen – Voest Alpine
Sent: Tuesday, December 14, 2004 2:01 PM
Subject: Pragmatic Solution / **Proposal for 36 kW Motors with MCFR patent.**

Dear George,

The 36 kW spinner motors that you purchase from Damel are fitted with aluminium rotors.
These rotors are subject to failure if the aluminium injection / casting has not been done been properly.
As you know, Femco has developed its own 36 kW spinner motor No FMM 0072 with a patented mixed-conductivity fabricated rotor.
This special rotor has the same torque characteristics as both the Loher and Damel motors with their aluminium rotors and will be able to run in tandem with either of them.
Given the current strength of the Rand and the attractive pricing from Damel in Poland, we have to be pragmatic and accept that our prices are not always competitive (given market fluctuation) and that it is unlikely that you will be able to order Femco motors permanently, in the foreseeable future.

Recently Peter requested at the Technical Committee that Femco test a 'brass bar' rotor that you had subcontracted to a third party in South Africa. It does not appear that this combination will give you the desired results.

Therefore, we propose that we investigate fitting the Damel motor with the Femco mixed-conductivity fabricated rotor on failure of its original aluminium rotor.

If you team agrees, we can pick this up in the Anglo Americans Technical Committee and come forward with a formal proposal.

Kind regards,
Bruno.

ANNEXURE 6.2: DESIGN ITERATIONS

Item / Steps	1	2	3a	3b	3c
Rated values					
Nnom [r/m]*	1482	1490	1484	1481	1479
Torque nom [Nm]	3222	3206	3216	3226	3228
Inom [A]	51.8	52.0	52.1	52.15	52.2
Temperature rise [C]	**100**				**100****
Effic. ή [%]	95.5	95.8	95.5	95.4	95.3+
Power factor	0.877	0.876	0.876	0.876	0.876
Io [A]	18.24	19.2	19.1	19.0	18.86
Po [kW]	10.1	10.6	10.6	10.6	10.6
Starting conditions	**+				
St.Tq [Nm]	7024	5451	6015	6624	7032
St.Crt. [A]	380	422	401	390	386
Run up time s	9.6	10.7	10.4	10	9.30
Wind.Trise[C]	18	28	23	20	18
Rotor Bars Trise	84	64	83	90	92
Rotor Ring Trise	41	31	38	45	49
Stall time [s]	17.2	29	23	18	14.5
P.O.T. [kNm]	9.8	9.97	10.0	10.1	10.26
@ speed [r/m]	1393	1432	1404	1380	1370

Comparing new design (3c) – Fig. 3 to the initial (1) or to a classic copper rotor replacement (2), some observations can be done:

* Rated speed value deviation from original is only 3 r/m, while a copper rotor (2) has a deviation of 8 r/m.

** Motor temperature rise was kept the same, with prospective of improving motor' internal ventilation by using at least one rotor radial vent; fanning effect on the rotor bars overhang should be considered, too.

\+ Motor efficiency with MCFR1 dropped 0.2%, but the application do not require continuous running regime, but frequent heavy starts.

**+ Starting performances confirms the motor capability to replace the existing one:

- Starting torque, starting current, run-up time and winding temperature rise per start values are the same or very close to the initial (1);
- Rotor bars and short-circuit rings temperature rises per start are slightly higher but proved their withstanding to thermal stress to be better than original;
- Stall time above 10 seconds is controlled by protection.

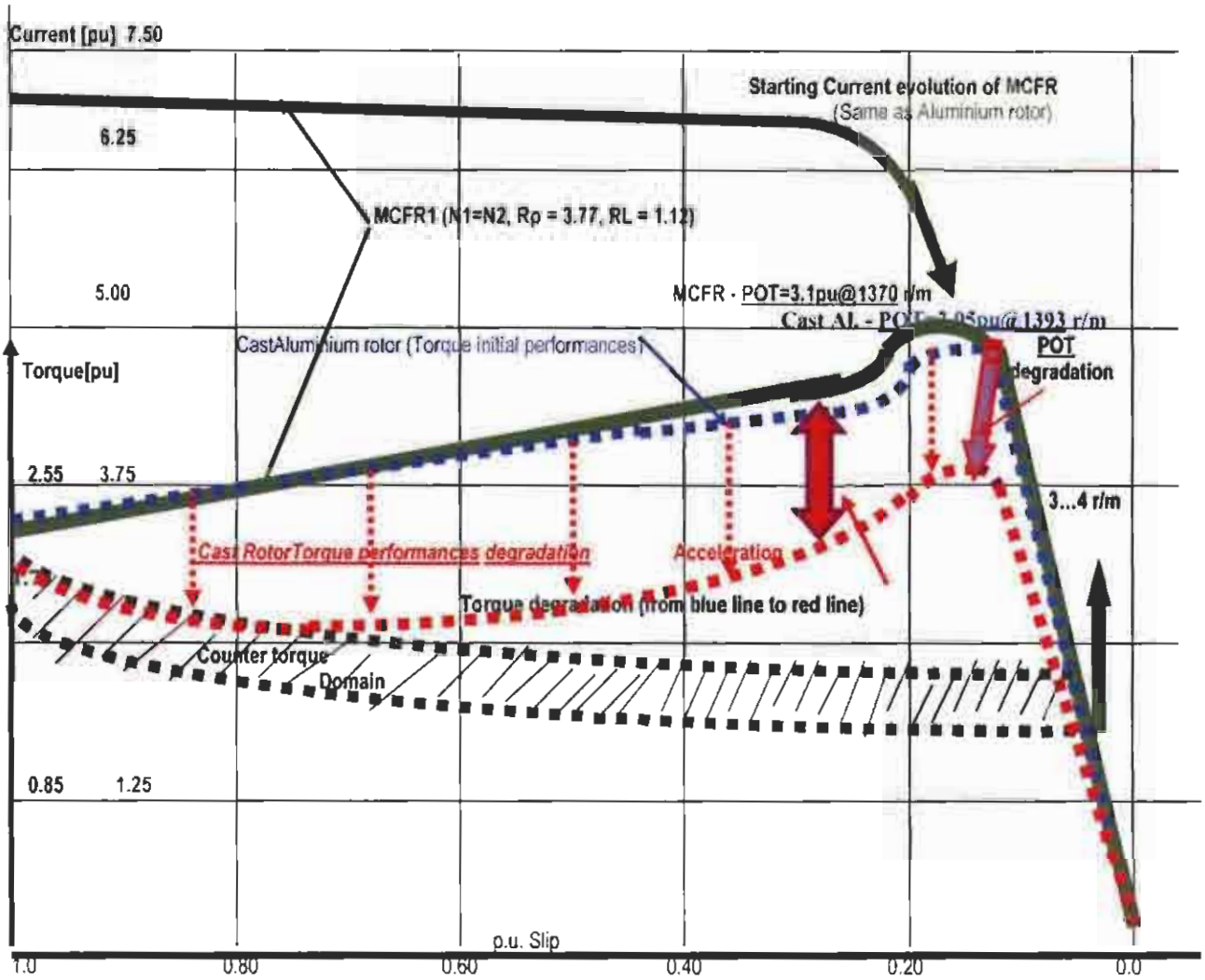

Speed Torque curves for a specific application where Aluminium rotors have been replaced with MCFR1

LEGEND

- **Black lines** = Load Counter-torque domain
- **Blue lines** = Aluminium cast rotor initial performances
- **Red lines** = Performances degradation evolution of a cast rotor
- **Light blue lines** = De-gradated performances to the extend motor beyond minimum requirements.
- **Green lines** = Performances of a motor with rotor replaced by a MCFR1 type.
- The green figures are for starting current scale in [pu]
- The black figures are for torque curve scale in [pu]

Pull-out torque (POT) value has been improved and this is one of the initial conditions taken into consideration when designed; however, reduced POT speed value is still in the requirements range. POT speed increase will be detrimental to starting performances.

ANNEXURE 7.1: MCFR1 DESIGN FOR THE 36 KW SPINNER MOTOR

```
                    *** SQUIRREL CAGE INDUCTION MOTOR ***
                    -------------------------------------

  ---------------------------------------------------------------------
  1 CUSTOMER:        Voest Alpine, MCFR              1 DATE:  Oct.2003   1
  1                                                  1 ORDER NO.:        1
  ---------------------------------------------------------------------
  1  FRAME  1  ENCLOSURE  1   KW   1 POLES 1 VOLTS  1 AMPS 1  PH  1  HZ 1
  1  E 200  1  Flproof    1   36   1   4   1  1000  1 27.7 1  3   1  50 1
  ---------------------------------------------------------------------
  1 EFFCY  1  P.FACT 1  SPEED     1 INSUL CLASS 1   WND SPECIFICATION   1
  1 91 %   1  0.85   1  1461  RPM 1       H     1   MCFR Patent         1
  ---------------------------------------------------------------------


  *** STATOR AND ROTOR SLOT CONFIGURATIONS ***
  -------------------------------------------

     STATOR              1  ..................................................
   ----------            1    284.00                                 26.00
SLOTS =   48.0           1                                          ----------
S/P/P =    4.0           1                        .............    .
WND TYPE = MUSH          1                        .     8.70   .
WND CONN = STAR          1                         .           .
PARALLEL CCT =  2.0      1                         .           .
COIL PITCH =  11.0       1                         .           .      24.00
COND/SLOT =   32.0       1          W1/3 =   6.45  .           .
IRON GRADE =    .0       1                         .           .
STACKING FACTOR = .941   1                         .   6.00    .            ---------
NO.ST.DUCTS =     .0     1                          \       /              TH=  2.50
WIDTH ST.DUCT=    .0     1  ........................1     1.............BD=    .50
KW/(DDLN) =     2.84     1    184.00                   3.20
GCL =   250.00           1             SSP =  12.04                GAP =     .80
                         1             RSP =   9.88
    ROTOR                1                              1.80
  ---------              1  ..........................    ........................
SLOTS =  58.0            1    182.40                  1    1                    1.50
WND TYPE = CU CAGE       1                          ..1    1..              --------
SKEW =    .0 (ST.SLOT)   1                          1         1
IRON GRADE =    .0       1                          1         1
STACKING FACT =  .90     1                          1         1       26.80
                         1                          1  3.25   1
                         1           W2/3 =   4.69  1         1
                         1                          1         1
                         1                          1.......1    ----------
                         1                                         31.90
                         1  ..................................................
                         1     65.00
VENTILATION:    AXIAL              HOLE SHAPE = CIRCULAR
                                   NO.ROT.VENTS =  2.0      DIAMETER =  2.00

  *** MAGNETIC CIRCUIT ***
  -----------------------
FLUX/POLE = .021399          DISPERSION COEFF =   .068      B(AV) =   .5923
```

	ST CORE	RT CORE	ST TEETH	RT TEETH	GAP
B(60)			1.4694	1.6842	.7267
B(MAX)	1.7512	1.4824	1.8221	2.0883	.9011
A-TURNS	133.76	16.43	53.13	195.71	579.22

TOTAL A-TURNS = 978.26 MAG CURRENT/PH = 14.50 XM = 39.81

*** NO LOAD LOSSES ***

F & W	ST TOOTH	ST CORE	SURFACE LOSS	(I**2)*R
275.00	133.18	335.36	325.29	366.83

TOTAL NO LOAD LOSSES = 1435.65

*** PERFORMANCE ***

	1.00 FL	.25 FL	.50 FL	.75 FL	1.25 FL
SC/PHASE	27.60	15.31	18.34	22.59	33.11
RC/PHASE	22.73	5.59	11.15	16.86	28.78
SLIP	.0257	.0062	.0124	.0189	.0329
RPM	1461.4	1490.7	1481.4	1471.6	1450.7
FW+IRON LOSS	1068.8	1068.8	1068.8	1068.8	1068.8
S CU LOSS	1328.0	408.5	586.8	889.7	1912.1
R CU LOSS	955.0	57.7	229.5	524.9	1531.2
STRAY L.LOSS	180.0	55.4	79.5	120.6	259.2
TOTAL LOSS	3531.7	1590.4	1964.7	2604.1	4771.3
EFFICIENCY	.910	.850	.902	.912	.904
POWER FACTOR	.8196	.3953	.6235	.7508	.8580

*** EQUIVALENT CIRCUIT (FULL LOAD) ***

PER UNIT QUANTITIES		ACTUAL VALUES (OHMS)	
X1 = .057	R1 = .0278	R1(HOT)= .5813	R2(HOT)= .6160
X2 = .0682	R2 = .0294	XS = .6485	XS = 1.0186
BM = .5256	GM = .0166	XEW = .4290	XEW = .2867
BASE OHMS = 20.9221		XZZ = .1408	XZZ = .1408
TRANSFORM RATIO = 12.57		XSK = .0000	XSK = .0000
		BR PERM = .1562	BR PERM = .8333
		SL PERM = 1.5764	SL PERM = 2.6564
ACTUAL BAR RESIST = .010916		RING RESIST = .000775	

STATOR		ROTOR	
FLCD (A/MM2) =	5.856	BARCD(A/MM2) =	3.811
AWPMM =	36.663	RING CD(A/MM2)=	2.199
EDDY CUR LOSS =	.000	CART COEFF =	1.072
CARTERS COEFF =	1.168	TO LAM WT(KG)=	30.776
SPACE FACTOR =	.488	BAR RESISTIVITY=	.38E-07
PITCH FACTOR =	.9914	BAR LENGTH(MM)=	290.00
DISTRIB FACT =	.9577	TOT BAR WT(KG)=	11.101
SLOT/P/P =	4.00	ENDR AREA(MM2)=	600.000
TOT LAM WT(KG)=	51.63	ENDR MEAN DIA(MM) =	155.000
COND./PHASE =	512.00	ENDRR WT(KG) =	5.142
CU WT(KG)APPROX=	15.269	ENDR RESISTIVITY=	.17E-07
WIRE SIZE (MM)=	1.00 BY 1.00	BAR DIMENS: BUW=	3.00 BUD= 25.00
	2.00 BY 1.00	TOW=	.00 TOD= .00

RECOMMENDED MIN GAP LENGTH = .70 MM
UMP = 255.90 KG

*** STARTING CHARACTERISTICS ***

UNSATURATED STARTING AT VOLTS = 1.0 PU

SLIP	TORQUE	ST.AMPS	P.F.	X1	X2	R1	R2
1.00	2.44	7.18	.46	.059	.066	.028	.039
.90	2.53	7.09	.47	.059	.067	.028	.038
.80	2.65	6.99	.49	.059	.068	.028	.036
.70	2.80	6.86	.51	.059	.068	.028	.035
.60	2.99	6.69	.53	.059	.069	.028	.033
.50	3.23	6.46	.57	.059	.069	.028	.032
.40	3.52	6.13	.61	.059	.070	.028	.031
.30	3.79	5.59	.68	.059	.070	.028	.030
.20	3.85	4.65	.77	.059	.070	.028	.030
.10	3.00	2.95	.87	.059	.071	.028	.030
.05	1.81	1.68	.89	.059	.071	.028	.029
.04	1.50	1.40	.88	.059	.071	.028	.029
.03	1.16	1.12	.84	.059	.071	.028	.029
.02	.79	.85	.76	.059	.071	.028	.029

PULL OUT TORQUE = 4.05 PU AT SLIP = .233

SATURATED STARTING AT VOLTS = 1.00 PU

SLIP	TORQ	ST.AMP	P.F.	TIME	L.T.	X1	X2	R1	R2
1.00	3.22	8.20	.53	.00	.00	.051	.052	.028	.039
.90	3.33	8.07	.54	.18	.01	.052	.053	.028	.038
.80	3.45	7.92	.56	.36	.04	.052	.054	.028	.036
.70	3.61	7.73	.58	.54	.09	.052	.055	.028	.035
.60	3.80	7.49	.60	.70	.17	.052	.055	.028	.033
.50	4.03	7.17	.63	.87	.26	.052	.056	.028	.032
.40	4.27	6.71	.68	1.02	.38	.052	.056	.028	.031
.30	4.43	6.00	.74	1.18	.52	.052	.057	.028	.030
.20	4.27	4.87	.82	1.34	.67	.052	.058	.028	.030
.10	3.10	2.99	.89	1.54	.85	.054	.061	.028	.030
.08	2.66	2.49	.90	1.60	.89	.054	.062	.028	.030
.06	2.13	1.96	.90	1.68	.93	.055	.064	.028	.029
.04	1.50	1.40	.88	1.82	.97	.057	.067	.028	.029
.02	.79	.85	.77	1.82	1.01	.058	.069	.028	.029

CALCS STOPPED AS NO MORE ACCELERATING TORQUE IS AVAILABLE.

RUN UP TIME = 1.82 SEC
LOAD + MOTOR INERTIA CONST = 3.00 (NOTE: THIS IS H NOT 2H)
TEMP RISE DURING STARTING (DEG C): STATOR WND = 12.71
ROT. BAR = 16.04
ROT. RINGS = 2.48
MAX STALL TIME = 16.6 SEC (LIMITED BY BAR TEMP)